Investigation of Fatigue Properties of Superpave HMA at the Virginia Smart Road

Stacey D. Diefenderfer

Dissertation submitted to the Faculty of the

Virginia Polytechnic Institute and State University

in partial fulfillment of the requirements for the degree of

Doctor of Philosophy

in

Civil Engineering

Gerardo W. Flintsch, Chair
Imad L. Al-Qadi, Chair
Scott W. Case
Amara Loulizi
Antonio A. Trani

October 12, 2009
Blacksburg, Virginia

Keywords: hot mix asphalt, Superpave, fatigue

Investigation of Fatigue Properties of Superpave HMA at the Virginia Smart Road

Stacey D. Diefenderfer

ABSTRACT

This study investigated the influence of material properties on fatigue life through laboratory fatigue testing of eleven Superpave hot mix asphalt (HMA) mixtures in use at the Virginia Smart Road. Mixtures were sampled from the plant and produced in the laboratory to investigate the influence of production method. Specimens were cut from the in-situ pavement and compacted in the laboratory to evaluate the influence of compaction method. Third point beam fatigue testing was performed at 25ºC and 10Hz. Additional testing at frequencies of 1 Hz and 5Hz, and at 10 Hz including rest periods of 0.4sec and 0.9sec were performed for one mixture to explore the impact of frequency and rest periods. Analyses were performed on the strain-life relationships and predicted endurance strain limits for the mixtures.

Investigation of strain-life relationships for several mixtures indicated that small differences in mixture volumetrics due to the production method have minimal impact on the laboratory fatigue performance of HMA. Comparisons of expected fatigue performance for one mixture indicated that shorter fatigue lives (under the same strain conditions) may be expected for laboratory-compacted specimens when compared to field-compacted specimens, despite visual observation of damage (surface cracking) in the field-compacted specimens. Testing performed on one mixture to determine the influence of different loading frequencies showed that fatigue life was independent of the frequencies tested. Investigation of rest period inclusion indicated no differences in fatigue life for loading conducted at 10 Hz frequency and no rest period, 0.4sec rest period, or 0.9sec rest period. The evaluation of specimens cut from the in-situ pavement indicated that location within the lane and orientation did not significantly affect laboratory fatigue performance. The effect of aggregate size was considered; however, results were inconclusive. Using predictive strain-life fatigue equations, the benefits of polymer-modification of binders and use of SMA were shown for mixtures produced in the laboratory according to the job mix formula and to match the plant-produced volumetrics. Evaluation of the predicted fatigue strain endurance limit was performed using an energy-based and an empirical method. The energy method was shown to estimate significantly higher endurance limit strains for mixtures.

ACKNOWLEDGEMENTS

I would like to thank my advisors, Dr. Imad Al-Qadi and Dr. Gerardo Flintsch, for their guidance, help, and patience throughout my graduate studies. Their expertise, assistance, and support have been invaluable. In addition, I would like to thank Dr. Scott Case, Dr. Amara Loulizi, and Dr. Antonio Trani for their support and help as members of my advisory committee. The journey to complete this work spanned a rather long period of time and many unusual circumstances, but their encouragement has not flagged.

I would also like to thank the friends and colleagues who have been instrumental in their support of this endeavor. From Virginia Tech, I would like to thank Alexander Appea, James Bryant, Alan Cristoe, Robin Davis, Mostafa Elseifi, Samer Lahouar, Samer Katicha, Edgar de León, and Kevin Siegel for their help and friendship. Also, special thanks are extended to William (Billy) Hobbs for all of his time and patience while producing all of the test specimens, performing all volumetric testing, and keeping the laboratory running smoothly. From VDOT and the Virginia Transportation Research Council, I would like to acknowledge Troy Deeds, Donnie Dodds, Mohamed Elfino, Bill Maupin, Kevin McGhee, and Michael Sprinkel for their support and assistance in completing this work.

My parents and family are credited for their support and encouragement. Finally, I cannot overstate the importance of the love, support, and encouragement of my husband Brian and the blessing of my son Ian, who have both provided great motivation to complete my degree.

TABLE OF CONTENTS

LIST OF FIGURES

LIST OF TABLES

1 INTRODUCTION

Decreasing highway funding and increasing expectations for performance and quality have created a situation wherein it is particularly important for pavement engineers to understand the effects of asphalt mixture properties on pavement performance. Public road mileage in 2007 in the United States reached almost 4.05 million miles (FHWA, 2007). Vehicle miles of travel reached an all-time a high of 3,049,027 million miles in the same year, while highway expenditures per vehicle mile of travel have continued a decreasing trend (FHWA, 2007). The increase in traffic and decrease in maintenance funding are causing pavement deterioration to become more readily apparent in the nation's highways. Part of the solution to deteriorating roadways lies in the choice of better construction materials, which require greater understanding of the fundamental behavior and properties of such materials.

1.1 BACKGROUND

Bituminous pavements comprise approximately 98% of the hard-surfaced pavements in the United States (FHWA, 2007). Considering this, the properties and performance of asphalt materials is an area of high importance to the highway infrastructure of the U.S. Bituminous mixtures, or hot mix asphalt (HMA), are complex mixtures composed of a bituminous binder and mineral aggregate. The binder acts as an adhesive, gluing the aggregate into a dense mass and waterproofing the aggregate particles. The aggregate, when bound together, acts as a stone framework to give strength and toughness to the composite system. Mixture performance is affected by both the aggregate and binder individual properties and interactions. Despite considerable research efforts to characterize mixture properties and performance, no consensus has been reached as to definitive relationships between the two.

Selection of appropriate highway materials with respect to climatic and loading conditions can significantly contribute to an increase in expected pavement service life and can lead to notable long-term national savings. With these considerations, the Superpave (Superior Performing Asphalt Pavements) mixture design protocol was developed as a product of the Strategic Highway Research Program (SHRP), a five-year, $150 million program designed to improve the performance and durability of US roads and highways (Asphalt Institute, 1996). The system is intended to incorporate performance-based materials characterization with design for environmental and traffic conditions to improve highway performance.

Employing an understanding of the interaction between climate, traffic, and pavement performance, Superpave mixtures are developed to perform under site-specific traffic and climatic loading conditions. They are designed to resist, in particular, deterioration due to low temperature cracking, fatigue, and permanent deformation. Low temperature cracking is caused by excessive tensile stresses induced over time by thermal gradients within pavements. Permanent deformation, commonly called rutting, is generally attributed to insufficiently designed pavements and is characterized as a permanent change in the form of a pavement or pavement layer (Roberts et al., 1996). Fatigue is the process by which the pavement deteriorates through cracking because of small built-up irrecoverable strains induced by repeated loading over time (Khalid, 2000a, 2000b).

The potential for these distresses is usually evaluated through laboratory testing performed on laboratory-produced specimens. However, production of laboratory specimens differs significantly from production of hot mix asphalt for roadways. Also, differences have been shown to exist for test results between specimens produced in the laboratory using different compaction methods and road cores (Button et al., 1994; Consuegra et al., 1989; Harvey and Monismith, 1993; Khan et al., 1998; Masad et al., 1999).

Effects of specimen preparation and compaction methods on the physical properties of HMA are not well-understood although are expected to be significant. Six different Superpave mixtures are in service at the Virginia Smart Road, offering the opportunity to evaluate these effects on HMA mixtures through in-service testing and laboratory characterization. Evaluation of compaction effects between the laboratory and field can give valuable insight into adjusting design procedures such that in situ material will more accurately reflect design performance.

1.2 PROBLEM STATEMENT

One of the most problematic deterioration modes in HMA pavements is fatigue. The occurrence of this distress may be reduced by proper design of highway pavements, which requires comprehensive knowledge of the material properties and performance. Hot mix asphalt characteristics and properties are commonly measured through volumetric analysis and laboratory performance testing. As HMA properties are significantly affected by specimen preparation, compaction, mixture inhomogeneity, and test method, a better understanding of the effects of these variables on response is needed.

1.3 OBJECTIVES OF RESEARCH

The primary objective of this research to determine the influence of field and laboratory production and compaction on the predicted fatigue performance of HMA. This will be accomplished by characterizing and evaluating the fatigue performance of six Superpave HMA mixtures commonly used in Virginia pavements under four production and compaction conditions.

1.4 SCOPE OF RESEARCH

To accomplish the objectives of this study, evaluation was performed on six Superpave HMA mixtures designed with several binders and differing gradations. In addition to the six mixtures, four combinations of production and compaction methods were considered: plant-produced and field-compacted; plant-produced and laboratory-compacted; laboratory-produced according to the mixture design and laboratory-compacted; and laboratory-produced to match plant-produced gradation and asphalt content and laboratory-compacted. Also, several mixtures were placed in multiple locations at the Smart Road; these were considered as unique mixtures for the purpose of mixture variation comparisons. Volumetric properties for each mixture were measured and evaluated. Fatigue characterization of each mixture was performed using third point beam fatigue testing. Results of fatigue testing were used to compare fatigue performance

of mixtures and to evaluate the differences in production and compaction methods on fatigue performance.

Chapter 2 provides an overview of material properties necessary to characterize hot mix asphalt and discusses the development and use of fatigue evaluation methods. The research approaches used in this study are presented in Chapter 3. Results of fatigue testing are offered in Chapter 4, along with discussion of the factors affecting fatigue response. The summary, findings, and conclusions of the research experiment are presented in Chapter 5 and Chapter 6 offers recommendations for further investigation.

2 BACKGROUND

2.1 MATERIAL PROPERTIES IN PAVEMENT DESIGN

Hot mix asphalt (HMA) is a composite material composed of aggregate, binder, and often, various admixtures. Although each constituent exhibits specific behavior under loading, this is not necessarily indicative of the performance of the composite. Aggregate is generally accepted to be an elastic material. Traditionally, pavement engineers and researchers assume that asphalt binders are linear viscoelastic materials (Christenson, 1998). This assumption is carried over to HMA for simplification of analyses, although HMA is significantly more complex than the binder alone. For temperatures below 0ºC, the assumption of linear elasticity may be justified; however, at temperatures above this, nonlinear elastic and viscoelastic behavior can become a problem in performing analyses (Roque and Buttlar, 1992; Buttlar and Roque, 1994). Despite this concern, historically most methods for determination of material properties have used linear elastic assumptions for calculations, due to the complications of introducing either linear viscoelastic or nonlinear elastic concepts. However, with advances in computing capabilities, models incorporating linear viscoelasticity are becoming more widely used.

In order to understand HMA properties, different behaviors should be noted and several mechanical concepts must be clarified. In general, it is accepted that four mechanical models exist to characterize fundamental material properties by relating stress to an applied strain; these are considered as elastic, viscous, viscoelastic, and plastic. Elastic strains are fully recoverable and are independent of time; this means that no permanent strains are generated in a loading/unloading cycle and this response is independent of the loading/unloading rate. Viscous strains are irrecoverable and time-dependent; this means that the magnitude of the strain depends on both load duration and rate of loading/unloading. Viscoelastic strains are recoverable and time-dependent; the strain magnitude depends on both load duration and rate of loading/unloading but is fully recoverable over time. Plastic strains are permanent but independent of time; this means for any loading history, regardless of rates of loading/unloading, the same magnitude of permanent strain is developed.

Unfortunately, it is difficult to isolate the three types of strains under most loading histories. This is because both viscous and plastic strains lead to permanent deformation. The importance of identifying strains related to each property comes from the fact that the constitutive equations describing each model are formulated differently. Constitutive equations for elasticity and viscosity, as well as viscoelasticity, do not impose limitations on stress magnitudes, which imply a relationship through a continuous operator of the stresses and strains or their derivatives. However, plasticity utilizes the yield condition, implying different operators separated by functions of stress, and in general, of strain, for the loading and unloading conditions.

During the pavement design process, the material responses to the applied stresses or strains are used to determine an appropriate design to resist the three primary modes of asphalt deterioration: rutting, thermal cracking, and fatigue. In Virginia, fatigue is generally considered to be the most widespread mode of deterioration for HMA pavements.

2.2 FATIGUE RESISTANCE

Fatigue is the process by which the pavement deteriorates through cracking because of small built-up irrecoverable strains induced by repeated loading over time (Khalid, 2000a, 2000b). These strains accumulate because of the viscoelastic properties of HMA. When loads are removed, induced strains are not completely recovered and these accumulate over time. Fatigue cracking is generally thought to begin at the bottom of the HMA layer, as this area is placed in a state of tensile strain from the stresses caused by repeated traffic loading. Fatigue is a two stage process consisting of microcrack growth and healing and macrocrack growth and healing. Both of these growth processes are thought to be governed by Paris' law (Little et al., 2001) which will be discussed in detail later. After crack initiation at the bottom of the asphalt layer, cracks propagate upward, and may eventually result in a network of cracks in the asphalt surface, which gives fatigue cracking its more common name, alligator cracking. Although less commonly accepted, fatigue may also initiate at the top surface of the pavement. This is hypothesized to be due to non-uniform three-dimensional contact traction and pressure distribution between the pavement and vehicle tire (Collop and Cebon, 1995). Temperature-induced fatigue cracking also may be initiated at both the top and bottom of asphalt layers due to horizontal tensile strains induced by daily temperature cycles (Collop and Cebon, 1995).

Fatigue cracking may be evaluated from one of two viewpoints: at the microscopic level and at the macroscopic level. These correspond to local and global fracture, respectively. The microscopic level is generally considered when investigating the initiation of cracking in HMA. If HMA is considered an inhomogeneous material, it is comprised of binder, aggregate particles and air voids. The boundaries where the aggregate particles and binder "bond" together act as stress concentration locations in the inhomogeneous material and are the initiation location of most cracking. Cracks then may propagate through the area of least resistance – the aggregate-binder interface. The analysis of these cracks is usually performed using plasticity methods, as the binder is considered a viscoelastic medium and plastic effects (such as crack-tip plasticity and cyclic opening/closing) play an important role in initiation and propagation. The microscopic level is also where the phenomenon of healing is thought to occur. Healing is described as either a reduction in crack length and retardation in the rate of propagation, or when used with fatigue concepts, crack closure. Under loading, cracks open; however, when plasticity is present, a plastic zone containing residual tensile stresses is formed ahead of the crack tip. During successive loading cycles, the plastic zone is deformed, causing compressive stresses to be exerted on the crack tip and closing it. This effectively retards the crack growth rate and can extend the life of the pavement.

The macroscopic level of HMA evaluation considers the HMA to be an inhomogeneous material that is described with uniform properties. In this case, cracks are assumed to propagate through the mixture without consideration for the constituent material (i.e. cracking may occur through individual aggregates, rather than though the binder aggregate interface). The effects of the individual constituent material properties are considered negligible when compared to the properties of the mixture as a whole. Analysis of the rate of crack growth is performed using fracture concepts and considering the HMA as a uniform material, rather than including the constituent properties of the binder and aggregate.

Many pavement researchers consider crack initiation to be best described at the local level, leading to use of plasticity analysis for crack initiation, while propagation is often described at the global level, and uses fracture mechanics in analysis. Laboratory testing of fatigue properties, such as the third point flexural beam test, use global methods of analysis for the determination of fatigue properties.

Other aspects of HMA behavior that must be accounted for in the analysis of fatigue include temperature and loading effects. As a viscoelastic material, asphalt mixtures are temperature sensitive in their response to applied loads. At high temperatures, HMA behaves as a viscous liquid; at low temperatures, it behaves as an elastic solid. Because of this, loads have greater effect at high temperatures. Additionally, the duration of loading itself affects response. Since fatigue is caused by an accumulation of strains, the ability of asphalt mixtures to recover strains upon unloading complicates the task of evaluating fatigue. Over time, the residual stress in pavements will dissipate since there are generally sufficient rest periods between loads. Fatigue specimens in the laboratory will also undergo this effect; however, as typically there are not sufficient rest periods between load applications for total recovery, the residual stresses will accumulate. This causes the fatigue life of laboratory specimens to be considerably shorter than the life expected in the field. The effects of temperature and rest periods have been addressed in fatigue evaluation previously by the introduction of shift factors (Balbissi, 1983; Tseng and Lytton, 1990); however, the accuracy of such factors depends on the availability of field data for calibration and verification.

The fatigue life of an asphalt mixture is generally characterized by performing fatigue tests, wherein a sample is repeatedly loaded, either in a strain- or stress-controlled mode until a predefined failure occurs, at which point the sample is determined to have reached the end of service life.

2.2.1 Effect of Material Properties on Fatigue

Several researchers have evaluated material effects on fatigue. Maupin (1972) performed controlled-strain beam fatigue testing on several mixtures and observed that oxidative aging reduced specimen fatigue life by approximately one tenth. Additionally, it was shown that binder stiffness had great influence on the mixture stiffness, and thus affected fatigue significantly.

Adedimila and Kennedy (1976) used indirect tensile fatigue testing to evaluate the effects of asphalt content, aggregate type, test temperature, and mixture air voids on the fatigue life. It was found that the optimum asphalt content for fatigue was less than that for density. Aggregate type and mixture air void content were not found to significantly affect fatigue life. Fatigue life was found to increase with decreasing test temperature.

Bell et al. (1984) evaluated the effects of various mixture properties on fatigue life using the indirect tensile mode and found that percent compact (or void content) was the most significant factor affecting fatigue performance.

Kim et al. (1992) evaluated the effects of mixture variables on diametral fatigue results and determined that asphalt type, aggregate type, and test temperature had significant effects on fatigue life. Improved life was demonstrated by mixtures having aggregate with a rough surface texture; this was postulated to occur due to improved interface bonding between the aggregate and binder. Other effects, such as air void content, asphalt content, and interactions between aggregate type and other factors were found to have no significant effect on fatigue life.

Harvey and Monismith (1993) evaluated the effects of binder type, aggregate type, fines content, air void content, compaction method, mixing viscosity, and compaction viscosity on the fatigue life of mixtures using the third point loading flexural beam test. It was found that mixture stiffness was sensitive to binder type, air void content, mixing viscosity, and compaction method. The fatigue life was found to be sensitive to binder type, fines content, air void content, mixing and compaction viscosities, and compaction method.

SHRP Project A-003 (SHRP, 1994) included the development of a standardized testing method for laboratory evaluation of fatigue. The resulting test method utilized the third point loading flexural beam fatigue test. During the test method development, experimentation was performed to evaluate the effects of asphalt content and air void content on the fatigue life of a single asphalt-aggregate mixture. It was found that the asphalt content and air void content had significant effects on initial flexural stiffness, fatigue life, and cumulative dissipated energy. Increasing the asphalt content resulted in decreased mixture stiffness, and increases in fatigue life and cumulative dissipated energy. Increasing the air voids resulted in decreases in mixture stiffness, fatigue life, and cumulative dissipated energy.

Deacon et al. (1995a) evaluated fatigue properties using the third point loading flexural beam fatigue test and concluded that aggregate structure, as induced by mixture compaction, has a significant effect on mixture fatigue properties.

Harvey and Tsai (1996) evaluated fatigue performance of several mixtures and determined that lower air voids are of clear benefit to fatigue life and initial stiffness. The study also found that increased asphalt content increased fatigue life and reduced mixture stiffness.

The effects of mixture segregation on fatigue life were evaluated by Khedaywi and White (1996) and it was found that fatigue life significantly decreased with increasing segregation.

2.3 FATIGUE TESTING

The characterization of fatigue life has been a well-recognized concern in pavement design for many years, since at least 1948 (Hveem and Carmany, 1948). Laboratory evaluation of fatigue generally focuses on direct applications of loads. There are several common methods of fatigue testing, including simple flexure, supported flexure, direct axial, and diametral (Matthews et al., 1993), as shown in Figure 2.1.

Simple flexure tests are the most common and include methods whereby loads are applied repeatedly or sinusoidally to rectangular beams with center point (Khalid, 2000a) or third-point loading (Deacon et al., 1994, 1995a, 1995b; Harvey and Monismith, 1993; Harvey et

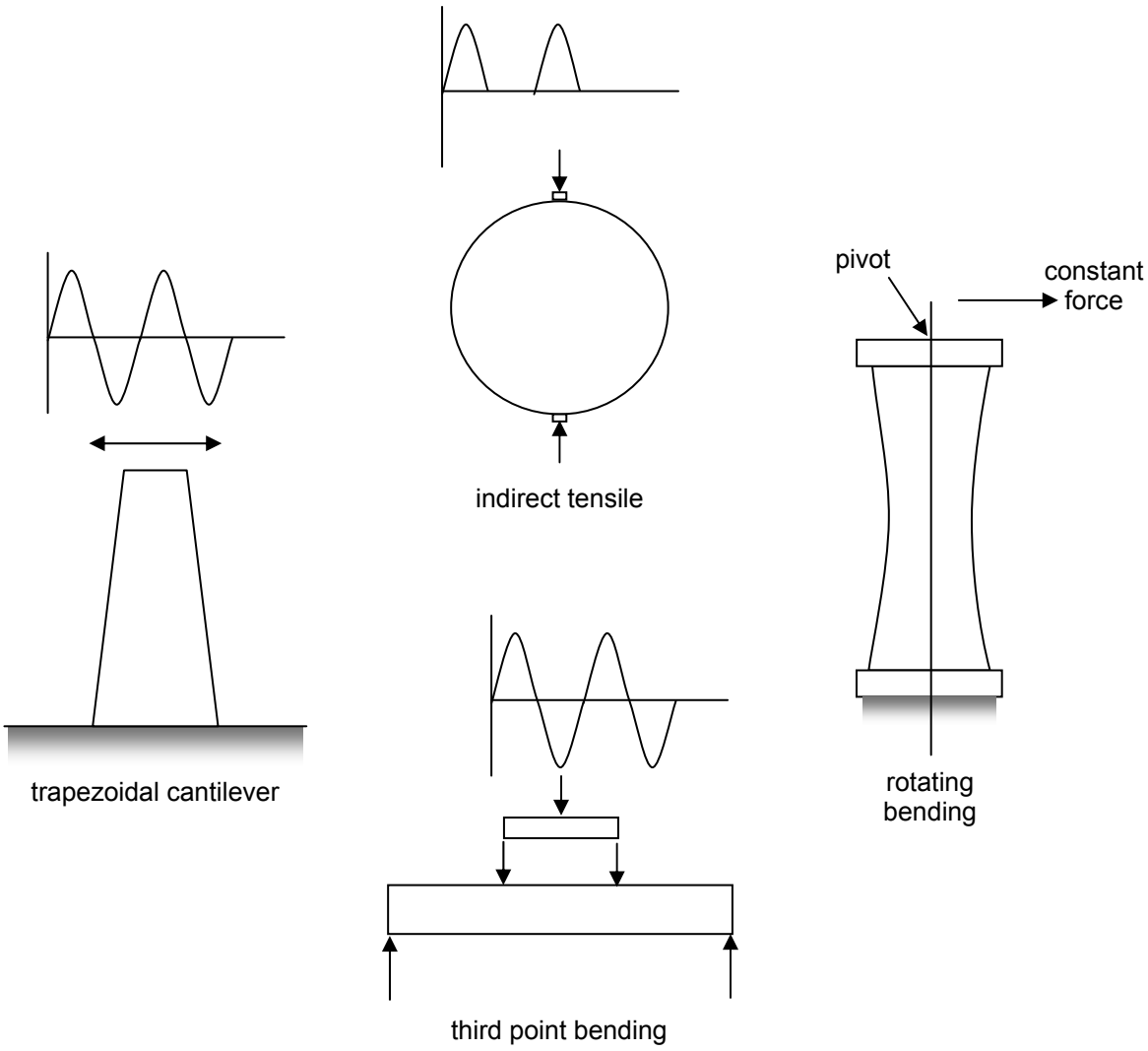

Figure 2.1 Examples of various fatigue testing modes.

al., 1994; Harvey and Tsai, 1996; Khalid, 2000b; Khedaywi and White, 1996; Maupin, 1972, 1977; Radziszewski, 1997; Read and Brown, 1996; Read and Collop, 1997; Sousa et al., 1998; Tayebali et al., 1992, 1994, 1996). Loads may also be applied sinusoidally to rotating cantilever beams (Pell and Cooper; 1975) or sinusoidally totrapezoidal beams (Francken and Verstraeten, 1974), although these modes are less common than the methods employing rectangular beams. Supported flexure tests apply loading to a beam supported on an elastic base; this better reflects actual field conditions but requires special equipment so is less generally performed (Matthews et al., 1993; Ramsamooj, 1980, 1991). Direct axial tests are performed by applying loads in the axial direction, similarly to the uniaxial methods discussed previously for creep compliance (Brennan et al., 1996; Von Quintus et al., 1982). Diametral testing is performed in the indirect tensile mode by applying a haversine loading pulse. This method of fatigue testing is commonly used as well (Adedimila and Kennedy, 1976; Baladi et al., 1988; Bell et al., 1984; Khalid, 2000b; Kim et al., 1992; Leahy et al., 1995; Von Quintus et al., 1982) and is considered an effective means of characterizing fundamental material properties.

Fatigue testing may be performed under two loading conditions: controlled-stress or controlled-strain. These are important as fatigue characteristics are generally expressed as relationships between the initial stress or strain and the number of load repetitions to failure. The determination of controlled-stress or –strain is important as it relates to the in-situ pavement structure. Controlled stress testing is associated with evaluation of thick asphalt layers (greater than approximately 150mm) except when the asphalt is extremely weak or the support exceedingly stiff, and controlled strain testing is associated with thin asphalt layers (less than approximately 50mm) unless the asphalt is extremely stiff or the support very weak (Monismith and Deacon, 1969). In reality, pavements experience an intermediate form of loading somewhere between constant stress and constant strain; because of this, Monismith and Deacon (1969) proposed a mode factor to take the loading mode effect into account:

$$MF = \frac{|A| - |B|}{|A| + |B|} \tag{2.1}$$

where

MF = mode factor,
A = percentage change in stress due to a stiffness decrement of C percent,
B = percentage change in strain due to a stiffness decrement of C percent, and
C = an arbitrary but fixed reduction in stiffness resulting from the accumulation of fatigue damage under repetitive loading.

The mode factor is assumed to be -1 for controlled stress testing, +1 for controlled strain testing, and -1<MF<+1 for intermediate modes of loading. The mode factor allows for estimates of the controlled strain curve from the controlled stress relationship (Monismith et al., 1977).

An energy based parameter (Ψ) was proposed by Van Djik (1975) to account for the mode of loading. The energy ratio Ψ is introduced as the ratio between the calculated dissipated energy, based on initial values of stress, strain, and phase angle, and the actual total dissipated energy. For controlled-stress testing $\Psi \leq 1$ and for controlled strain testing $\Psi \geq 1$.

It has been reported that fatigue lives under controlled-strain conditions are approximately 2.4 times greater than those under controlled-stress conditions (Tayebali et al., 1994). However, it has also been found that the ranking of mixtures, in terms of fatigue performance, is not affected by the mode of loading (SHRP, 1994). This determination from fatigue testing through the SHRP A-003 program has resulted in specifications for a third-point bending fatigue test in the controlled-strain mode (Deacon et al., 1995a, 1995b; Matthews and Monismith, 1993; Matthews et al., 1993; SHRP, 1994; Tayebali et al., 1992, 1996).

2.3.1 Methods of Analysis

Several methods have been introduced for the analysis of fatigue response. The primary methods include traditional phenomenological approaches relating applied stress or strain and number of applied cycles to failure, development of constitutive continuum models related to materials properties, fracture mechanics-based analysis, and analysis of energy and dissipated energy. Several other researchers have developed prediction or analysis methods that utilize other relationships or approaches.

Phenomenological Approach

Results of fatigue testing are generally interpreted in terms of a relationship between applied stress or strain and fatigue life. For the strain approach, such as recommended by SHRP, this results in a relationship of the following form, introduced by Pell (1967):

$$N_f = k_1\left(\frac{1}{\varepsilon_t}\right)^{k_2} \tag{2.2}$$

where

N_f = fatigue life,
k_1 and k_2 = mix-dependent constants (Irwin and Gallaway, 1974;Matthews and Monismith, 1993; van Dijk and Visser, 1977), and
ε_t = initial tensile strain.

Adedimila and Kennedy (1976) determined that the relationship between initial strain and fatigue life was as follows for several unmodified mixtures:

$$N_f = 9.38\times10^{-8}\left(\frac{1}{\varepsilon_t}\right)^{2.76} \tag{2.3}$$

In addition, they determined that fatigue life could be related to a stress-strength ratio, defined as the ratio of the applied repeated stress to the estimated indirect tensile strength. This relationship is similar in form to that relating fatigue life and strain and is given as:

$$N_f = 1.97\times10^{7}\left(\frac{1}{SSR}\right)^{3.18} \tag{2.4}$$

where SSR is the stress-strength ratio.

Maupin (1977) developed sets of equations for fatigue life prediction from beam fatigue testing under controlled-stress and –strain conditions. For stress-controlled testing failure was defined as specimen collapse; the prediction relationships are described as:

$$N_f = k_1\left(\frac{1}{\sigma}\right)^{n_1} \tag{2.5}$$

$$k_1 = e^{n_1\cdot\ln(12.6\cdot\sigma_{IT}-558)} \tag{2.6}$$

$$n_1 = 11.6 - 0.000396\cdot E_{IT} \tag{2.7}$$

where

N_f = number of cycles to failure,
k_1 and n_1 = constants dependent on mixture properties,
σ_{IT} = indirect tensile strength, and
E_{IT} = indirect tensile stiffness.

For strain-controlled testing, failure was defined as being when the initial stiffness was reduced by one-third; the prediction relationships are described as:

$$N_f = k_2 \left(\frac{1}{\varepsilon_t} \right)^{n_2} \tag{2.8}$$

$$\log k_2 = 7.92 - 0.122 \sigma_{IT} \tag{2.9}$$

$$n_2 = 0.0374 \sigma_{IT} - 0.744 \tag{2.10}$$

where k_2 and n_2 are constants that are dependent on mixture properties. These equations were used to formulate a mixture design procedure: a mixture having known field fatigue performance was tested to determine indirect tensile strength and stiffness, and the fatigue relations shown in equation 2.5 and 2.8 were plotted; the potential mixture under question was designed and tested for indirect tensile strength and stiffness; and fatigue life of this mixture was calculated and compared to the known performance to determine suitability of the proposed mixture.

The Asphalt Institute method of mix design (Asphalt Institute, 1981) utilizes the following:

$$N_f = 18.4 C \left[4.325 \times 10^{-3} \cdot (\varepsilon_t)^{-3.291} \cdot (S_{mix})^{-0.854} \right] \tag{2.11}$$

$$C = 10^{4.84\left(\frac{V_B}{V_V + V_B} - 0.69 \right)} \tag{2.12}$$

where

ε_t = tensile strain,
S_{mix} = mixture stiffness for a particular time and loading temperature,
V_V = volume of air voids, and
V_B = volumetric asphalt content.

Rauhut and Kennedy (1982) offered modifications of the values of k_1 and k_2 found in equation 2.2 to account for differences in temperature. The relation given for determination of K_0 is as follows:

$$\log \left[\frac{k_1(T_1)}{k_1(T_2)} \right] = 0.00058 (T_1 - T_2) \tag{2.13}$$

where

k_1 = regression constant seen in equation 2.2, and
T_1 and T_2 = temperatures of interest, wherein $k_1(T_1)$ is normalized by $k_1(T_2)$.

The value of k_2 is determined from that of k_1 as follows:

$$k_2(T) = 1.75 - 0.252 \log k_1(T) \tag{2.14}$$

Monismith et al. (1985) determined that stiffer mixtures generally have shorter fatigue lives in laboratory controlled-strain tests. Thus, an additional parameter was introduced into the general fatigue life equation to account for variations the material:

$$N_f = k_1 \left(\frac{1}{\varepsilon_t} \right)^{k_2} \left(\frac{1}{S_0} \right)^{k_3} \tag{2.15}$$

where S_0 is the mixture initial stiffness and k_1, k_2, and k_3 are regression constants. However, Harvey and Tsai (1996) offer experimental results that indicate that stiffness should not be

included in models used for evaluation of fatigue life, as conflicting results were found as to the effect of stiffness on fatigue life.

Medani and Molenaar (2000) present a method using repeated load indirect tensile tests to estimate fatigue life by determining the values of the constants k_1 and k_2 in equation 2.2. Repeated load indirect tensile tests are performed to evaluate the relationship between the mixture stiffness and loading time and a master curve is determined to define the following relationship:

$$\log S_m = f(\log t) \tag{2.16}$$

where

S_m = mixture stiffness modulus at the temperature of interest, and
t = loading time.

The n-value is then determined from the master curve as:

$$n_{mas} = \frac{2}{m} = \frac{2}{\frac{d(\log S_m)}{d(\log t)}} \tag{2.17}$$

where

n_{mas} = n-value from the mastercurve, and
m = slope of stiffness master curve.

The estimated, corrected k_2 value for use in equation 2.2 is determined as:

$$n_{est} = \frac{n_{mas}}{CF} \tag{2.18}$$

$$CF = 0.541 + 0.173\, n_{mas} - 0.0352\, V_a \tag{2.19}$$

where

n_{est} = k_2 value used in Wöhler equation (equation 2.2),
CF = correction factor, and
V_a = volume percentage of voids.

The value of k_1 for use in equation 2.2 is determined as:

$$\log k_1 = 6.589 - 3.762\, n_{est} + \frac{3209}{S_m} + 2.332 \log V_b + 0.149 \frac{V_b}{V_a} + 0.928\, PI - 0.721\, T_{R\&B} \tag{2.20}$$

where

K_0 = parameter used in Wöhler equation (equation 2.2),
V_b = volume percentage of binder,
PI = penetration index, and
$T_{R\&B}$ = ring and ball temperature (ºC) of binder.

This procedure is promoted as a feasible alternative to the performance of time-consuming fatigue tests. The procedures were developed using both unmodified and modified binders.

Although widely used, the phenomenological approach is essentially an empirical approach and does not provide a relationship between loading and any form of damage accumulation in the mixture. The approach also cannot be directly applied to complex loading scenarios, such as those commonly seen in the field. Additionally, the strain fatigue life

relationship is treated linearly, which has been found to be inappropriate at low strains (Carpenter et al, 2003). As a result, more fundamental approaches, such as continuum damage mechanics, fracture mechanics, and dissipated energy approaches, that seek to more thoroughly capture the complex responses involved in fatigue have been applied.

Continuum Approach

An alternative approach to fatigue analysis is the use of a constitutive model calibrated to material properties of the HMA, and fitted to fatigue test data. This results in a predictive relationship for similar HMA materials. This continuum approach is so-called because it utilizes principles of continuum mechanics to assign the HMA response under fatigue loading to three mechanisms (Kim et al., 1998): linear viscoelasticity, fatigue damage, and microdamage healing. The time dependent effects of linear viscoelasticity are classified using the correspondence principle, which utilizes a data transformation to remove the expected linear viscoelastic behavior from the total measured response to yield "pseudo strain". This principle was first introduced by Schapery (1984) and assumes that all deviations from linear viscoelastic behavior represent some form of damage.

As the constitutive model is continuum-based, the damage is considered very general and is not distinguished as specifically fracture or evolving in other forms such as plastic deformation. This allows all damage to be assigned to one variable, denoted by an internal state function. The general form of the constitutive relationship is as follows (Little et al., 2001):

$$\sigma = \sigma\left(\varepsilon^R, S_m\right) \tag{2.21}$$

where

σ = stress,
ε^R = pseudo strain, and
S_m = internal state variable of damage.

The general constitutive model accounts for the response of the viscoelastic body and damage by a function "C" expressed as:

$$\sigma = C\left(S_m\right)\varepsilon^R \tag{2.22}$$

where $C(S_m)$ is the internal function of damage.

Since the relaxation modulus, E^R, is assumed to be constant in linear viscoelasticity, the damage function above correlates damage with a change in the material stiffness. The changes in stiffness are categorized into three functions in the following relationship:

$$\sigma = I\left(\varepsilon^R\right)\left[F + G + H\right] \tag{2.23}$$

where

I = initial pseudo stiffness,
F = damage function fit to the change in the slope (pseudo stiffness) of each transformed hysteresis loop of stress versus pseudo strain,
G = hysteresis function delineating loading versus unloading paths, and
H = healing function representing the change in pseudo stiffness due to rest periods.

The G function may be omitted when the equation is applied to predictive analysis, such as determining the life of the specimen. The damage function, F, is an adjustment of the pseudo stiffness to account for the loading mode and rate of stiffness loss:

$$F = \left\{ \frac{\varepsilon^R{}_m}{\varepsilon^R{}_m - \varepsilon^R{}_s} \right\} C_1(S_{1n}) \tag{2.24}$$

$$C_1(S_{1n}) = C_{10} - C_{11}(S_{1n})^{C_{12}} \tag{2.25}$$

where

$\varepsilon^R{}_m$ = peak pseudo strain in each cycle,

$\varepsilon^R{}_s$ = shift in pseudo strain due to accumulated permanent deformation in the stress-controlled mode,

S_{1n} = normalized pseudo stiffness factor, and

C_{10}, C_{11}, C_{12} = coefficients of regression.

The healing function, H, expresses three types of behavior observed by Kim et al. (1998) during model calibration: immediate recovery, more rapid loss of pseudo stiffness upon commencement of cyclic loading, and settling out of the effect defined when the curve becomes more stable and assumes the characteristic exponential decline of stiffness during fatigue testing. The healing function is expressed as:

$$H = \sum_{j=1}^{i} \left(S^R_{B,j} - S^R_{C,j} \right) \quad \text{when} \quad S^R < S^R_{B,i} \tag{2.26}$$

$$C_2(S_2) = C_{20} + C_{21}(S_2)^{C_{22}} \tag{2.27}$$

$$C_3(S_3) = C_{30} + C_{31}(S_3)^{C_{32}} \tag{2.28}$$

where

$S_{B,i}{}^R = S^R$ (pseudo stiffness) before the i^{th} rest period,

$S_{C,i}{}^R = S^R$ without rest period at the point where S^R is equal to $S_B{}^R$ for the case with a rest period,

C_2 (S_2) = function representing the increase of S^R during rest periods due to microdamage healing, and

C_3 (S_3) = function representing the reduction in S^R after rest periods due to damage evolution.

The failure criterion for this method is an adjustment of the traditional approach, as:

$$C_1 + H \le 0.5 \tag{2.29}$$

where C_1 is equivalent to the effect of fatigue damage in reducing pseudo stiffness. This approach judges the sample to be failed when the pseudo stiffness falls below half of its original value, and is compatible with the traditional assumption of failure at 50% reduction of measured stiffness.

Due to the complicated nature of the constitutive model, Lee et al. (2000) developed a continuum model that assumes generic "damage" while still addressing realistic loading conditions and healing effects. The model incorporates three important aspects: a pseudo strain

energy density function, a stress-strain relationship, and a damage evolution law. The total fatigue life (including healing) as:

$$N_{f,total} = N_{f,w/oRP} + \sum_{i=1}^{M} \Delta N_{f,i} \tag{2.30}$$

where

M = number of rest periods.

The fatigue life without rest periods is determined as follows:

$$N_{f,w/oRP} = \frac{f(S_{1f})^{p_1}}{p_1(0.125 I C_{11} C_{12})^{\alpha_1}} |E^*|^{-2\alpha_1} \varepsilon_0^{-2\alpha_1}$$
$$p_1 = 1 + (1 - C_{12})\alpha_1 \tag{2.31}$$

where

$N_{f,w/o\,RP}$ = number of load cycles to failure without rest periods,
f = loading frequency,
S_{1f} = value of damage parameter S_1 at failure,
I = initial pseudo stiffness,
C_{11} and C_{12} = regression coefficients,
|E*| = dynamic modulus, and
α_1 = material constant.

The healing effects due to rest periods are considered by the following:

$$\Delta N_{f,i} = \frac{f(S_{3e})^{p_3}}{p_3\left[0.125 I (C_2 + S_B^R) C_{31} C_{32}\right]^{\alpha_3}} |E^*|^{-2\alpha_3} \varepsilon_0^{-2\alpha_3}$$
$$p_3 = 1 + (1 - C_{32})\alpha_3 \tag{2.32}$$

where

$\Delta N_{f,i}$ = increase in number of load cycles to failure due to the i^{th} rest period,
S_{3e} = value of damage parameter S_3 immediately before the rest period,
C_2 = recovery of pseudostiffness during the rest period,
S_B^R = pseudostiffness immediately before the rest period,
C_{31} and C_{32} = regression coefficients, and
α_3 = material constant.

Once the continuum model is constructed from test data, it may be used to evaluate the healing effects of rest periods of differing duration. The model has been successfully applied to asphalt mixtures tested under cyclic loading by Lee (1996) and Kim et al. (1997). The model presents good potential in predicting fatigue performance with realistic loading; however there are deficiencies. First, the creep compliance test is necessary to obtain model parameters rather than a fatigue test. Additionally, the model considers only microcracking and assumes continuous crack growth, which does not adequately describe actual crack propagation.

The difficulty with use of the continuum approach is the lack of relation between fundamental properties and the evolution of damage and recovery. Pseudo stiffness is the only measurable property directly incorporated into the model. Additionally, the predictive model requires calibration that relies on observed failure states, undermining the assessment of damage across the boundaries of test and sample conditions.

Fracture Mechanics Approach

Fracture mechanics is also utilized to analyze fatigue from the mechanistic standpoint. In this mechanistic approach, fatigue is considered a continuous damage process, and damage accumulation is assumed to follow a crack propagation law.
The fracture mechanics approach uses three stages to characterize fatigue cracking: crack initiation, stable crack propagation, and unstable crack fracture. The crack opening and length (or plastic zone) are necessary to obtain stress intensity factors at the crack tip used to determine fatigue life during the crack propagation stage (Majidzadeh et al, 1971; Monismith and Salam, 1973).

A model based on Paris' law is commonly used to describe crack propagation, which consumes most of the fatigue life (Majidzadeh et al, 1971):

$$\frac{dc}{dN} = A K_I^{\,n} \tag{2.33}$$

where

dc/dN = rate of crack propagation,
A and n = material constants, and
K_I = Mode I stress intensity factor.

The stress intensity factor is dependent on the specimen configuration, boundary conditions, temperature (for viscoelastic materials) and load effects. The stress intensity factor is normally evaluated from fracture toughness tests and can be calculated from the following for Mode I loading cases:

$$\sigma_y = \frac{K}{\sqrt{2\pi r}}\cos\frac{\theta}{2}\left(1+\sin\frac{\theta}{2}\sin\frac{3\theta}{2}\right)$$

$$\sigma_x = \frac{K}{\sqrt{2\pi r}}\cos\frac{\theta}{2}\left(1-\sin\frac{\theta}{2}\sin\frac{3\theta}{2}\right)$$

$$\tau_{xy} = \frac{K}{\sqrt{2\pi r}}\left(\sin\frac{\theta}{2}\cos\frac{\theta}{2}\cos\frac{3\theta}{2}\right) \tag{2.34}$$

It has been observed (Witczak, 1976) for thick pavement systems or specimens tested at low temperatures that fracture is governed by the critical stress intensity factor, K_c, and thus the critical crack size c_f is a fraction of the pavement or specimen thickness. This implies that pavements or specimens tested at high temperatures are not governed in fracture by K_c; this is explained as the value of c_f under such conditions being greater than the thickness of the pavement or specimen. In this case, failure as defined by the mechanistic approach does not occur.

Using the following relationship, fatigue life can be predicted if the initial and critical crack lengths are known (Majidzadeh et al., 1971):

$$N_f = \int_{c_0}^{c_f} \frac{dc}{A K_c^n} \tag{2.35}$$

where c_0 is the initial crack length and c_f is the critical crack length. An average value of 0.635 mm was determined for c_0 for an asphalt mixture having a nominal maximum aggregate size of 9.5 mm.

Ramsamooj (1980) evaluated fatigue prediction for asphalt beams supported on an elastic solid and used the theory to predict fatigue life for full-depth asphalt pavements with reasonable agreement. The crack propagation law for beams supported on elastic foundation is given as:

$$\frac{dc}{dN} = \frac{\pi}{24 K_{Ic}^2 \sigma_y^2}\left[(\Delta K_I)^4 - K_0^4\right] \tag{2.36}$$

where

K_{Ic} = critical value of plane strain stress intensity factor,
σ_y = yield stress in tension,
ΔK_I = increment in stress intensity factor, and
K_0 = value of stress intensity factor at endurance limit.

This is verified to also be equivalent to the rate of crack growth per cycle in the opening mode. Integration for the fatigue life, assuming that $K_0 \sim 0$, gives:

$$N_f = \frac{\pi}{24 K_{Ic}^2 \sigma_y^2} \int_{c_0}^{c_f} \frac{1}{(\Delta K_I)^4} dc \tag{2.37}$$

where

c_0 = initial crack length, and
c_f = crack length at failure.

Experimental results showed reasonably good agreement with theoretical results, with order-of-magnitude agreement being observed between the predicted life and design life of tested specimens.

Liang and Zhou (1997) offer a prediction model based on fracture mechanics which utilizes a two-stage plastic zone model. The model is presented as:

$$N_f = \frac{(1-\alpha)^2}{\delta_c} \int_{a_0}^{a_f} \frac{1}{\left[\left(\frac{K_I}{K_c}\right)^2 - \alpha\right]} da$$

$$\frac{K_I}{\sigma\sqrt{H}} = f\left(\frac{a}{H}\right)$$

$$f\left(\frac{a}{H}\right) = 6.898\left(\frac{a}{H}\right) - 17.425\left(\frac{a}{H}\right)^2 + 22.438\left(\frac{a}{H}\right)^3 \tag{2.38}$$

where

α = strength reduction factor per cycle of loading / unloading,
δ_c = critical single stage process zone length at failure,
a_f = critical value of fatigue crack,
a_0 = initial value of fatigue crack,

K_I = stress intensity factor for three point bending beam, and
K_c = critical value of stress intensity factor.

This model was found to predict a much faster crack growth rate when compared to Paris' law. Additionally, the model is reported to show more sensitivity of crack growth rate to the ratio of the initial stress intensity factor to its critical value (K_0 / K_c), and predicts fatigue lives that are slightly conservative as compared to fatigue data points.

Other work on the crack growth phenomenon in asphalt mixtures (Jacobs et al., 1996) indicates that macro cracks in asphalt mixtures grow discontinuously, and that the discontinuity increases with increasing aggregate size; in addition, it was determined that the fracture process consists of three parallel occurring processes: cohesive crack growth through the binder, adhesive crack growth separating the aggregate from the binder, and crack retarding caused by changes in the crack direction due to aggregate or air voids.

Fracture mechanics is also used to address the healing phenomenon. Schapery (1984) derived a fundamental fracture mechanics law describing the fundamental relation of cohesive fracture mechanics from the first principles of fracture:

$$2\Gamma_f = E_R D_f(t_d) J_v \tag{2.39}$$

where

Γ_f = surface energy density of a crack surface, FL^{-1},
E_R = reference modulus, FL^{-1},
$D_f(t_d)$ = tensile creep compliance of the material corresponding to the time, t_d, required for a crack to move through a distance the length of the fracture process zone ahead of the crack tip, and
J_v = viscoelastic J-integral, defined as the change of dissipated pseudo-strain energy per unit of crack area from one tensile load cycle to the next.

The law is based on energy balance. Energy released by the right hand side of the equation is taken up by the newly created crack surface on the left hand side of the equation. Following this law, Schapery (1989) then developed a healing model for linear, isotropic viscoelastic material that assumed interfacial forces of attraction and external or applied loading:

$$\dot{h}_2 = \left[\frac{2\gamma_m E_R^2 D_{1c} \Gamma_h}{(1-\nu^2) c_m^{1/m_c} H_v} \right]^{1/m_c} \beta \tag{2.40}$$

where

$\dot{h}_2$ = long term healing rate,
γ_m, c_m = fitting constants,
E_R = references modulus derived from the stress transformation,
D_{1c} = compressive creep compliance constant (D_0 is assumed to be zero),
Γ_h = wetting surface energy,
ν = Poisson's ratio,
m_c = creep compliance slope,
H_v = healing integral, and
β = size of the crack healing zone.

Schapery's healing equation indicates a direct relationship between surface energy density and the rate of microfracture healing. Additionally, this form of the equation assumes that the D_0 component of the power law model of creep compliance is zero. Otherwise, the healing rate equation would take on a significantly more complex form (Little et al., 2001)

Lytton et al. (1998) used Schapery's fundamental fracture equation to postulate a direct parallel cohesive healing process as the reversal of fracture:

$$\dot{h}_1 = \left[\frac{k_{th} D_{1c} E_R H_v}{2\Gamma_h}\right]^{1/m_c} \beta \tag{2.41}$$

where k_{th} is a fitting constant. This is an inverse of the relationship between healing rate and surface energy Γ_h and the healing integral H_v. This results in a relationship where surface energy is seen as an inhibitor to the healing process. The surface energy is considered the energy density required to close a given area of surface crack, thus the lower the surface energy density, the greater the healing that can proceed under equivalent conditions. This interpretation views surface energy acting as an impedance toward closure or reformation of the cracked surface rather than acting as an attractive force between the asphalt surfaces on either side of a crack face.

The two models (equations 2.40 and 2.41) were studied by Little et al. (2001) and it was observed that Schapery's healing rate is more related to long-term healing, while Lytton's healing rate is more descriptive of short-term healing, although in practice the two rates occur simultaneously. Because the actual healing is governed by both short-term and long-term healing rates, a unified model of fracture healing was developed:

$$\dot{h} = \dot{h}_2 + \frac{\dot{h}_1 - \dot{h}_2}{1 + \frac{\dot{h}_1 - \dot{h}_2}{h_\beta}(\Delta t)_h} \tag{2.42}$$

where

$\dot{h}$ = actual healing rate,

$\dot{h}_1, \dot{h}_2$ = short-term and long-term healing rates, respectively,

h_β = factor varying between 0 and 1 representing the maximum degree of healing that can be achieved by the asphalt binder, and

$(\Delta t)_h$ = rest period between load applications.

This combined model assumes that the total healing rate is the result of the external energy contribution which is converted into the formation of the "closed surface." The rate at which this happens is the sum of the two effects explained by Schapery and Lytton. Schapery's theory explains the contributions expected from polar interactions across the fracture surface and within the resulting mixture by polar forces and acid-base interactions, while Lytton's theory explains the resistance offered by the Lifshitz-Van der Waals component. However, despite these components, the model must still be considered empirical as the h_β parameter is empirically dependent on the ratio of surface energies (the polar divided by the non-polar component) and the asphalt mixture compliance (Little et al., 2001).

Although fracture mechanics approaches show promise in dealing with fatigue and healing, there are deficiencies. The testing associated with these approaches is generally too extensive for routine mix design and analysis and large data sets are required to determine the crack initiation process and crack growth rate. Also, the fracture mechanics models require the assumption of inherent cracks or flaws, so do not describe crack initiation, and only address the stage II stable crack propagation.

Dissipated Energy Approach

Another method of evaluating fatigue in viscoelastic materials utilizes the concept of dissipated energy. The energy input into a material during external loading is determined as the area under the stress-strain curve. For non-pure-elastic materials, the loading and unloading process is associated with energy dissipation since the loading and unloading paths do not overlap, a phenomenon called hysteresis. The dissipated energy for one loading-unloading cycle can be defined as the area inside of the stress-strain hysteresis loop. Fatigue damage is related to this energy that is dissipated in the specimen during testing.

One drawback to the apparent straightforwardness of this approach is the presence of viscoelastic damping. Viscoelastic materials can both store and dissipate mechanical energy. During loading, energy may be dissipated as thermal energy through the damping process and thus reduce the material's fatigue damage. As this energy is not then available for fatigue crack propagation, it should not be considered as part of the dissipated energy used to determine fatigue failure.

In general, the dissipated energy approach is considered appropriate for asphalt mixtures, as the dissipated energy can be used to explain the decrease in mechanical properties, such as flexural stiffness, during testing. The dissipated energy per unit volume per cycle is determined as:

$$w_i = \pi \sigma_i \varepsilon_i \sin \phi_i \tag{2.43}$$

where

w_i = dissipated energy at load cycle i,
σ_i = stress amplitude at load cycle i,
ε_i = strain amplitude at load cycle i, and
ϕ_i = phase angle between stress and strain wave signals.

Over the previous decades, many interpretations and applications of dissipated energy concepts have been proposed.

Initial Dissipated Energy

The initial dissipated energy is that measured at a defined number of initial loading cycles. Typically, the first 50 cycles are regarded as conditioning cycles and the dissipated energy at the 50^{th} loading cycle is determined to be the initial dissipated energy.

Rowe (1993) noted that initial dissipated energy can be a good indicator of fatigue performance for similar mix types. Ghuzlan (2001) found initial dissipated energy to be one of the most important factors affecting HMA fatigue behavior. A model was introduced in the

SHRP-A-404 study (SHRP, 1994) to relate initial dissipated energy to fatigue life based on 44 different mixes:

$$N_f = 2.365e^{0.069\,VFB}\left(w_0\right)^{-1.882} \tag{2.44}$$

where

N_f = number of cycles to failure,
VFB = percentage of voids filled with asphalt, and
w_0 = initial dissipated energy per cycle, psi.

A disadvantage of the initial dissipated energy approach is that it is not appropriate for the whole range of loading. Shen and Carpenter (2005) found that good correlations no longer exist when dealing with low strain fatigue tests. In addition, this approach has no means of accounting for the effects of healing.

Cumulative Dissipated Energy Approach

The total, or cumulative dissipated energy can be determined for a fatigue test as:

$$W_f = \sum_{i=1}^{n} w_i \tag{2.45}$$

where W_f is the cumulative dissipated energy at failure. The cumulative dissipated energy may be related to fatigue life as follows (Van Dijk, 1975):

$$W_f = A\left(N_f\right)^z \tag{2.46}$$

where

N_f = number of cycles to failure, and
A and z = experimentally determined coefficients.

The relationship is not affected by loading mode, effects of frequency (between 10 Hz and 50 Hz), temperature (between 10º and 40ºC), or the occurrence of rest periods. However, it has been found to be highly dependent on the mixture formulation (Tayebali et al., 1992; Van Dijk, 1975; Van Dijk and Visser, 1977).

Pronk and Hopman (1991) proposed that the dissipated energy per cycle is responsible for fatigue damage. An equation was developed using the total dissipated energy combined with Wöhler's curve to determine a fatigue equation:

$$N_t' = \frac{N_0}{3}\left(\frac{3}{\beta}\right)^{\frac{b}{2}} \tag{2.47}$$

where

N_t' = predicted fatigue life for the composed strain-signal,
N_0 = fatigue life according to the Wöhler curve for the maximum strain amplitude,
β = dissipated energy ratio, and
b = Wöhler curve coefficient.

Tayebali et al. (1992) introduced the stiffness ratio, defined as the ratio of the stiffness at load cycle i to the initial stiffness, and the dissipated energy ratio, defined as the ratio of cumulative dissipated energy up to load cycle i to the cumulative dissipated energy up to the

fatigue life. The study suggested that a unique relationship exists between the stiffness ratio and energy ratio that is independent of mixture type. A relationship between cumulative dissipated energy and the fatigue life was also seen, but was not unique and was dependent on the mode of loading and temperature. This was further verified by the SHRP-A-404 study (SHRP, 1994).

Radzisewski (1997) performed flexural fatigue testing on mixtures made with unmodified and modified binders as well as rubber modified mixtures and determined fatigue equations using the dissipated energy approach and having the linear form:

$$\log N_f = a_1 + b_1 \cdot \log \varepsilon_0 \tag{2.48}$$

where

a_1 and b_1 = regression coefficients, and

ε_0 = initial strain.

The dissipated energy was calculated as:

$$\log W_f = a_2 + b_2 \cdot \log \varepsilon_0 \tag{2.49}$$

where a_2 and b_2 are regression coefficients. The regression models reported for the mixture fatigue data are as follows:

(a) conventional binder

$$N_f = 0.055 \cdot W_f^{0.60} \tag{2.50}$$

(b) SBS-modified binder

$$N_f = 0.041 \cdot W_f^{0.67} \tag{2.51}$$

(c) EVA-modified binder

$$N_f = 0.012 \cdot W_f^{0.78} \tag{2.52}$$

(d) fine-grained and coarse-grained rubber-modified mixtures

$$N_f = 0.031 \cdot W_f^{0.71} \tag{2.53}$$

A universal fatigue prediction model found using results from all mixtures is expressed as:

$$N_f = 3.20 \times 10^4 \cdot W_f^{1.09} \cdot \varepsilon^{1.43} \tag{2.54}$$

Correlation coefficient analysis indicated that the fatigue life, tensile strain, and cumulative dissipated energy to failure are all highly interrelated.

Work Ratio Approach

The work ratio approach was first introduced by Van Dijk and Visser (1977) wherein a parameter Ψ is introduced as the ratio between the calculated total dissipated energy and the real total dissipated energy per volume:

$$\Psi = \frac{W_0}{W_f} \tag{2.55}$$

$$W_0 = \pi N_f \sigma_0 \varepsilon_0 \sin \phi_0 \tag{2.56}$$

where

Ψ = the energy ratio factor,

W_0 = calculated total dissipated energy based on initial values for stress, strain, and phase angle,

W_f = total dissipated energy per volume,

σ_0 = initial stress,
ε_0 = initial strain, and
ϕ_0 = initial phase angle.
The energy ratio was found to be less than or equal to one in controlled-stress tests and equal to or greater than one in controlled strain tests.

Rowe (1993) carried out controlled stress and strain testing in sinusoidal loading using trapezoidal specimens and determined as model to predict fatigue life to crack initiation as a function of initial dissipated energy:

$$N_i = 205 \cdot V_b^{6.44} \cdot W_0^{-2.01} \cdot \Psi_i^{1.64} \tag{2.57}$$

where
V_b = volume of binder,
W_0 = initial dissipated energy, and
Ψ_i = energy ratio at the number of cycles at crack initiation.
This energy ratio is defined as:

$$\Psi_i = \frac{N_i \cdot W_0}{W_i} \tag{2.58}$$

where W_i is the cumulative dissipated energy at crack initiation N_i. An alternative calculation method to cumulative dissipated energy was reported by Matthews et al. (1993), from data gathered by Van Dijk (1975) wherein the energy ratio, Ψ, is calculated as:

$$\Psi = \frac{W_i}{W_{total/cycle}} = \frac{\pi \cdot \sigma_0 \cdot \varepsilon_0 \cdot \sin\phi_0}{A\, N^{z-1}} \tag{2.59}$$

where A and z = material constants.
The fatigue life is solved for as follows:

$$N = \left[\frac{\pi \cdot S_0 \cdot \sin\phi_0}{A \cdot \Psi}\right]^{\frac{1}{z-1} \cdot \varepsilon_0 \left(\frac{2}{z-1}\right)} \tag{2.60}$$

where S_0 is initial stiffness modulus. The permissible strain for a given number of load applications is described as:

$$\varepsilon_p = \left[\frac{A \cdot \Psi}{\pi \cdot S_0 \cdot \sin\phi_0}\right]^{\frac{1}{2}} \cdot N^{\frac{z-1}{2}} \tag{2.61}$$

The energy ratio can be applied to the prediction of crack initiation. Pronk (1997) found that if the ratio of dissipated energy up to a number of cycles, N_i, to dissipated energy at that N_i is plotted versus N_i, microcrack initiation can be determined as the point where a sharp change in the slope of the line is observed.

Ratio of Dissipated Energy Change

Another alternative approach using the dissipated energy concept is the ratio of dissipated energy change. This approach initially considered the dissipated energy ratio (DER) as a parameter to evaluate fatigue life. The DER approach postulates that not all dissipated energy is responsible for material damage; the energy due to material mechanical work and other environmental influence remains nearly constant. Thus the development of damage can be

assessed by the change in dissipated energy. This approach has been examined and refined by Ghuzlan and Carpenter (2000), Ghuzlan (2001), and Carpenter et al. (2003). Carpenter et al. (2003) found that the relationship between DER and fatigue life is fundamental as it is independent of load level, mode of loading, and mixture type.

Shen and Carpenter (2005) and Shen (2006) rename the DER approach as the ratio of dissipated energy change (RDEC) approach to better describe its use of the ratio of the change in dissipated energy between loading cycles to represent damage generation.

$$RDEC = \frac{\left(DE_{n+1} - DE_n\right)}{DE_n} \tag{2.62}$$

where

RDEC = ratio of dissipated energy change,
DE_{n+1} = dissipated energy produced in load cycle n+1, and
DE_1 = dissipated energy produced in load cycle n.

The RDEC approach is considered a fundamental approach and has shown validity for different testing methods such as flexural beam fatigue testing (Ghuzlan and Carpenter, 2000; Ghuzlan, 2001; Carpenter et al., 2003; Shen and Carpenter, 2005; Shen, 2006) and uniaxial tension testing (Daniel et al., 2004) as well as for various materials such as asphalt mixtures and Portland cement concrete materials (Daniel and Bisirri, 2005).

Plotting the curve represented by the RDEC versus the loading cycles produces a characteristic damage curve (Ghuzlan, 2001), as shown in Figure 2.2. This curve can be divided into three distinct stages, of which the plateau stage indicates a period during which a constant portion of energy is being turned into damage (Carpenter et al., 2003). This plateau value is proposed as a fundamental damage parameter uniquely related to failure despite mixture type, test mode, and other testing conditions (Shen and Carpenter, 2005). Further work by Shen (2006) developed a relationship between the RDEC and plateau value and the predicted fatigue endurance limit and also investigated the use of the RDEC and plateau value to evaluate the role of healing on fatigue life.

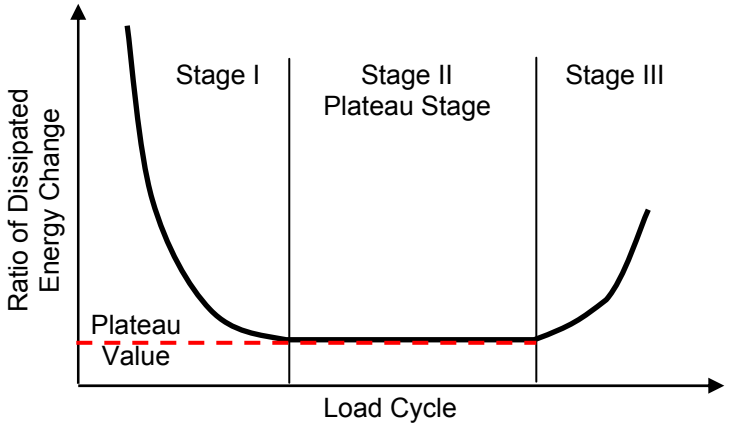

Figure 2.2 Characteristic plot of ratio of dissipated energy change.

Shen and Carpenter (2007) proposed an equation to determine the plateau value for mixtures without extensive testing:

$$PV = 44.422\,\varepsilon^{5.140}\,S^{2.993}\,VP^{1.850}\,GP^{-0.4063}$$

$$VP = \frac{AV}{AV + V_b}$$

$$V_b = 100 \times \frac{G_{mb}\,P_b}{G_b}$$

$$GP = \frac{P_{NMAS} - P_{PCS}}{P_{200}} \qquad (2.63)$$

where

PV = plateau value,

ε = tensile strain, in/in,

S = flexural stiffness of the mixture from the laboratory fatigue test, MPa,

VP = volumetric parameter,

GP = gradation parameter,

AV = mixture air voids, %,

V_b = mixture asphalt content by volume, %,

G_{mb} = mixture bulk specific gravity,

P_b = mixture asphalt content by total weight of mix, %,

G_b = asphalt binder specific gravity (generally assumed 1.03),

P_{NMAS} = aggregate percent passing the nominal maximum sieve size,

P_{PCS} = aggregate percentage passing the primary control sieve (PCS = NMAS × 0.22), and

P_{200} = aggregate percentage passing the No. 200 (0.075mm) sieve.

Other Approaches

Several other prediction methods have been developed by various researchers. Francken and Verstraeten (1974) offered a prediction methodology for the modulus and fatigue life of mixtures based on stress-controlled sinusoidal bending tests. The value of the modulus was found to depend only on mixture composition and is given as:

$$E_\infty = 1.436 \times 10^{10}\ R^{0.55}\ e^{-5.84 \times 10^{-2} \cdot v}$$

$$R = \frac{V_a}{V_L} \qquad (2.64)$$

where

E_∞ = purely elastic modulus characterizing the mixture at very low temperatures or very high frequencies or both,

R = ratio between aggregate percentage volume and binder percentage volume,

v = void content,

V_a = aggregate percentage volume, and

V_L = binder percentage volume.

The fatigue law was given as:

$$\varepsilon_r(N) = \overline{\Lambda}\, G\left(\frac{V_L}{V_L + v}\right)\left(\frac{N}{10^6}\right)^{-0.21} \tag{2.65}$$

where

$\varepsilon_r(N)$ = initial strain,

$\overline{\Lambda}$ = coefficient dependent on the asphaltene content of the binder,

G = empirical factor equal to unity when: aggregate volume is between 78 and 85%; binder content is such that aggregates are fully coated without having excessive amounts; aggregates contain at least 50% coarse aggregate; and

$0.5 \times 10^{-4} \le \varepsilon_r (N=10^6) \le 1.3 \times 10^{-4}$, and

N = number of cycles to failure.

Bonnaure et al. (1980) developed a nomograph for prediction of the mixture stiffness modulus, and thus fatigue life, based on knowledge of the binder modulus and volumetric composition of the mixture. The nomograph was developed for constant strain and constant stress tests from the following, respectively:

$$\varepsilon = \left(4.102\,PI - 0.205 \cdot PI \cdot V_b + 1.094\,V_b - 2.707\right) S_m^{-0.36}\, N^{-0.2} \tag{2.66}$$

$$\varepsilon = \left(0.300\,PI - 0.015 \cdot PI \cdot V_b + 0.080\,V_b - 0.198\right) S_m^{-0.28}\, N^{-0.2} \tag{2.67}$$

where

ε = initial strain,

PI = penetration index of the binder,

V_b = volumetric binder content,

S_m = stiffness modulus of the mixture, and

N_f = number of cycles to failure.

Equations 2.66 and 2.67 can be solved for N to determine the fatigue life.

2.3.2 Fatigue Endurance Limit

The concept of an endurance limit for fatigue was first proposed by Wöhler for metallic materials. The fatigue endurance limit is considered to be the applied stress below which a material will not continue to accumulate fatigue damage leading to failure, thus providing essentially an infinite life. The classical stress versus cycles to fatigue curve assumes a hyperbolic shape having an asymptote parallel to the cycles to fatigue axis, implying that there is an applied load below which the material does not incur continuing damage in fatigue, as shown in Figure 2.3. This asymptote represents the fatigue endurance limit.

Although the concept of an endurance limit has been widely studied for metals and other materials, considerably less work has been done relative to HMA until recently due to interests in perpetual pavements. Monismith et al. (1961) observed during laboratory testing that when applied bending stresses were very low, around 100 microstrain, that HMA beams were able to endure large numbers (approximately 1million) load repetitions without failure. An endurance limit of 70 microstrain was later proposed by Monismith and McLean (1972) when it was observed that the log-log relationship between strain and applied cycles converged at approximately this value at approximately 5 million cycles. A similar convergence was noted by Maupin and Freeman (1976).

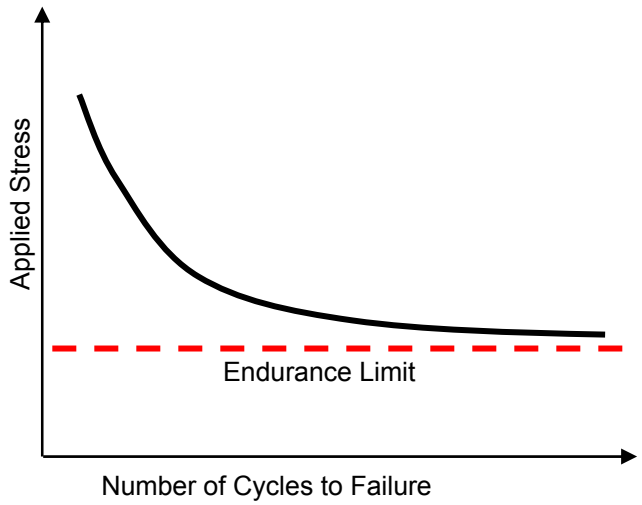

Figure 2.3 General concept of the fatigue endurance limit.

Shen and Carpenter (2005) propose that extrapolation to the endurance limit can be performed from testing performed to 500,000 repetitions using the ratio of dissipated energy change and plateau value. They found no statistical difference in plateau values predicted at failure (used to predict the endurance limit) extrapolated from testing performed to 500,000, 1 million, 3 million, and 5 million cycles. Prowell and Brown (2006) describe the required loading repetitions in the laboratory equivalent to the endurance limit to be 500 million, based on assumptions regarding maximum vehicle lane capacities, typical axle weights, and shift factors between laboratory and in-situ loading.

Shen and Carpenter (2007) manipulated the predictive equation for the plateau value (equation 2.63) which results in a predictive model for the strain level at the fatigue endurance limit that does not require extensive fatigue testing:

$$\varepsilon_L = 0.0123 S^{-0.5832} VP^{-0.3599} GP^{0.0790} \quad (2.68)$$

where ε_L is the strain based fatigue endurance limit. The model assumes that the plateau value at the endurance limit, PV_L, is equivalent to 6.74×10^{-9}.

2.3.3 Healing of Fatigue Damage

The concept of healing in HMA is important in the context of pavement design. Fatigue is recognized as one of the primary modes of pavement failure, and the fatigue life evolves as the result of the competing mechanisms of damage and healing. While measuring fatigue damage is relatively simple, the study of healing is much more complicated.

Pulsed loading was used by Deacon and Monismith (1967) to simulate the recovery of asphalt concrete pavement due to the viscoelastic nature of the material. Research performed by Bazin and Saunier (1967) showed clear evidence of healing, as they reported that ordinary dense graded HMA could recover 90 percent of its initial resistance to cracking after 3 days of rest at 77ºF. They also concluded that pressure on the crack faces had a great influence on healing. Unfortunately, the duration of rest periods investigated (1 to 100 days) was too long to realistically evaluate field conditions. Raithby and Sterling (1970) performed uniaxial tensile

cyclic tests on hot-rolled asphalt beam samples using pulsed loads with rest periods up to three times the load cycle duration. They observed that the strain recovery during the rest periods resulted in a fatigue life over five times longer than the fatigue life under simple loading. A new expression for the cumulative cycle damage ratio in Miner's law was developed by Francken (1979) by accounting for rest period effects. Bonnaure et al. (1982) investigated the effects of rest periods by means of a three point bending test and determined that higher test temperatures and softer binders increased the beneficial effect of rest periods.

Kim et al. (1990) suggest the presence of two main healing mechanisms in a partially cracked asphalt pavement: relaxation of stresses in the system due to the viscoelastic nature of HMA, and chemical healing across microcrack and macrocrack faces. Since both of these mechanisms occur simultaneously, a method was developed to quantify chemical healing by the separation of the viscoelastic relaxation using Schapery's correspondence principle of nonlinear viscoelastic media.

Little et al. (1999) show that surface energy is responsible for microcrack damage rate. When surface energy is less than dissipated energy, the healing potential is negative, and the material will tend to create more surface energy through the creation of more surfaces (i.e. crack initiation and propagation). However, if surface energy is greater than dissipated energy, the desire for equilibrium between the two will drive a decrease in surface energy, though the closing of crack surfaces by the healing process. Lytton (2000) explained the fracture and healing process using the dissipated pseudo strain concept and noted that the dominating mechanism (either surface energy storage or surface energy release) is related to the polar or non-polar characteristics of the asphalt binder.

In general, the literature emphasizes the importance of healing on the fatigue behavior of HMA. However, the true mechanisms and the contribution of these to the fatigue endurance limit are still unclear. Further evaluation is still needed to resolve these issues.

2.3.4 Third Point Loading Test

The third point beam fatigue test applies loading at points located at one-third distances from the beam ends, as shown in Figure 2.4. This produces uniform bending in the central third of the specimen and significantly simplifies analysis. The general equations for analysis of a simply supported beam are as follows (Khalid, 2000a):

$$\sigma_t = \frac{3PL}{2bd^2} \tag{2.69}$$

$$\varepsilon_t = \frac{3PL}{2Ebd^2} \tag{2.70}$$

$$\delta = \frac{PL^3}{48EI} \tag{2.71}$$

where

σ_t = tensile stress at the bottom of the beam,
ε_t = tensile strain,

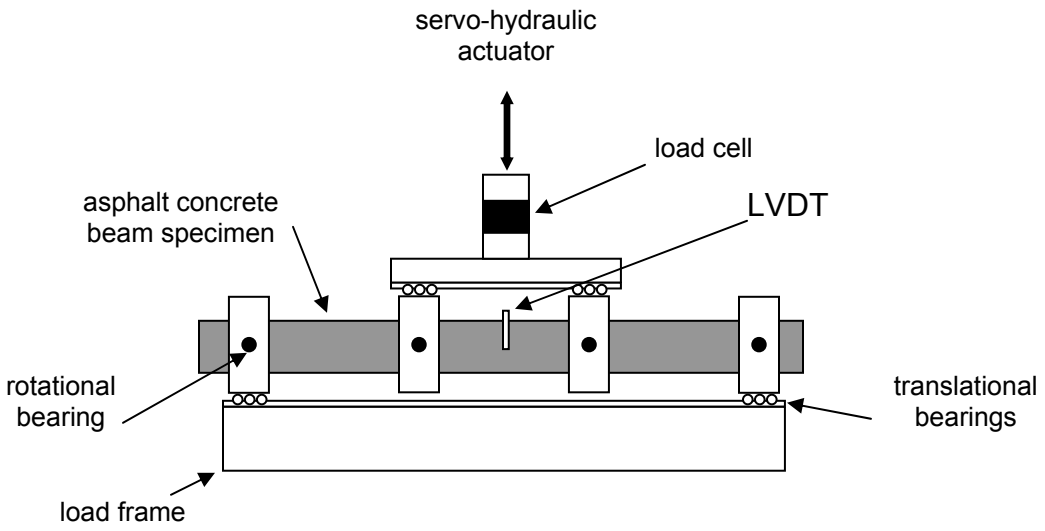

Figure 2.4 Third point loading mode fatigue test apparatus.

δ = vertical deflection,
P = applied load,
L = beam span,
b = beam width,
d = beam depth,
E = Young's modulus, and
I = section modulus, equivalent to ($bd^3/12$).

Hadley and Vahida (1983) performed finite element analysis and laboratory testing of beam fatigue samples to modify elastic equations for use with the third point beam fatigue test. The flexural stress, modulus, and tensile strain are expressed as follows (Hadley and Vahida, 1983):

$$\sigma_f = \frac{3 a P K_4}{K_1 b d^2} \tag{2.72}$$

$$E_f = a P K_2 \left(3l^2 - 4a^2\right) 48 l d K_3 \tag{2.73}$$

$$\varepsilon_f = \frac{\sigma_f}{E_f} \tag{2.74}$$

$$K_1 = 1.005 + 2.195(1+\nu)\left(\frac{d}{l}\right)^2$$

$$K_2 = 1.034 + 9.233(1+\nu)\left(\frac{d}{l}\right)^2 - 46.828(1+\nu)\left[\left(\frac{d}{l}\right) - 0.208\right]^2 - 0.389\nu$$

$$K_3 = \begin{cases} 1.00 \text{ if deflection measured at third point} \\ 0.835 + 0.115\left(\frac{d}{l}\right) \text{ if deflection measured at center point} \end{cases} \quad (2.75)$$

$$K_4 = \begin{cases} 1.00 \text{ if deflection measured at third point} \\ 0.981 + 0.375\left(\frac{d}{l}\right) \text{ if deflection measured at center point} \end{cases}$$

where

σ_f = flexural stress,
E_f = modulus,
ε_f = tensile strain,
a = distance from reaction to applied load,
P = total applied load,
b = beam width,
d = beam height, and
l = reaction span length.

SHRP offers a methodology for characterizing the fatigue response of a mixture within a short time period using the third-point loading test (SHRP, 1994). The procedure utilizes four specimens tested at four strain levels to determine the fatigue characteristics of the mixture. The strain levels are chosen such that the specimen life ranges from approximately 5000 to 500000 cycles. Testing is performed in the controlled-strain mode of loading at a frequency of 10Hz. Results from the four tests are utilized for fatigue characterization by calculating resulting stresses, strains, stiffness, and dissipated energy at each load cycle (AASHTO TP8-94, SHRP M-009).

The peak-to-peak stress is computed as:

$$\sigma_t = \frac{3\,a\,P}{w\,h^2} \quad (2.76)$$

where

σ_t = peak-to-peak maximum tensile stress, N,
a = L / 3, mm,
L = beam span, mm,
P = applied peak-to-peak load, N,
w = beam width, mm, and
h = beam height, mm.

Peak-to-peak strain is determined as:

$$\varepsilon_t = \frac{12\,h\,\delta}{3L^2 - 4a^2} \quad (2.77)$$

where

ε_t = peak-to-peak maximum tensile strain, mm/mm, and
δ = beam deflection at neutral axis, mm.

Stiffness is calculated as follows:

$$S = \frac{\sigma_t}{\varepsilon_t} \tag{2.78}$$

where S is the beam stiffness in Pa.

The phase angle is expressed as:

$$\phi = 360 \cdot f \cdot s \tag{2.79}$$

where

ϕ = phase angle, ^{o},
f = load frequency, Hz, and
s = time lag between P_{max} and δ_{max}, sec.

Dissipated energy per cycle is computed as:

$$D = \pi \sigma_t \varepsilon_t \sin \phi \tag{2.80}$$

where D is the dissipated energy per cycle, expressed in Pa. The cumulative dissipated energy was determined as by summing the dissipated energy per cycle over the life of the specimen.

The test is run until failure occurs; however, there is dispute concerning the definition of failure for the controlled strain test as it is very difficult to reach a physical failure via fracture. Currently, specifications (AASHTO TP8-94 and SHRP M-009) set the criteria for failure as occurring when there is a 50% reduction in the measured stiffness; initial stiffness is measured after 50 applied load cycles. Several researchers (Ghuzlan and Carpenter, 2000; Kim et al., 1997; Van Dijk, 1975; Van Dijk and Visser, 1977) have introduced alternative methods to this, each of which have been proposed to avoid the issues of mode-of-loading, temperature, loading frequency, and rest periods, which have been shown to influence fatigue life. However, none of these methods has been fully validated, nor proven to be uninfluenced by the aforementioned issues.

Ghuzlan and Carpenter (2000) propose to use the change in dissipated energy per cycle related to the total dissipated energy per cycle as a measure of failure. The change in dissipated energy, ΔDE, is calculated between cycles a and a+1 and divided by the total dissipated energy, DE, of load cycle a. This ratio (ΔDE/DE) is plotted versus the number of load cycles to characterize the mixture performance. It is reported that the curve will decrease during the first portion of loading, as larger portions of the dissipated energy are being converted to damage as the mixture reorients itself to the loading. Following this, the curve will remain constant, indicating stable fatigue damage resistance. Upon failure, the damage rate will increase rapidly. For this method, failure is defined as the number of loading cycles wherein the energy ratio begins to increase rapidly.

2.3.5 Applications in Pavement Design

It is well documented in the literature that laboratory fatigue responses are considerably more conservative than the actual response seen in pavements. This has been postulated to be due to differences in crack propagation, healing effects due to rest periods, use of simple loading patterns, temperature effects, and influences of surface cracking. Additional differences are due

to the use of different fatigue design criteria amongst researchers. This shift factors have been introduced to attempt to relate laboratory results with expectations for in-situ pavements. Many of these factors are simply general factors applied to the expected life and based on phenomenological fatigue studies, rather than mechanistic evaluation. These factors are reported by a number of researchers and range in value from approximately 0.95 to 20 (Majidzadeh et al., 1973; Monismith, 1981; Van Dijk, 1975), depending on the method of laboratory testing and the make-up of the applicable pavement.

Temperature Effects

One aspect of fatigue testing that has created many questions is that of temperature. It has been well-documented that changes in laboratory test temperature affect fatigue response; additionally, the relationships between laboratory test temperature and effective pavement temperature are necessary to predict pavement performance. Witczak reports the use of an "effective temperature concept" for use in fatigue analysis (Witczak, 1976). An effective design temperature, q_e, is defined as the unique pavement temperature at which the repetitions to failure determined using a cumulative damage law is equivalent to the repetitions to failure determined by evaluating the pavement at the same temperature (stiffness) for tensile strain. The evaluation for tensile strain, usually through multiplayer elastic theory, must utilize a value for the elastic modulus, E_1, that corresponds to the effective temperature. This value may be determined as:

$$E_1 = \frac{3.8 \times 10^6}{1.0046^{q_e^{1.45}}} \tag{2.81}$$

where

E_1 = HMA elastic modulus at the effective temperature, and
q_e = effective design temperature.

Additionally, temperature is found to affect the stiffness of HMA and thus the fatigue properties found in the lab. Pulse loads are utilized in the laboratory to better simulate loading experienced in the field; however, this loading results in curves that are temperature-dependent. These curves have been reported by various researchers and their results fall into one of two categories: parallel (apparently shifted) curve sets and intersecting curve sets. Summaries of studies having these characteristics is presented by Witczak (1976) and the observation is made that the studies resulting in parallel curve sets did not account for nonlinearity in the stress response when calculating the tensile strain in the mix. These studies were found to utilize a linear modulus in the determination of the calculated strains. Witczak (1976) reports that this phenomenon occurs because laboratory fatigue tests are performed utilizing large stress/strain levels such that failure occurs within a relatively short time, such that nonlinear stresses/strains are introduced, especially in the case of high temperatures. Following this, if linear methods are utilized to calculate response, the fatigue curve will have a lesser slope than that resulting from nonlinear analysis, and curves may appear to be parallel.

Effect of Rest Periods

Van Dijk et al. (1972) reported laboratory results demonstrating marked increases in fatigue life of specimens due to the effect of rest periods between load pulses. Shift factors are recommended by SHRP (Lytton et al., 1993) to relate three separate processes occurring in

HMA: healing, residual stresses, and resilient dilation. The healing shift factor is a function of the rest period, and extends the fatigue life. According to Lytton et al. (1993), the form of the equation for the healing shift factor is as follows:

$$SF_h = 1 + a(t_r)^b \tag{2.82}$$

where

SF_h = shift factor due to healing, commonly ranging between 1 and 10,
a, b = healing coefficient and exponent, respectively, and
t_r = rest period, sec.

An alternative form, presented by Little et al. (2001) from the same study is as follows:

$$SF_h = 1 + \left(\frac{n_n}{N_0}\right) a \left(\frac{t_r}{t_0}\right)^h \tag{2.83}$$

where

n_n = number of rest periods,
N_0 = number of cycles to fatigue failure,
t_0 = time between cyclic loads in the fatigue test,
t_r = rest period, and
a and h = coefficient and exponent related to the healing index measured by Kim (1988).

The healing index is expressed as (Kim, 1988):

$$HI = \left(\frac{\phi_{after} - \phi_{before}}{\phi_{before}}\right) = \frac{a\, t_r{}^h}{1 + a\, t_r{}^h} \tag{2.84}$$

where

HI = healing index,
ϕ_{before} = pseudo dissipated energy before the rest period, and
ϕ_{after} = pseudo dissipated energy after the rest period.

The relationship expressed above rises from 0 to 1 to the far right as the length of the rest period increases. The number will rise more quickly for mixtures that heal well.

Test Variability

A review of previous fatigue work indicates that there is great scatter or variability in fatigue results. Monismith et al. (1970) and Pell (1973) found that the distribution of fatigue life for HMA at particular stress levels could be represented by a normal distribution if a log transformation is used on the values of the fatigue life. With this, they confirmed the validity of the following relationship for the frequency distribution of fatigue life:

$$f(y) = \frac{1}{\sigma\sqrt{2\pi}} e^{\frac{-(y-m)^2}{2\sigma^2}} \tag{2.85}$$

where

f(y) = normal density of Y,
Y = transformed life (log N),
M = mean of Y, and
σ = variance of distribution of Y.

This distribution is applicable for each particular strain level.

2.4 SUMMARY

As can be seen from the previous discussion, the fatigue life of HMA has been studied using many different methodologies. It has been shown that the differences between in-situ and laboratory fatigue life can be attributed to several variables. The quantification of these has previously been performed on limited numbers of mixtures. If these can be determined for a wider variety of mixtures designed using the current Superpave practice it will be beneficial to pavement researchers as a means to improve the accuracy of laboratory fatigue life prediction.

3 EXPERIMENTAL METHODS

One of the most problematic deterioration modes in asphalt pavements in Virginia is fatigue. The occurrence of fatigue may be reduced by the proper design of highway pavements, which requires comprehensive knowledge of the material properties and performance. As HMA properties are significantly affected by specimen preparation, compaction, mixture inhomogeneity, and test method, a better understanding of the effects of these variables on response is needed. Testing for the evaluation of permanent deformation and fatigue properties was performed on surface mixtures used at the Virginia Smart Road in Blacksburg, Virginia. Fatigue testing was performed using a third-point beam fatigue testing method under controlled strain conditions on 50.8 mm x 63.5 mm x 381 mm rectangular beam specimens. Specimens were representative of surface mixtures from the Virginia Smart Road.

3.1 VIRGINIA SMART ROAD

Construction of the Virginia Smart Road began in 1997 to provide a direct connection between the town of Blacksburg, Virginia and Interstate 81. Through cooperation between Virginia Tech and the Virginia Department of Transportation (VDOT), the Virginia Smart Road also became a test facility incorporating various types of transportation related research, including a pavement test facility. The pavement test facility is approximately 2.5 km in length, of which 1.3 km is flexible pavement that is divided into 12 sections of approximately 100 m each. Each flexible pavement test section is comprised of a multi-layer pavement system and possesses a unique structural configuration. Each layer in each section is instrumented to measure quantitative pavement responses to traffic loading and environmental conditions using instruments such as pressure cells, strain gages, resistivity probes, thermocouples, and time domain reflectometry (TDR) probes. One underground bunker, containing a data acquisition system, collects data from all instrument types for every two pavement sections. During instrument installation, all the wires from each instrument in the two sections were brought to their respective bunker and were connected to the data acquisition system. Each of the six data acquisition systems is connected to the Virginia Smart Road control center where the data can be remotely retrieved and stored.

The Virginia Smart Road differs from other types of pavement testing (e.g., LTPP) in that the instruments were placed in the roadbed during the construction process and not "retrofitted" after construction. The 12 pavement structural configurations are designated as Sections A through L. Sections A through E are located in a fill area with approximately 1-3.5% longitudinal slope and Sections F through L are located in a cut area having a longitudinal slope of approximately 4-6%. The structural configurations of the 12 pavement sections are shown in Table 3.1.

Six surface mixtures are employed among the 12 test sections, as indicated in Table 3.2:

- Section A has SM-12.5D.
- Sections B, E through H, and J have SM-9.5D.
- Section C has SM-9.5E.
- Section D and I have SM-9.5A.

Table 3.1 Structural configuration of the Virginia Smart Road.

Material	Section / Thickness (mm)								
	A - D	E	F	G	H	I	J	K	L
OGFC[a] HMA Wearing Surface	-	-	-	-	-	-	-	19	-
HMA Wearing Surface	38	38	38	38	38	38	38	19	38
HMA Base	150	225	150	100	100	100	225	225	150
HMA Surface (placed as base)	-	-	-	50	50	50	-	-	-
Asphalt Stabilized OGDL[b]	75	-	-	-	75	75	75	-	-
Cement Stabilized OGDL	-	-	-	-	-	-	-	75	75
Cement Stabilized Aggregate Base	150	150	150	150	150	150	-	-	150
21B Aggregate Base	175	75	150	150	75	75	150	150	75

[a]OGFC = Open graded friction course.
[b]OGDL = Open graded drainage layer.

Table 3.2 HMA mixtures used at the Virginia Smart Road.

Section	Wearing Surface	Characteristics
A	SM-12.5D	12.5mm nominal maximum aggregate size PG 70-22 binder
B, E - H, J	SM-9.5D	9.5mm nominal maximum aggregate size PG 70-22 binder
C	SM-9.5E	9.5mm nominal maximum aggregate size PG 76-22 binder
D, I	SM-9.5A	9.5mm nominal maximum aggregate size PG 64-22 binder Section I designed with high lab compaction
K	OGFC	12.5mm nominal maximum aggregate size PG 76-22 binder
L	SM-12.5	12.5mm nominal maximum aggregate size PG 76-22 binder
Section	Base	Characteristics
all	BM-25.0	25.0mm nominal maximum aggregate size PG 64-22 binder

- Section K has an open-graded friction course (OGFC) surface.
- Section L has SMA-12.5.

The mixtures are designated by their use (surface mixture [SM]), nominal maximum aggregate size (12.5 mm and 9.5 mm), and performance graded binder (PG 64-22, 70-22, and 76-22 as A, D, and E, respectively). The OGFC mixture found on the surface of Section K is designed to promote drainage and increase tire friction but was not evaluated during this study. The HMA base mixture, designated BM-25.0 provides structural support to the pavement and serves as a base layer over which the surface mixtures are placed.

3.2 MIXTURE PREPARATION

Specimens for testing were prepared from all surface mixtures except the OGFC found in Section K. Specimens were given four designations, with the first term designating the production source and the second term designating the compaction location:

- *Field-field* specimens were cores taken from the Smart Road and are representative of in-situ as-placed material.
- *Field-lab* specimens were compacted in the laboratory from loose HMA gathered in the field at the time of construction of the Smart Road. These specimens were intended to be used to evaluate the differences between laboratory and field compaction.
- *Lab-lab* specimens were laboratory prepared and compacted specimens that were prepared to match the mixture properties of the field-lab mixture. These properties were determined through ignition testing for asphalt content and sieve analysis for aggregate gradation. Lab-lab specimens were intended to be used to evaluate the effects of batch-plant and laboratory production practices on mixture response.
- *Design-lab* specimens were laboratory prepared and compacted according to the original design batch sheets (job mix formulas) provided by the contractor to VDOT during construction of the Smart Road. These specimens were included to compare the performance of the designed mixture with that of the mixtures found in-place at the Smart Road.

Mixture designs and gradations for all specimens are presented in Appendices A and B.

Aggregate and binder were procured from the sources used during construction. Laboratory procedures for mixture preparation followed practices required by Superpave and VDOT. Mixtures were prepared in large batches to reduce variability attributable to batching and mixing. After mixing, HMA batches were placed in storage bags until compaction was performed; this was done so that compaction of specimens could be performed at different times. Bagged samples were stored at 25ºC. Short term aging as prescribed by Superpave was not performed before the HMA mixtures were bagged. Prior to compaction, bagged samples were short-term aged in accordance with Superpave requirements, heated to compaction temperatures, and compacted into test specimens.

Volumetric analysis was performed on all specimens after compaction. Specifications for compaction temperatures and for compaction and volumetric properties are presented in Table 3.3 and Table 3.4, respectively.

Table 3.3 VDOT specifications for mixing and compaction temperatures.

Mixture Designation	Mix Temperature	Compaction Temperature
A, Base	300-310ºF	285-290ºF
D	310-320	295-300

For mixtures using PG 76-22 or other modified binder, temperatures shall be based on documented supplier's recommendations.

Table 3.4 VDOT specifications for compaction and volumetric properties.

Mixture	VTM	VFA	VMA	F/A Ratio	N_{ini}	% density at N_{ini}	N_{design}
SM-9.5A	2.5 – 5.5	68 – 84	15	0.6 – 1.2	7	≤ 90.5	65
SM-9.5D	2.5 – 5.5	68 – 84	15	0.6 – 1.2	7	≤ 89	75
SM-9.5E	2.5 – 5.5	68 – 84	15	0.6 – 1.2	7	≤ 89	75
SM-12.5D	2.5 – 5.5	65 – 83	14	0.6 – 1.2	7	≤ 89	75
SMA-12.5	2.5 – 5.5	65 – 83	14	0.6 – 1.2	7	≤ 90.5	65

Beam specimens for fatigue testing were prepared as rectangular beams approximately 50.8 mm by 63.5 mm by 381 mm. The exceptions to this were the field-field beam specimens, which were approximately 35 to 45 mm in thickness, because of the thickness of the wearing surface at the Smart Road. A summary of fatigue testing specimens is presented in Table 3.5.

Compaction of the field-lab, lab-lab, and design-lab beam fatigue specimens were performed using a PTI asphalt vibratory compactor shown in Figure 3.1. After compaction, specimens were measured and weighed to determine their volumetric properties. Specimens were stored at 25ºC in a manner providing full support to prevent warping of the beams until testing. Fatigue specimen properties are presented in Appendix C. Specimens were stored at a temperature of 25ºC in a manner providing full support to prevent warping of the beams until testing was performed.

3.3 VOLUMETRIC ANALYSIS

Volumetric analysis is important in the characterization of HMA. Acceptable ranges for various component properties have been established by Superpave to produce mixtures that perform reliably as expected. The volumetric properties were determined for companion gyratory specimens:

- asphalt content (AASHTO T308-99)
- specific gravity of material components (G_{sb}, AASHTO T 166-00; G_{mm}, AASHTO T 209-99; $G_{sb,}$ AASHTO T84-00 and ASHTO T85-91;)
- bulk density

Table 3.5 Summary of fatigue specimens.

Mixture	Section	Field-Field	Field-Lab	Design-Lab	Lab-Lab
SM-9.5A	D	-	10	10	10
	I[a]	-	10	10	10
SM-9.5D	B	-	10	10	10
	E	-	10	-	-
	F	-	10	-	-
	G	-	10	-	-
	H	-	10	-	-
	E-H	-	-	-	10
	J	-	10	-	10
SM-9.5E	C	36	10	48	10
SM-12.5D	A	-	10	10	10
SM-12.5A	L	-	10	10	10

[a]Designed with high laboratory compaction.

Figure 3.1 PTI Vibratory compactor (photo by author).

- density at N_{ini}
- percent passing No. 200 sieve
- voids in total mix (VTM)
- voids in mineral aggregate (VMA)
- voids filled with asphalt (VFA)
- percent of maximum density at N_{ini}
- fines to asphalt (F/A) ratio.

A summary of volumetric properties for all mixtures is presented in Appendix B.

3.4 THIRD POINT BEAM FATIGUE TEST

Fatigue life testing was performed using the third-point mode of loading flexural test under controlled-strain conditions, as specified in the AASHTO TP8-94 protocol. This method of testing was chosen because of its ease of use and understanding and its adoption as a standard. In pavement analysis, generally, conditions of stress-control may be assumed to represent in-situ response as the surface course is considered to be integral with the base course, creating a thick-layer system. However, as this study sought to quantify properties of the surface mixtures individually, it was felt that following the recommended AASHTO test method was appropriate.

The third-point beam fatigue test applies loading at points located at one-third distances from the beam ends. This produces uniform bending in the central third of the specimen and significantly simplifies analysis. The test is run until failure occurs; however, there is dispute concerning the definition of failure for the controlled strain test, as it is very difficult to reach a physical failure via fracture. The AASHTO specification sets the criterion for failure as

occurring when there is a 50% reduction in the measured stiffness; initial stiffness is measured after 50 applied load cycles. Several researchers (Ghuzlan and Carpenter, 2000; Kim et al., 1997) have introduced alternative methods to this, each of which have been proposed to avoid the issues of mode-of-loading, temperature, loading frequency, and rest periods, which have been shown to influence fatigue life. However, none of these methods has been fully validated, nor proven to be uninfluenced by the aforementioned issues. For this work, the 50% reduction of initial stiffness was utilized as failure criteria in accordance with the AASHTO TP8-94 specification. "True failure" in fatigue has been shown to be correlated strongly with the 50% reduction of initial stiffness (Carpenter et al., 2003):

$$N_{true\ failure} = 21758 + 1.30727 \cdot N_{50\%\,K} \qquad R^2 = 0.91 \qquad (3.1)$$

where

$N_{true\ failure}$ = number of cycles to failure

$N_{50\%\,K}$ = number of cycles required to reduce the initial stiffness by 50%.

This method of failure definition was chosen to comply with specifications and to provide a standard method of test comparable to that performed by other researchers in the assumption that future comparisons may be made. In addition, although fatigue life response will be different depending on the mode of loading, the overall rankings of mixtures are not significantly changed because of the mode of loading (SHRP, 1994).

Fatigue testing was performed on the specimens previously shown in Table 3.5. Fatigue beams cut from the Smart Road (designated section C, mixture SM-9.5E, field-field) were evaluated by location and with respect to the direction of compaction; wheelpath and center-of-lane specimens reflect the effect of traffic compaction, whereas beams cut with the longitudinal length parallel with or perpendicular to traffic reflect the effect of construction compaction, as the roller compacts mixtures parallel with the roadway direction. In addition, evaluations of loading frequency and rest period effects were performed by evaluating specimens using three load frequencies and two rest period lengths, summarized in Table 3.6. These combinations were evaluated for only one surface mixture, SM-9.5E, located in section C, and one production condition, design-lab.

All fatigue tests were performed at 25ºC. The strain levels for the replicate sets of four specimens each were chosen such that the specimen life ranged from approximately 5,000 to 300,000 cycles, with the failure criterion being 50% reduction of the initial stiffness. Testing was performed in the controlled-strain mode of loading at a frequency of 10 Hz, with the exception of the testing designed to evaluate frequency and rest period changes. Results from each set of tests were used in calculating resulting stresses, strains, stiffness, and dissipated energy at each load cycle (according to AASHTO TP8-94), as discussed previously in Chapter 2. Additional analysis details will be discussed in Chapter 4.

Table 3.6 Summary of loading frequencies and rest periods to be tested.

Load Frequency	Rest Period
10 Hz	-
5 Hz	-
1 Hz	-
10 Hz	0.4 sec, 0.9 sec

4 FATIGUE RESPONSE

Fatigue is one of the major modes of failure found in pavements and occurs as accumulated strains from traffic loading exceed the strength of the component materials. In the laboratory, fatigue resistance is evaluated by the application of repeated stresses or strains to the HMA specimen until failure. A characteristic curve may be compiled from the results of several tests performed at differing applied stresses or strains, such that the fatigue life at any stress or strain may be predicted. These predictions are utilized in conjunction with pavement design methodologies to predict pavement performance and optimize design.

Controlled-strain laboratory fatigue testing was performed during this study and characteristic strain-life curves were determined for each mixture. Additionally, investigation of the complex stiffness response of each mixture was performed, and the storage and loss of energy during fatigue loading was considered. The measured responses to fatigue loading were evaluated to identify mixture characteristics having significant effects upon the fatigue service life of HMA and the fatigue strain endurance limits of the mixtures were investigated.

4.1 RESULTS OF FATIGUE TESTING

As discussed in Chapter 3, fatigue life testing was performed using the third-point mode of loading flexural test under controlled-strain conditions, following procedures specified in AASHTO TP8-94. Measured responses from the testing included applied deflections, load response, and time lag between the applied deformation and resulting load response. Applied strains, resulting stresses, phase angle, mixture stiffness, dissipated energy per cycle, and cumulative dissipated energy were calculated. An evaluation of the storage and loss of energy was performed.

4.1.1 Strain-Life Evaluation

Characteristic plots of fatigue life versus applied strain are presented for each mixture in Appendix D. These curves can be described using the form:

$$N_f = K_1 \varepsilon^{-K_2} \qquad (2.2)$$

where

N_f = fatigue life, cycles,
ε = applied strain, mm/mm, and
K_1 and K_2 = regression coefficients.

It is reported that K_1 and K_2 are dependent on mixture properties (Irwin and Gallaway, 1974; Van Dijk and Visser, 1977); however, analysis of the mixtures used in this study could not determine the validity of property-based relationships. This may be due to the limited range of values found for the mixture properties, as seen in Table 4.1. Table 4.2 summarizes the coefficients K_1 and K_2 for each Smart Road section and mixture. In this study, it was observed that a logarithmic relationship exists between the values of K_1 and K_2; this relationship is illustrated in Figure 4.1.

Table 4.1 Average statistics on volumetric values determined for all mixtures and specimens used in this study.

	Asphalt Content	% Passing #200 Sieve	G_{mm}	G_{mb}	VTM
Average	5.8	7.81	2.475	2.262	8.6
Std. Deviation	0.5	1.70	0.032	0.039	1.8
Max. Value	6.8	12.28	2.524	2.373	14.2
Min. Value	4.7	5.52	2.402	2.071	3.8
Range of Values	2.1	6.76	0.122	0.301	10.4

Figure 4.2 demonstrates the expected average fatigue life for the five mixture types evaluated at the Smart Road under various applied strains. The expected fatigue life was determined using the average mixture values for K_1 and K_2 shown in Table 4.2; it should be noted that these are average values and include the variation in performance due to the different sample preparation methods (i.e., field-field and field-lab). Figure 4.2 indicates that the SMA-12.5 mixture had the best expected fatigue life performance when compared to that of the other mixes. The benefits are present throughout the range of investigated applied loading strains. Better performance is also predicted for the SM-9.5E mixture at applied strains above approximately 300microstrain, indicating the potential benefits of the use of polymer modified binders (SM-9.5E utilizes a modified PG76-22 binder). Further discussion of mixture performance is presented in Section 4.2.

An alternative to the form expressed in equation 2.2, introduced by Monismith et al. (1985), that includes the mixture stiffness as a factor is:

$$N_f = K_0 \varepsilon^{-K_1} S_0^{-K_2} \tag{2.5}$$

where

S_0 = initial mixture stiffness, Pa, and
K_2 = regression coefficient.

It is thought that the quantities K_0, K_1, and K_2 are related to mixture properties; however, specific relations are not well supported in the literature. To examine this, a preliminary evaluation of the use of equation 2.5 was performed; however, for 23 of the 31 sets of fatigue beams used in this study, the initial mixture stiffness was found to be statistically insignificant in fitting the model. Thus, investigation of the potential relationships between K_0, K_1, ad K_2 and mixture properties was not performed. In addition, Harvey and Tsai (1996) offer experimental results indicating that stiffness should not be included in models used for fatigue life evaluation, as conflicting results were found as to the effect of stiffness on fatigue life.

Additional potential equations for the prediction of fatigue response were considered in this study:

$$N_f = K_0 \cdot \varepsilon^{K_1} \cdot CDE^{K_3} \tag{4.1}$$

$$N_f = K_0 \cdot \varepsilon^{K_1} \cdot S_0^{K_2} \cdot CDE^{K_3} \tag{4.2}$$

where

Table 4.2 K_1 and K_2 coefficients for fatigue characterization from equation (2.2).

Mixture	Section	Preparation Method	K_1	K_2	R^2
SM-9.5A	D	field-lab	1.1591×10^{17}	-4.1864	0.9816
		lab-lab	1.1929×10^{18}	-4.6674	0.9855
		design-lab	7.5088×10^{18}	-4.9437	0.9803
	I[a]	field-lab	5.1929×10^{20}	-5.5745	0.9895
		lab-lab	2.2741×10^{18}	-4.8336	0.9906
		design-lab	5.1567×10^{17}	-4.6670	0.9537
	Mixture Average Value		3.8435×10^{17}	-4.5091	0.8788
SM-9.5D	B	field-lab	7.4846×10^{15}	-3.8650	0.8393
		lab-lab	4.7460×10^{19}	-5.2555	0.9791
		design-lab	1.6466×10^{20}	-5.3580	0.9544
	E	field-lab	5.6342×10^{19}	-5.2267	0.9752
	F	field-lab	1.4247×10^{20}	-5.3073	0.9648
	G	field-lab	5.4076×10^{19}	-5.2077	0.9160
	H	field-lab	2.5000×10^{19}	-5.1073	0.9875
	E - H	lab-lab	5.4768×10^{19}	-5.1814	0.9760
	J	field-lab	7.4318×10^{18}	-5.0413	0.9598
		lab-lab	3.6831×10^{20}	-5.5657	0.9890
	Mixture Average Value		2.7933×10^{15}	-3.7885	0.7280
SM-9.5E	C	field-lab	3.4440×10^{24}	-6.5922	0.9282
		lab-lab	2.1103×10^{16}	-3.9916	0.9142
		design-lab	5.9337×10^{22}	-6.1179	0.9395
		design-lab (0.4sec rest period)	1.1099×10^{16}	-3.7988	0.9470
		design-lab (0.9sec rest period)	2.1508×10^{21}	-5.5201	0.9580
		field-field (all specimens)	2.7098×10^{17}	-4.4111	0.8291
		field-field (center of lane)	1.3194×10^{18}	-4.5846	0.8536
		field-field (outer wheelpath)	3.0676×10^{16}	-4.0459	0.8928
		field-field (inner wheelpath*)	1.6084×10^{22}	-6.1547	0.9478
		field-field (inner wheelpath**)	1.7161×10^{20}	-5.4374	0.9310
	Mixture Average Value		1.4113×10^{17}	-4.2681	0.7739
SM-12.5D	A	field-lab	1.0422×10^{21}	-5.6455	0.9476
		lab-lab	5.5532×10^{19}	-5.1962	0.9782
		design-lab	1.1000×10^{19}	-4.9849	0.9798
	Mixture Average Value		7.9046×10^{19}	-5.2648	0.9623
SMA-12.5	L	field-lab	1.5353×10^{24}	-6.5740	0.8699
		design-lab	5.4898×10^{14}	-3.3251	0.6920
	Mixture Average Value		3.1845×10^{17}	-4.2674	0.6923

* Beams cut with longitudinal axis perpendicular to direction of traffic

** Beams cut with longitudinal axis parallel to direction of traffic

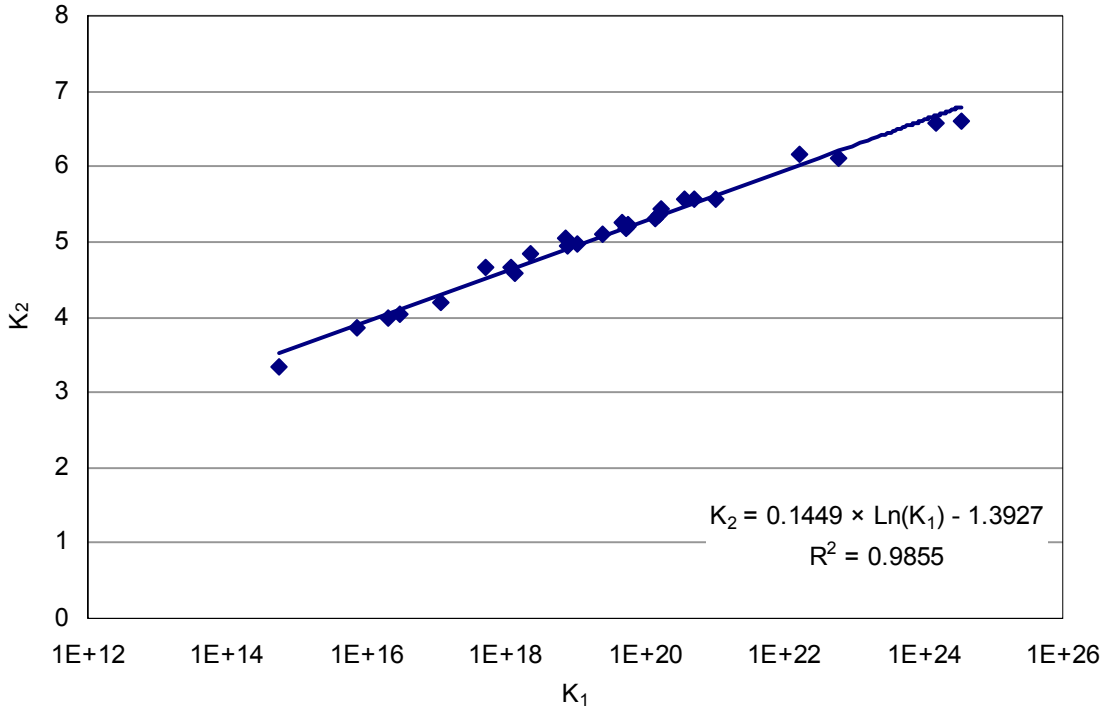

Figure 4.1 Relationship between K_1 and K_2 found in this study.

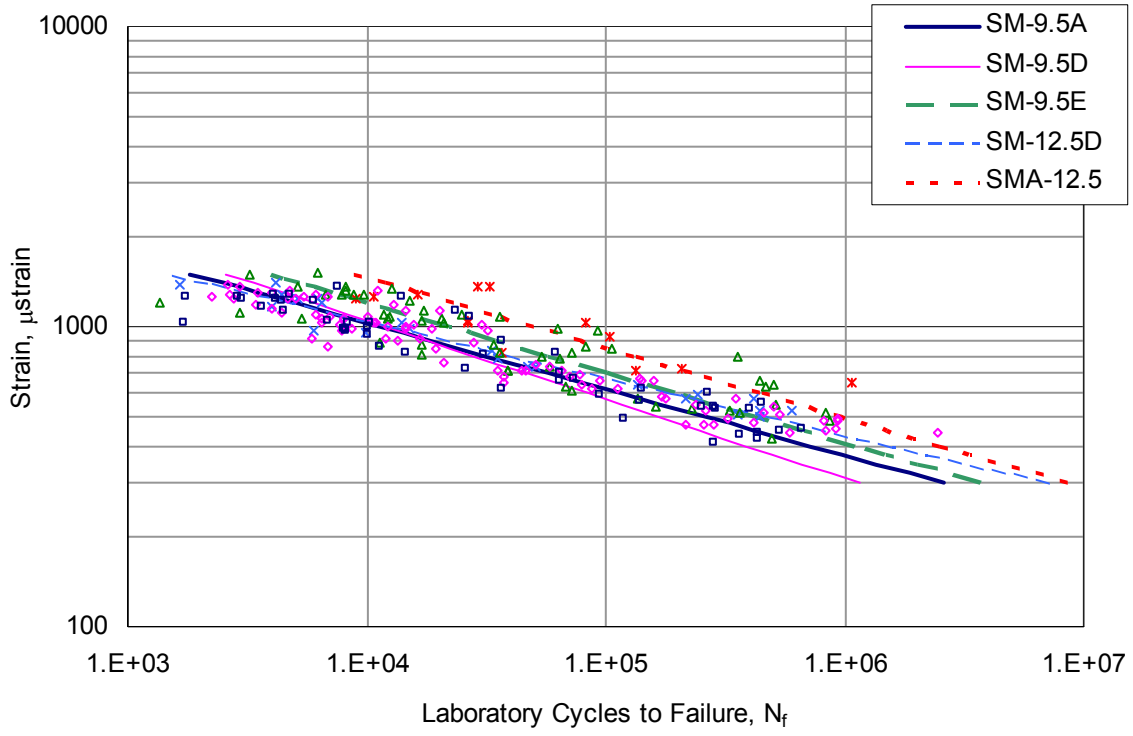

Figure 4.2 Expected mixture performance based on mixture average $K_1$and K_2 values from Table 4.2.

CDE = cumulative dissipated energy at failure, kN-mm/mm^3, and
K_3 = regression coefficient.
Details of the evaluation of these equations and their use in evaluating mixture performance will be discussed in Section 4.2.

4.1.2 Dissipated Energy Concepts

For viscoelastic materials, fatigue damage is related to the amount of energy dissipated in the specimen during testing. This relationship is suitable for asphalt mixtures as the dissipated energy can be used to explain the decrease in mechanical properties, such as flexural stiffness, during testing. An example hysteresis loop for a linear viscoelastic material under an oscillating load is shown in Figure 4.3; the elliptical shape is a characteristic of a linearly viscoelastic material. In nonlinear materials, the hysteresis loop may exhibit pointed ends.

The elliptical plot of the hysteresis loop encloses an area that represents energy per unit volume dissipated in the material per cycle. This dissipated energy can be calculated by integrating the stress-strain curve over one full cycle. The dissipated energy per unit volume per cycle was shown in Chapter 2 to be:

$$w_i = \pi \sigma_i \varepsilon_i \sin \phi_i \tag{2.43}$$

Stored energy cannot be calculated directly for a full cycle in the case shown in Figure 4.3; since the material returns to its starting configuration the net stored energy is zero. However, the stored energy can be evaluated over one-quarter of the cycle as follows:

$$W_s = \frac{1}{2} S' \varepsilon_0^2 \tag{4.3}$$

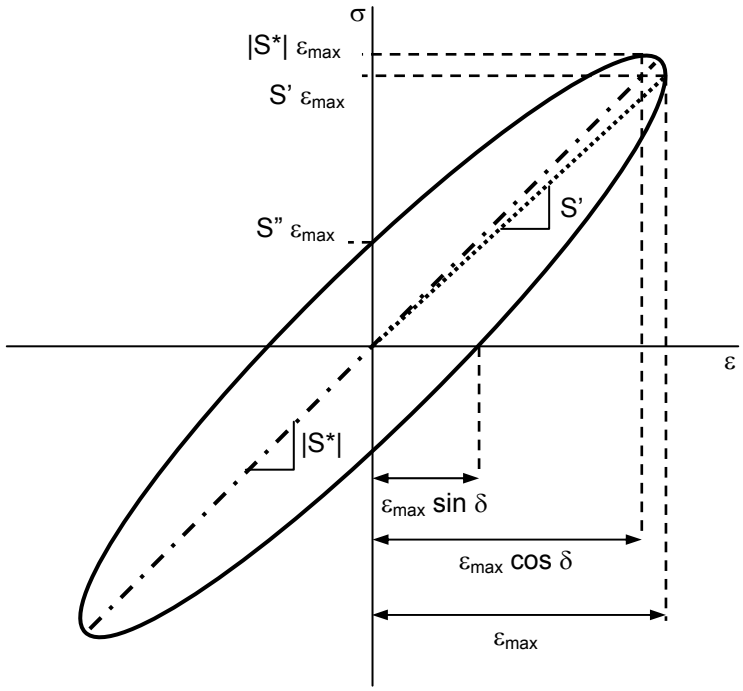

Figure 4.3 Hysteresis curve showing complex stiffness for purely elastic material.

where S' is the storage stiffness and ε_0^2 is the strain amplitude. Then, the dissipated energy over one-quarter cycle can be determined by taking one quarter of the integral of the stress-strain curve over a full cycle, so that:

$$W_d = \frac{\pi}{4} S'' \varepsilon_0^2 \tag{4.4}$$

where S" is the loss stiffness.

In addition, the accumulation of damage can be evaluated by considering the total energy dissipated during loading. Thus, the total, or cumulative, dissipated energy is then determined as:

$$W_{fat} = \sum_{i=1}^{n} w_i \tag{2.45}$$

The cumulative dissipated energy may be related to fatigue life as follows (Van Dijk, 1975):

$$W_{fat} = A \cdot \left(N_f\right)^z \tag{2.46}$$

Characteristic plots of cumulative dissipated energy versus fatigue life are presented in Appendix E for each mix. Table 4.3 summarizes the values of A and z for each mixture. Evaluation of these values indicates that there is a moderate relationship between A and z, as shown in Figure 4.4. Regression analysis to evaluate relationships between volumetric properties and the coefficients A and z showed no significant relationships; this is likely due to the limited range of volumetric quantities, as discussed previously and presented in Table 4.1.

An alternate evaluation using dissipated energy is to look at the change in energy dissipated from cycle to cycle (Ghuzlan, 2001). The ratio of dissipated energy per cycle (RDEC) changes depending on the damage state of the HMA and reaches a plateau value that is closely related to the fatigue life of the mixture. The plateau value can be determined by one of two methods: a manual method based on the results of testing or a calculation method using material properties.

Shen (2006) provides a description of determining the plateau value manually from test data as follows:

- Obtain the dissipated energy versus loading cycle (DE-LC) relationship:

$$DE = A \cdot LC^k \tag{4.5}$$

where A and k are regression constants. In Shen's analysis, the DE-LC curve was found to follow a power law relationship with low variability. However, the choice of number of cycles used to perform the regression may vary by operator, introducing additional variability, so a process was developed to determine the relationship. It was recommended to use the segment of the DE-LC curve with the highest R^2 value to regress the power law model. Shen suggested using the Excel spreadsheet function "RSQ" to determine the regression starting from each cycle of the test data to determine the best fit. Additionally, it was determined that no less than half of the fatigue life should be used to ensure that the fitted curve is representative of the overall DE-LC curve trend.

Table 4.3 Values of A and z for all mixtures from equation (2.46).

Mixture	Section	Preparation Method	A	z	R^2
SM-9.5A	D	field-lab	0.5169	0.5160	0.9757
		lab-lab	0.1357	0.5840	0.9874
		design-lab	0.1429	0.5806	0.9916
	I[a]	field-lab	0.0950	0.6338	0.9925
		lab-lab	0.1374	0.5751	0.9901
		design-lab	0.0991	0.5801	0.9781
SM-9.5D	B	field-lab	0.0905	0.6263	0.9672
		lab-lab	0.0908	0.6228	0.9938
		design-lab	0.0854	0.6361	0.9871
	E	field-lab	0.0828	0.6414	0.9899
	F	field-lab	0.1404	0.6077	0.9801
	G	field-lab	0.0866	0.6409	0.9690
	H	field-lab	0.1154	0.6166	0.9918
	E, F, G, H	lab-lab	0.1349	0.6028	0.9874
	J	field-lab	0.0778	0.6178	0.9850
		lab-lab	0.0559	0.6562	0.9975
SM-9.5E	C	field-lab	0.1573	0.6150	0.9882
		lab-lab	0.2372	0.5467	0.8880
		design-lab	0.0407	0.7228	0.9834
		field-field (all specimens)	0.1095	0.6165	0.9072
SM-12.5D	A	field-lab	0.0465	0.6860	0.9716
		lab-lab	0.1127	0.6128	0.9929
		design-lab	0.1196	0.6059	0.9880
SMA-12.5	L	field-lab	0.0352	0.7507	0.9794
		design-lab	0.2038	0.5666	0.8796

[a]Designed with high laboratory compaction.

- Calculate the average RDEC per 100 cycles as:

$$RDEC_a = \frac{1-\left(1+\frac{100}{a}\right)^k}{100} \tag{4.6}$$

where
$RDEC_a$ = the average ratio of dissipated energy change at cycle a, comparing to the next cycle, and
k = the exponential slope of the power equation for the regressed DE-LC curve.

- Calculate the plateau value (PV) as:

$$PV = \frac{1-\left(1+\frac{100}{N_{f50}}\right)^k}{100} \tag{4.7}$$

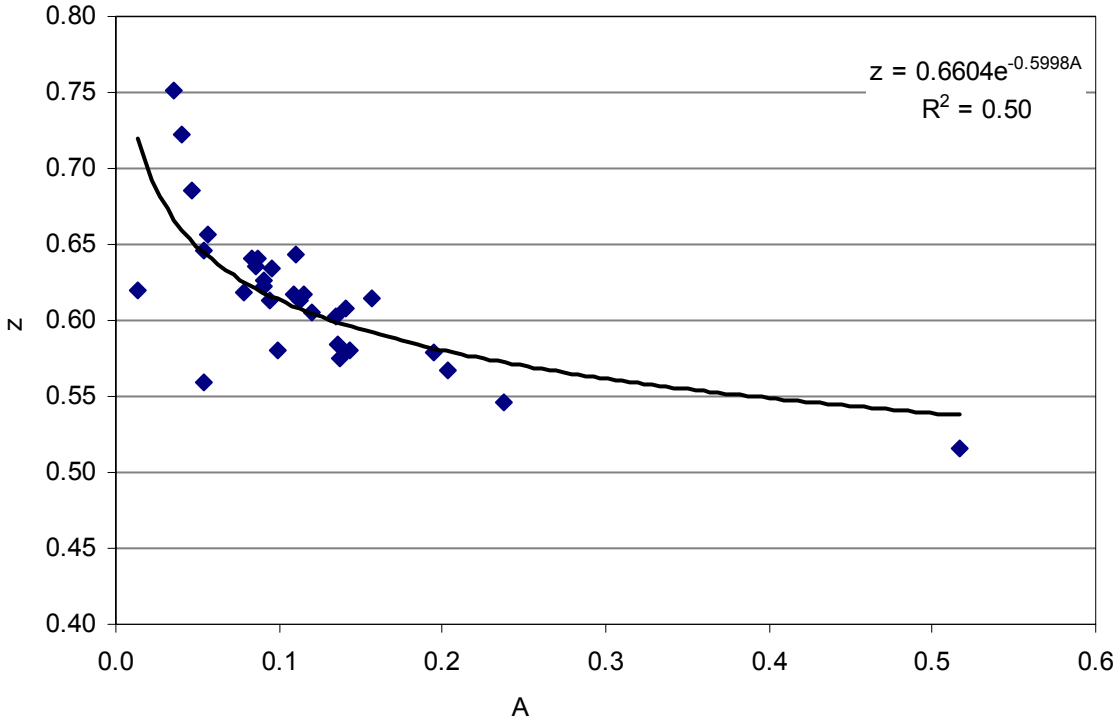

Figure 4.4 Relationship between A and z from Table 4.3.

where
PV = plateau value defined as the RDEC value at N_{f50}, and
N_{f50} = 50% stiffness reduction failure point.

Shen and Carpenter (2007) offer an alternative method to calculate the PV that does not require extensive fatigue testing. The PV is determined as:

$$PV = 44.422\,\varepsilon^{5.140}\,S^{2.993}\,VP^{1.850}\,GP^{-0.4063} \tag{4.8}$$

where
PV = plateau value,
ε = tensile strain, in/in,
S = flexural stiffness of the mixture from laboratory testing, MPa,
VP = volumetric parameter (defined in equation 2.63), and
GP = aggregate gradation parameter (defined in equation 2.63).
This formula was calibrated using data collected from five material sources, 89 different mixtures, and a total of 372 samples.

Plateau values were determined for all mixes tested in this study using both methods and then compared using the paired t-test for means. The results are presented in Table 4.4 through Table 4.8. Areas having a p-value of less than 0.10 are shaded, indicating that the probability of the sample means being equivalent is less than 10%. From these results, it can be seen that the PV determined from the fatigue data is not always equivalent with that determined from the formula. The difference is likely due to variability in the data and discrepancies in the curve

Table 4.4 Plateau values and t-test results for SM-9.5A mixes.

Section	D					
Preparation Method	FL		LL		DL	
Specimen Plateau Value	Formula	Data	Formula	Data	Formula	Data
	1.95E-04	8.04E-06	4.71E-05	1.56E-05	9.07E-06	3.76E-05
	7.38E-05	6.84E-06	1.17E-05	1.08E-05	6.27E-06	1.79E-05
	2.08E-05	[a]	1.77E-06	1.66E-06	1.37E-06	4.79E-06
	3.28E-06	[a]	2.80E-07	8.12E-08	1.26E-07	3.74E-07
	1.07E-04	8.65E-06	3.41E-05	3.88E-05	4.24E-06	2.67E-05
	5.70E-05	1.80E-06	2.57E-05	1.44E-05	4.74E-07	1.19E-05
	2.80E-05	[a]	7.71E-07	8.23E-07	5.44E-07	2.24E-06
	4.94E-06	1.60E-07	2.72E-07	9.70E-08	1.05E-07	3.75E-07
Average	6.12E-05	5.10E-06	1.52E-05	1.03E-05	2.78E-06	1.27E-05
Std. Deviation	6.49E-05	3.86E-06	1.82E-05	1.33E-05	3.39E-06	1.37E-05
p-value[b]	0.0524[c]		0.2699		0.0341	
Section	I					
Preparation Method	FL		LL		DL	
Specimen Plateau Value	Formula	Data	Formula	Data	Formula	Data
	1.21E-04	2.99E-05	1.05E-05	7.95E-05	2.58E-05	6.25E-05
	4.17E-05	1.35E-05	1.28E-06	1.31E-05	1.43E-05	1.75E-04
	1.19E-05	1.75E-06	1.27E-07	4.21E-06	8.34E-06	1.63E-05
	2.54E-06	1.90E-07	2.57E-09	5.69E-08	5.45E-07	1.65E-06
	4.67E-05	2.80E-05	5.59E-06	1.55E-05	4.29E-05	1.18E-04
	4.29E-05	1.82E-05	4.92E-07	1.35E-05	1.23E-05	1.28E-05
	6.65E-06	2.45E-07	2.37E-08	8.57E-07	1.76E-06	6.90E-06
	1.93E-06	3.05E-07	1.92E-09	3.00E-07	2.25E-07	1.96E-07
					2.00E-07	1.62E-07
Average	3.45E-05	1.15E-05	2.25E-06	1.59E-05	1.18E-05	4.37E-05
Std. Deviation	3.99E-05	1.27E-05	3.82E-06	2.65E-05	1.45E-05	6.30E-05
p-value	0.0631		0.1377		0.1171	

[a]Plateau value was unable to be calculated for this specimen.
[b]*p*-value indicates probability of the sample means being equivalent. Shaded cells indicate significant differences (α=0.10).

fitting process used to determine the PV, despite following the recommendations for minimizing such issues. It was quite difficult in practice to follow the recommended procedure for determining the PV using the curve fitting process; in fact, several specimen data sets did not work with the fitting method such that the PV could not be calculated. Additionally, as calculation of the PV for each specimen is much more reasonable in terms of time required to perform using the formula, it is recommended that the formula presented in equation (4.8) be the preferred method for determining the plateau value.

Table 4.5 Plateau values and t-test results for SM-9.5D mixes.

Section	B						J			
Preparation Method	FL		LL		DL		FL		LL	
Specimen Plateau Value	Formula	Data	Formula	Data	Formula	Data	Formula	Data	Formula	Data
	1.87E-04	7.84E-06	3.96E-05	6.91E-05	1.36E-05	2.59E-05	1.66E-04	2.09E-05	5.55E-05	6.93E-05
	6.61E-05	6.00E-06	6.33E-06	2.57E-05	5.23E-06	1.18E-05	3.75E-05	3.07E-05	3.57E-05	2.54E-05
	3.89E-05	3.19E-06	1.23E-06	1.71E-06	3.13E-06	3.11E-06	1.14E-05	2.32E-06	5.40E-06	2.50E-06
	1.05E-04	[a]	3.21E-07	2.47E-07	3.07E-07	8.62E-08	1.61E-06	3.27E-07	4.50E-07	1.13E-08
	1.09E-05	4.97E-06	2.24E-05	6.10E-05	2.25E-05	2.92E-05	1.29E-04	4.97E-05	4.15E-05	1.78E-05
	1.29E-04	7.18E-05	7.93E-06	1.03E-05	1.12E-05	2.16E-05	2.93E-05	2.29E-05	1.41E-05	1.00E-05
	4.84E-05	9.73E-06	7.47E-07	1.17E-06	1.72E-06	1.88E-06	3.20E-06	2.25E-07	2.01E-06	4.51E-07
	3.51E-05	[a]	1.50E-07	3.32E-08	5.65E-07	7.40E-07	1.53E-06	1.02E-07	1.54E-06	1.67E-07
	1.22E-04	[a]								
	3.37E-06	4.97E-08								
Average	7.46E-05	1.48E-05	9.83E-06	2.12E-05	7.28E-06	1.18E-05	4.75E-05	1.59E-05	1.95E-05	1.57E-05
Std. Deviation	5.91E-05	2.53E-05	1.41E-05	2.85E-05	7.86E-06	1.21E-05	6.39E-05	1.83E-05	2.16E-05	2.36E-05
p-value[b]	0.0515		0.0801		0.0420		0.1350		0.3381	

Section	E		F		G		H		EFGH	
Preparation Method	FL								LL	
Specimen Plateau Value	Formula	Data	Formula	Data	Formula	Data	Formula	Data	Formula	Data
	2.68E-04	5.65E-05	1.13E-04	1.17E-05	2.00E-04	4.22E-05	1.64E-04	5.22E-05	1.33E-04	2.39E-05
	8.23E-05	1.84E-05	5.74E-05	7.17E-06	9.25E-05	1.32E-05	4.65E-05	7.04E-06	4.73E-05	1.36E-05
	7.28E-06	8.48E-07	1.21E-05	3.25E-06	1.22E-05	5.34E-06	1.76E-05	1.89E-06	4.21E-06	8.28E-07
	1.84E-06	1.89E-07	2.72E-06	2.49E-08	3.99E-06	2.34E-07	2.39E-06	1.69E-07	8.04E-07	1.19E-07
	8.70E-05	1.35E-05	2.05E-04	5.56E-06	3.26E-04	1.75E-05	1.40E-04	2.94E-05	1.10E-04	1.90E-05
	2.67E-05	6.16E-06	1.01E-04	4.75E-06	9.34E-05	[a]	4.26E-05	2.23E-05	1.52E-05	9.19E-06
	7.59E-06	3.25E-06	9.74E-06	[a]	1.83E-05	[a]	9.94E-06	7.59E-07	3.90E-06	6.95E-07
	2.04E-06	8.33E-08	4.30E-06	1.28E-07	7.03E-06	7.50E-07	6.36E-06	[a]	6.08E-07	2.36E-08
					1.68E-06	3.66E-09				
Average	6.04E-05	1.24E-05	6.31E-05	4.65E-06	8.39E-05	1.13E-05	5.37E-05	1.63E-05	3.94E-05	8.42E-06
Std. Deviation	9.11E-05	1.91E-05	7.23E-05	4.09E-06	1.12E-04	1.53E-05	6.32E-05	1.95E-05	5.33E-05	9.54E-06
p-value	0.1017		0.0516		0.1163		0.0482		0.0885	

[a]Plateau value was unable to be calculated for this specimen.

[b]*p*-value indicates probability of the sample means being equivalent. Shaded cells indicate significant differences (α=0.10).

Table 4.6 Plateau values and t-test results for SM-9.5E mixes.

Section	C							
Location	Outer wheelpath		Center of lane		Inner wheelpath PP[a]		Inner wheelpath PL[b]	
Preparation Method	FF							
Specimen Plateau Value	Formula	Data	Formula	Data	Formula	Data	Formula	Data
	3.21E-05	1.17E-05	9.27E-05	3.11E-06	3.77E-05	2.35E-06	2.54E-05	3.83E-05
	8.33E-05	1.76E-06	2.67E-05	2.59E-05	9.05E-06	7.09E-05	7.88E-06	2.77E-05
	1.30E-05	1.72E-05	6.05E-06	2.92E-05	1.46E-06	2.77E-05	1.69E-06	5.51E-06
	1.18E-05	3.79E-07	1.18E-06	1.88E-06	5.26E-05	5.34E-07	1.02E-06	5.34E-07
	8.39E-05	9.39E-06	1.82E-04	2.16E-05	5.97E-06	1.54E-06	1.55E-07	1.54E-06
	6.05E-05	6.85E-06	5.68E-05	8.62E-08	1.49E-06	5.51E-06	2.44E-07	2.35E-06
	2.96E-06	1.33E-07	5.87E-06	7.40E-07	[c]	1.23E-07		
	1.87E-06	7.22E-08	1.02E-05	1.18E-05				
Average	3.62E-05	5.94E-06	4.77E-05	1.18E-05	1.80E-05	1.55E-05	6.06E-06	1.27E-05
Std. Deviation	3.49E-05	6.43E-06	6.29E-05	1.21E-05	2.17E-05	2.63E-05	9.89E-06	1.62E-05
p-value[d]	0.0423		0.1477		0.9976		0.0996	

Section	C					
Preparation Method	FL		LL		DL	
Specimen Plateau Value	Formula	Data	Formula	Data	Formula	Data
	1.55E-04	4.55E-05	1.21E-04	1.02E-05	1.78E-05	2.77E-05
	3.00E-05	9.55E-06	2.76E-05	4.81E-06	8.51E-06	5.51E-06
	1.34E-05	1.50E-06	4.32E-06	1.97E-06	2.09E-06	5.34E-07
	2.75E-06	6.18E-08	1.82E-06	2.80E-07	7.13E-07	7.12E-08
	1.22E-04	1.59E-05	1.10E-04	8.47E-06	1.36E-05	1.40E-05
	3.26E-05	2.22E-06	2.42E-05	6.96E-06	3.86E-06	2.35E-06
	1.10E-05	1.56E-06	1.11E-06	1.15E-06	1.23E-06	1.54E-06
	1.37E-05	5.54E-07	2.46E-06	2.26E-08	1.25E-07	1.23E-07
Average	4.76E-05	9.61E-06	3.66E-05	4.23E-06	6.00E-06	6.47E-06
Std. Deviation	5.77E-05	1.55E-05	4.99E-05	3.95E-06	6.65E-06	9.75E-06
p-value	0.0445		0.0892		0.7450	

[a]PP - perpendicular to direction of traffic.
[b]PL - parallel to direction of traffic.
[c]Plateau value was unable to be calculated for this specimen.
[d]*p*-value indicates probability of the sample means being equivalent. Shaded cells indicate significant differences (α=0.10).

Table 4.7 Plateau values and t-test results for SM-12.5D mixes.

Section	A					
Preparation Method	FL		LL		DL	
Specimen Plateau Value	Formula	Data	Formula	Data	Formula	Data
	1.09E-04	5.47E-05	7.44E-05	2.58E-05	3.78E-05	3.66E-05
	4.11E-05	7.67E-05	2.49E-05	6.59E-06	1.00E-05	1.72E-05
	2.84E-06	5.24E-07	4.82E-06	2.88E-06	2.05E-06	1.76E-06
	2.99E-06	4.37E-07	4.55E-07	2.21E-08	2.94E-07	1.33E-07
	1.59E-05	6.26E-05	5.20E-05	1.52E-05	2.60E-05	1.17E-05
	1.47E-05	[a]	1.90E-05	6.61E-06	4.25E-06	6.85E-06
	2.52E-06	[a]	6.78E-06	1.26E-06	3.45E-07	3.79E-07
			9.83E-07	2.99E-08	1.93E-07	7.22E-08
Average	2.69E-05	3.90E-05	2.29E-05	7.29E-06	1.01E-05	9.33E-06
Std. Deviation	3.85E-05	3.60E-05	2.70E-05	8.99E-06	1.42E-05	1.27E-05
p-value[b]	0.8027		0.0446		0.7272	

[a]Plateau value was unable to be calculated for this specimen.
[b]*p*-value indicates probability of the sample means being equivalent. Shaded cells indicate significant differences (α=0.10).

Table 4.8 Plateau values and t-test results for SMA-12.5 mixes.

Section	L			
Preparation Method	FL		DL	
Specimen Plateau Value	Formula	Data	Formula	Data
	1.10E-06	3.79E-06	8.23E-06	1.32E-05
	1.91E-07	4.65E-06	3.34E-06	4.50E-06
	4.51E-06	8.93E-06	7.52E-07	1.35E-06
	1.05E-06	4.76E-06	6.72E-06	9.33E-06
	3.72E-08	3.25E-07	6.01E-06	4.26E-06
	1.30E-08	2.97E-08	1.58E-06	7.53E-07
			5.47E-07	1.13E-06
Average	1.15E-06	3.75E-06	3.88E-06	4.93E-06
Std. Deviation	1.72E-06	3.29E-06	3.11E-06	4.71E-06
p-value[b]	0.0246		0.2579	

[a]Plateau value was unable to be calculated for this specimen.
[b]*p*-value indicates probability of the sample means being equivalent. Shaded cells indicate significant differences (α=0.10).

The plateau values determined from the formula presented in equation (4.8) for each mixture were also compared to determine if significant differences were present due to production method. Results of this analysis are presented in Table 4.9 and Table 4.10. This table shows that in only four cases were significant differences observed between the differing production methods for the mixtures. Analysis of the differences between the SM-9.5D mixture in sections E, F, G, and H, shown in Table 4.11, indicated that no significant differences exist between the sections.

Table 4.9 Comparison of plateau values for significant differences between production methods (level of significance, α = 0.05).

Mixture	Section	Comparison	DL	FL
SM-9.5A	D	FL	sig	-
		LL	NS	NS
	I[a]	FL	NS	-
		LL	NS	NS
SM-9.5D	B	FL	sig	-
		LL	NS	sig
	E	FL	NS	-
		LL	NS	NS
	F	FL	NS	-
		LL	NS	NS
	G	FL	NS	-
		LL	NS	NS
	H	FL	NS	-
		LL	NS	NS
	J	FL	NS	-
		LL	NS	NS
SM-12.5A	A	FL	NS	-
		LL	NS	NS
SMA-12.5	L	FL	NS	-

[a]Designed with high laboratory compaction.
sig - significant difference between regressors.
NS - no significant difference between regressors.

Table 4.10 Comparison of plateau values for significant differences between production methods for SM-9.5E, section C (α = 0.05).

Mixture	Production Method	FL	LL	DL
SM-9.5E Section C	FF	NS	NS	sig
	FL	-	NS	NS
	LL	-	-	NS

sig - significant difference between regressors.
NS - no significant difference between regressors.

Table 4.11 Comparison of plateau values for significant differences between SM-9.5D sections E through H (α = 0.05).

Mixture	Section	F	G	H
SM-9.5D	E	NS	NS	NS
	F	-	NS	NS
	G	-	-	NS

NS - no significant difference between regressors.

Table 4.12 summarizes the investigation of differences due to the location of sampling for the SM-9.5E section C field-produced, field-compacted mixture. The only significant difference in plateau values were found between the specimens taken from the center of the lane and those cut from the outer wheelpath parallel to the direction of traffic.

Table 4.12 Comparison of plateau values for significant differences between locations, SM-9.5E, section C, field produced, field compacted specimen sets ($\alpha = 0.05$).

Mixture	Location	CL	IWP PP	IWP PL
SM-9.5E section C FF	OWP	NS	NS	sig
	CL	-	NS	NS
	IWP PP	-	-	NS

OWP - outer wheelpath; CL - center of lane; IWP PP - inner wheelpath perpendicular to traffic; IWP PL - inner wheelpath parallel to traffic.
sig - significant difference between regressors.
NS - no significant difference between regressors.

4.2 EVALUATION OF MIXTURE RESPONSE

Goals of this study included investigating the factors affecting mixture response to fatigue loading and comparatively evaluating mixture performance to identify better performing mixtures. The methods used to perform the comparative analyses included analysis of variance (ANOVA) and general linear modeling (GLM) techniques. These techniques require the assumption of normally distributed variables; however, it is reported in the literature (Tayebali et al, 1994) that fatigue data are approximately log-normally distributed, and thus the log-transformed data may be used for analysis. The models considered were generally of a power nature; following the recommendation of the literature (Tayebali et al., 1994), log-transformations were applied. A convenient result of this transformation was the linearization of the proposed models presented in Section 4.1.1, which enhanced the ease of analysis.

Evaluation included the consideration of significant regressors and evaluation of the coincidence of slopes and intercepts to determine the effectiveness of models for predicting fatigue response. Factors thought to have influence on fatigue performance included production practice (plant or laboratory procedures), compaction, test loading frequency, presence and duration of rest periods during loading, and in situ location and orientation of the mixture. Additionally, categorized mixture performance was considered.

4.2.1 Production Effects

One focal point of this study was the evaluation of effects on laboratory performance of asphalt mixtures attributable to the differences between field and laboratory production practices. Analyses of combinations of production methods were performed to assess these effects. A coincidence of slopes and intercepts methodology was used initially for analysis as it can identify data sets for which fitted models are statistically identical. A summary of the results obtained by evaluating the differences between the K_1 and K_2 terms previously presented in Table 4.2 is shown in Table 4.13. It should be noted that either a slope or intercept can be significantly different, leading to the conclusion that the treatments (in this case, production method) may have a significant effect on response, generally causing either a shift in response (significantly different intercepts) or a change in behavioral pattern (significantly different slopes).

Table 4.13 Results of analysis comparing production effects using coincidence of slopes and intercepts ($\alpha = 0.05$)

Mixture	Section	Intercept	Contrast	DL	FL	Slope	Contrast	DL	FL
SM-9.5A	D	K_1	FL	NS	-	K_2	FL	NS	-
			LL	NS	NS		LL	NS	NS
	I[a]	K_1	FL	sig	-	K_2	FL	NS	-
			LL	NS	NS		LL	NS	NS
SM-9.5D	B	K_1	FL	sig	-	K_2	FL	sig	-
			LL	NS	NS		LL	NS	sig
	E	K_1	FL	NS	-	K_2	FL	NS	-
			LL	NS	NS		LL	NS	NS
	F	K_1	FL	NS	-	K_2	FL	NS	-
			LL	NS	NS		LL	NS	NS
	G	K_1	FL	NS	-	K_2	FL	NS	-
			LL	NS	NS		LL	NS	NS
	H	K_1	FL	NS	-	K_2	FL	NS	-
			LL	NS	NS		LL	NS	NS
	J	K_1	FL	NS	-	K_2	FL	NS	-
			LL	NS	NS		LL	NS	NS
SM-9.5E	C	K_1	FL	NS	-	K_2	FL	NS	-
			LL	NS	NS		LL	NS	NS
SM-12.5A	A	K_1	FL	NS	-	K_2	FL	NS	-
			LL	NS	NS		LL	NS	NS
SMA-12.5	L	K_1	FL	NS	-	K_2	FL	NS	-

[a]Designed with high laboratory compaction.
sig = significant difference between regressors.
NS = no significant difference between regressors.

Effects of Plant and Laboratory Production

The differences between field-lab and lab-lab fatigue specimens were evaluated to investigate the effects of plant production processes as compared to laboratory production processes. From Table 4.13, it can be seen that the SM-9.5D mixture in section B was associated with a significant difference in the value of K_2, the slope coefficient, and exhibits different responses at differing strains. As shown in Figure 4.5,the field-lab mixture is expected to perform better than the lab-lab mixture across most of the evaluated strain range. The cause of the difference in performance of the SM-9.5D field-lab and lab-lab mixtures is unclear; **Error! Reference source not found.** shows that the field-lab mixture had a slightly lower asphalt content and higher air void content, both of which typically contribute to reduced fatigue life.

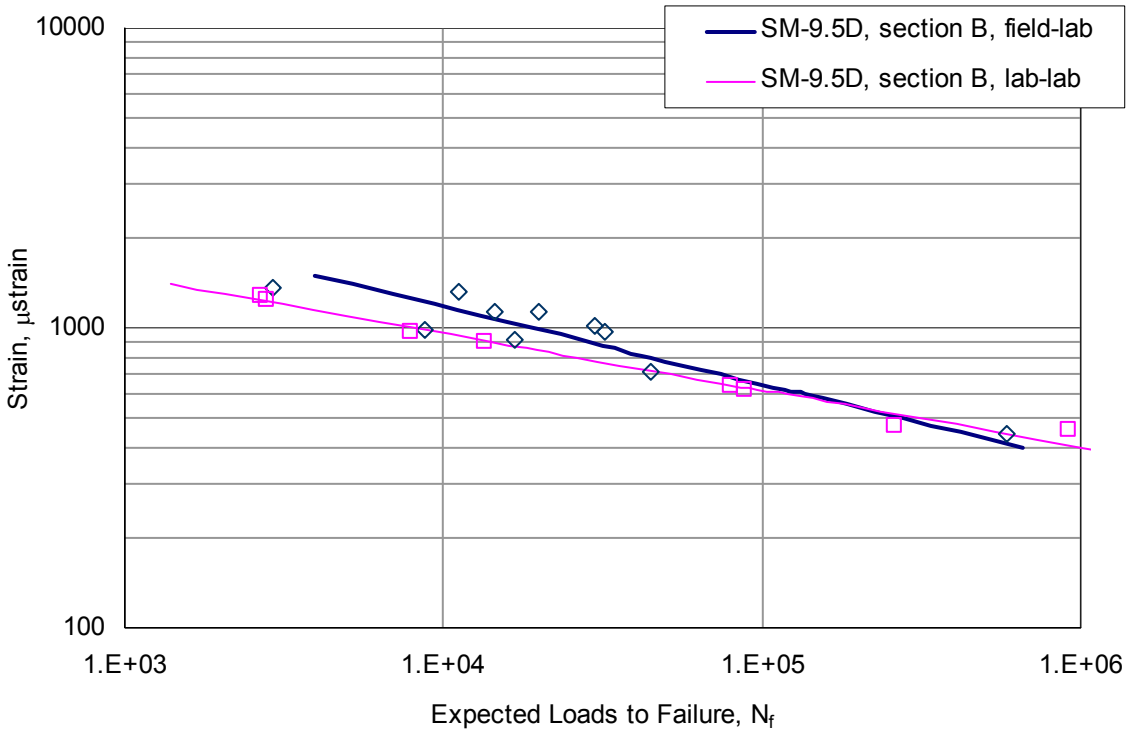

Figure 4.5 Expected fatigue performance of SM-9.5D, section B.

Table 4.14 Average volumetric values for field-lab and lab-lab fatigue specimens.

Mix	Section	Asphalt (%)			VTM (%)		
		FL	LL	difference	FL	LL	difference
SM-9.5A	D	6.3	6.8	0.5	5.1	8.2	3.1
	I[a]	5.4	5.3	0.1	6.1	10.2	4.1
SM-9.5D	B	4.7	5.4	0.6	9	7.7	1.3
	E	5.9	6	0.1	7.2	8.2	1
	F	5.4		0.6	8.3		0.1
	G	6.3		0.3	8.8		0.6
	H	5.6		0.4	8.6		0.4
	J	4.9	5.1	0.2	11.3	10.5	0.8
SM-9.5E	C	5.8	6	0.2	7.3	8.9	1.6
SM-12.5A	A	5.9	5.9	0	7.6	11.2	3.6

[a]Designed with high laboratory compaction.

Effects of Production Mixture Differences

Potential differences in performance between lab-lab and design-lab mixtures are due to deviations in the produced mixture as compared to the mixture design. For this evaluation, both mixture types were produced in the laboratory to eliminate the additional variability found between field-lab mixtures and focus on the differences in mixture properties between the job mix formula and plant-produced material. Table 4.13 indicates that there were no significant

differences in response for these mixtures. Table 4.15 summarizes the differences in asphalt and air void contents for the mixtures and shows that some differences are present; however, these did not appear to affect performance. In general, the findings for these mixtures and sections indicate that the differences in as-produced material and the job-mix-produced material do not significantly affect the fatigue performance.

Differences between the field-lab and design-lab mixtures were evaluated to investigate the differences in fatigue performance between mixtures produced in the laboratory and at the plant from the job mix formula. From Table 4.13, it can be seen that significant differences in both K_1 and K_2 are significant for the SM-9.5D mixture in section B. Consideration of the differences in asphalt and air void contents for the SM-9.5D mixture, shown in Table 4.16, does not indicate a clear cause for the difference in performance. Table 4.13 also indicates that a significant difference exists between the intercept coefficient, K_1, for the SM-9.5A mixtures in section I. This mixture shows a differences of 4.7% in the air void contents between the field-lab and design-lab specimens, which likely explains the difference in performance.

Table 4.15 Average volumetric values for design-lab and lab-lab fatigue specimens.

Mix	Section	Asphalt (%)			VTM (%)		
		DL	LL	difference	DL	LL	difference
SM-9.5A	D	6.3	6.8	0.5	7.9	8.2	0.3
	I[a]	5.4	5.3	0.1	10.8	10.2	0.6
SM-9.5D	B	5.3	5.4	0.1	9.6	7.7	1.9
	EFGH		6.0	0.7		8.2	1.4
	J		5.1	0.3		10.5	0.9
SM-9.5E	C	6.2	6.0	0.2	8.0	8.9	0.9
SM-12.5D	A	5.6	5.9	0.4	8.9	11.4	2.5

[a]Designed with high laboratory compaction.

Table 4.16 Average volumetric values for field-lab and design-lab fatigue specimens.

Mix	Section	Asphalt (%)			VTM (%)		
		FL	DL	difference	FL	DL	difference
SM-9.5A	D	6.3	6.3	0.0	5.1	7.9	2.8
	I[a]	5.4	5.4	0.1	6.1	10.8	4.7
SM-9.5D	B	4.7	5.3	0.6	9.0	9.6	0.6
	E	5.9		0.5	7.2		2.4
	F	5.4		0.1	8.3		1.3
	G	6.3		1.0	8.8		0.8
	H	5.6		0.3	8.6		1.0
	J	4.9		0.4	11.3		1.7
SM-9.5E	C	5.8	6.2	0.4	7.3	8.0	0.7
SM-12.5D	A	5.9	5.6	0.3	7.6	8.9	1.3
SMA-12.5	L	6.8	6.3	0.5	5.9	10.9	5.0

[a]Designed with high laboratory compaction.

In summary, the data from this portion of the study show that slight differences in asphalt content (up to 0.7%) has a minimal impact on the presence of significant differences in fatigue performance, regardless of the production method or accuracy of production in replicating the job mix formula. Differences in the intercept coefficient, which may be considered similar to a low-strain fatigue limit, appear to be influenced by the air void content, which is expected and is well-documented in the literature; however, a clear trend in the minimum difference required for the air void content to affect the strain-life relationship significantly was not apparent.

These data study also show that the responses of mixes prepared using either laboratory or plant production methods do not differ significantly in terms of mixture fatigue performance. In addition, it was found that volumetric differences between the mixtures produced at the plant and those produced to match the job mix formula did not significantly influence the expected laboratory fatigue performance.

4.2.2 Compaction Effects

One goal of this study was to evaluate the effect of compaction on the fatigue life of mixtures, including the differences between laboratory compaction of fatigue specimens and of specimens cut from the in-situ pavement. However, difficulties were encountered in the collection of the field specimens that might diminish the accuracy of this evaluation. Field specimens were cut from slabs removed from the pavement during installation of a weigh-in-motion facility. Unfortunately, the fatigue specimens were not collected from the slabs until approximately 1 year after the construction of the weigh-in-motion facility. This meant that the field specimens over-wintered as part of these separated slabs and were subjected to different climatic conditions than the in-place pavement; in addition, the slabs sustained some damage during removal that likely affected the fatigue response of the specimens. With these cautions, the following evaluation is offered.

Comparisons between the production/compaction methods indicated that no significant differences existed in the intercept coefficient for the field-lab, design-lab, or lab-lab specimen sets when compared to the field-field specimens; this can be seen in Table 4.17. Figure 4.6 illustrates the expected fatigue performance of each of the mixtures, while Table 4.18 presents the volumetric values for the mixtures. The order of rankings from this figure generally follow the order of the mixtures with respect to decreasing air void content; improved fatigue performance is expected with decreasing air void content. The impact of asphalt content on fatigue performance was not apparent, and is not particularly surprising as the asphalt content only varied by 0.4% amongst the mixtures.

Table 4.17 Results of analysis comparing compaction effects using coincidence of slopes and intercepts (α=0.05).

Mixture	Section	Intercept	Contrast	FF	Slope	Contrast	FF
SM-9.5E	C	K_0	DL	NS	K_1	DL	NS
			FL	NS		FL	NS
			LL	NS		LL	NS

sig - significant difference between regressors.
NS - no significant difference between regressors.

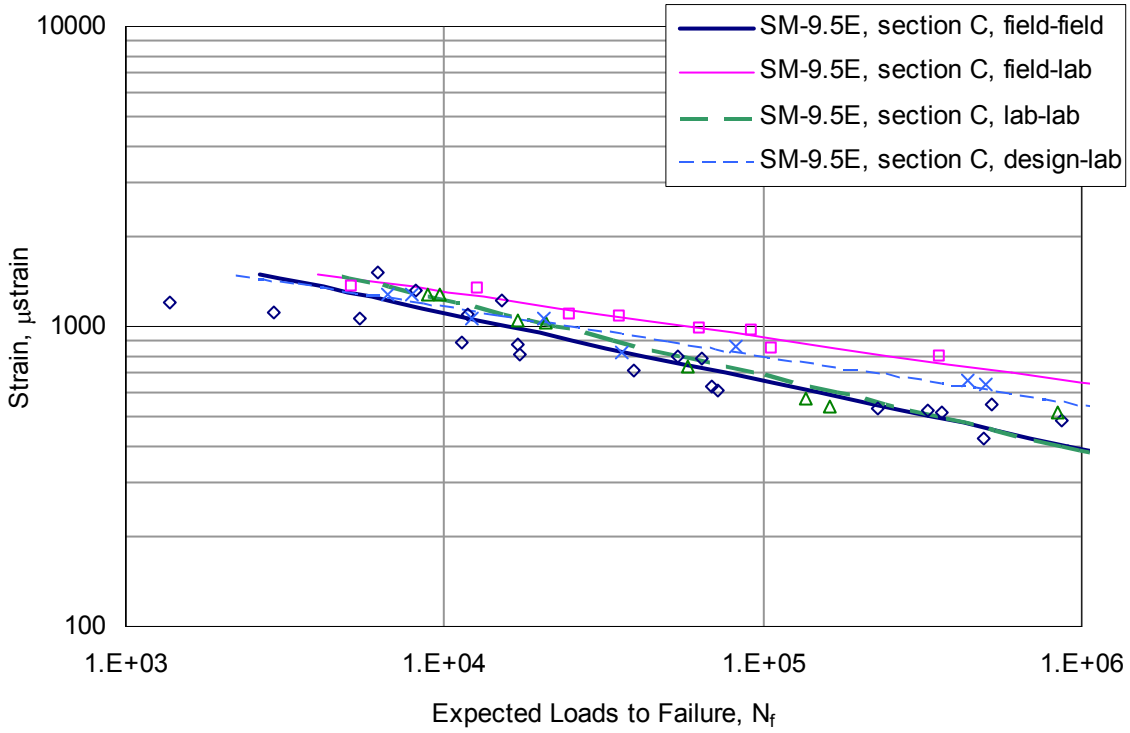

Figure 4.6 Expected fatigue performance of SM9.5E section C mixtures.

Table 4.18 Average volumetric values for SM-9.5E section C mixtures.

Mixture	Sample	Asphalt (%)	VTM (%)
SM-9.5E section C	FF	5.8%	8.6%
	FL	5.8%	7.3%
	LL	6.0%	8.9%
	DL	6.2%	8.0%

4.2.3 Loading Frequency

The effects of frequency of loading on fatigue life were evaluated as part of this study. Design-lab specimens of the SM-9.5E mixture were tested using loading frequencies of 1, 5, and 10 Hz. Results of testing were expressed in terms of applied stress and strain, stiffness, cumulative dissipated energy, and fatigue life. A summary of the test results for the 28 specimens in this portion of the study is shown in Table 4.19.

An initial evaluation was performed to determine if correlations existed between test frequency, fatigue life, applied strain, cumulative dissipated energy, and initial stiffness. Significant correlations were found for several relationships using a sensitivity of α=0.05. A summary of the correlation analysis is presented in Table 4.20, showing the Pearson correlation coefficients and the *p*-values. Applied strain was found to be highly correlated to the cumulative

Table 4.19 Summary of fatigue results using 1, 5, and 10Hz loading frequencies.

Frequency, Hz	Measured Strain, μstrain	Fatigue Life	Initial Stiffness, kN/mm	Cumulative Dissipated Energy, kN-mm/mm^2
1	1220	9641	1103	18.60
	1184	9967	1233	19.81
	1054	48181	1236	72.40
	1053	5686	1379	9.94
	782	69387	1608	70.94
	665	355174	1513	283.73
	586	539882	1292	287.55
	583	702830	1572	435.99
5	1205	5383	2386	16.87
	1187	6887	3100	26.19
	995	7404	3183	18.93
	989	12308	2542	28.01
	796	116170	2389	168.82
	782	268566	2137	356.49
	667	783319	2396	798.37
	567	965060	2732	829.16
10	1277	6686	2347	25.53
	1269	7879	2705	32.27
	1069	12233	2632	33.29
	1064	20463	2705	60.14
	862	81970	2802	152.06
	820	35888	2619	58.76
	664	437513	3123	545.92
	639	502838	2815	512.30

Table 4.20 Pearson correlation coefficients for significant effects between variables.

Pearson Correlation *p*-value ($\alpha = 0.05$)	Frequency	Applied Strain	Cumulative Dissipated Energy	Initial Stiffness
Frequency	1.00000	0.11904 0.5796	0.03147 0.8839	0.80531 < 0.0001
Applied Strain		1.00000	-0.78540 < 0.0001	-0.00783 0.9710
Cumulative Dissipated Energy			1.00000	0.15853 0.4594
Initial Stiffness				1.00000

Note: Shaded cells indicate significant effects between variables.

dissipated energy; this was expected, since the dissipated energy is a function of the applied strain. This is presented graphically in Figure 4.7. A strong correlation was also seen between test frequency and initial stiffness.

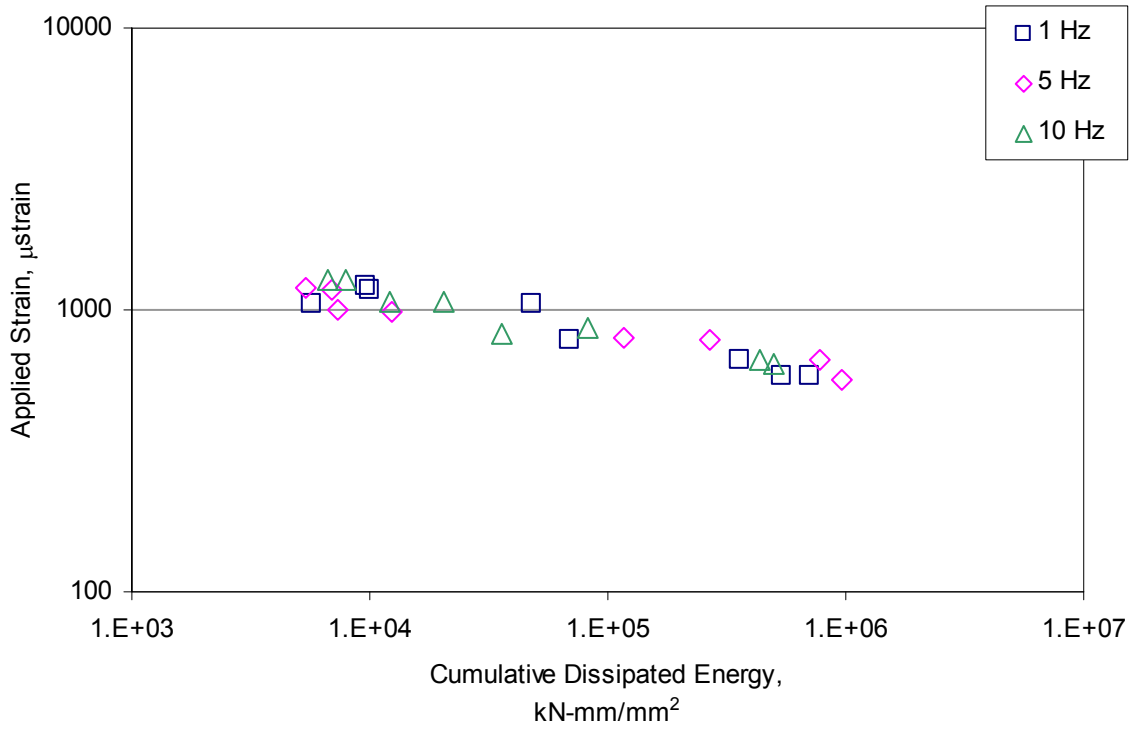

Figure 4.7 Applied strain versus cumulative dissipated energy for varying load frequencies.

Regression analyses were performed to evaluate the trends in performance seen in the fatigue data; the results are presented in Table 4.21. The equations used for analysis were equations 2.2, 4.1, and 4.2. Equation 2.2 is commonly accepted as a suitable relationship for fatigue. An investigation of the differences in the intercept term, denoted K_0, and the coefficient of the applied strain, denoted K_1, indicated that no trends were apparent for these terms with respect to frequency. Further statistical analysis of the equations indicated that no significant differences exist between the K_0 terms nor between the K_1 terms. Thus, Equation 2.2 can be utilized for the prediction of fatigue life from applied strain without regard to the testing frequency. The relationship between fatigue life and applied strain is also presented in Figure 4.8, where the similarity in the relationship for all tested frequencies can be seen. This indicates that for the mixture tested, fatigue life is independent of the frequency of the applied strains.

Equation 4.1 was investigated to determine the correlation effects between the applied strain and the cumulative dissipated energy. These models were found to have very low RMSE values, indicating a well-fitting model. This was somewhat surprising, as a significant correlation was found between the strain and cumulative dissipated energy; usually this indicates that one of the variables will be found extraneous to the model, which was not the case here. It is postulated that, despite the correlation, each variable captures independent significant influences on the fatigue life of the tested mixture.

Table 4.21 Regression results for evaluation of models.

$N_f = K_0 \times \varepsilon^{K_1}$ Equation (2.2)						
Frequency	K_0	K_1	K_2	K_3	RMSE	Adjusted R^2
1	1.1435×10^{22}	-5.887	-	-	0.6642	0.8822
5	9.2646×10^{27}	-7.901	-	-	0.6408	0.9162
10	5.9365×10^{22}	-6.118	-	-	0.4528	0.9295
All	9.1756×10^{23}	-6.531			0.5939	0.9006
$N_f = K_0 \times \varepsilon^{K_1} \times CDE^{K_2}$ Equation (4.1)						
Frequency	K_0	K_1	K_2	K_3	RMSE	Adjusted R^2
1	1.2103×10^{7}	-1.445	1.053	-	0.0814	0.9982
5	2.0095×10^{7}	-1.595	1.065	-	0.0980	0.9980
10	1.9479×10^{9}	-2.187	0.931	-	0.0482	0.9992
All	1.9565×10^{10}	-2.469	0.879		0.2373	0.9841
$N_f = K_0 \times \varepsilon^{K_1} \times S_0^{K_3}$ Equation (2.5)						
Frequency	K_0	K_1	K_2	K_3	RMSE	Adjusted R^2
1	7.8246×10^{32}	-6.689	-	-2.7086	0.6575	0.8846
5	3.9469×10^{36}	-7.443	-	-2.9232	0.5336	0.9419
10	1.6256×10^{7}	-5.290	-	-3.8171	0.4287	0.9368
All	4.2205×10^{24}	-6.536		-0.1950	0.6038	0.8972
$N_f = K_0 \times \varepsilon^{K_1} \times CDE^{K_2} \times S_0^{K_3}$ Equation (4.2)						
Frequency	K_0	K_1	K_2	K_3	RMSE	Adjusted R^2
1	1.6572×10^{10}	-1.794	1.016	-0.652	0.0454	0.9995
5	1.6948×10^{11}	-2.034	0.972	-0.718	0.0305	0.9998
10	3.0789×10^{11}	-2.129	0.981	-0.719	0.0624	0.9996
All	8.8565×10^{10}	-1.993	0.985	-0.680	0.0383	0.9996

Shaded cells indicate that regressor is not statistically significant.

Regarding the effects of frequency on the coefficients, clear trends can be seen for some coefficients. Increasing the testing frequency results in the following trends: the intercept term, K_0, increases; and the strain coefficient, K_1, decreases. There appears to be no clear relationship between frequency and the energy coefficient, K_2. Statistical analysis of the differences between frequencies for all coefficients indicated that changes in coefficients are not significant between the three test frequencies, resulting in the conclusion that one model is sufficient to capture the fatigue performance at test frequencies below 10Hz. This finding contradicts previous evaluations by Monismith et al. (1961) and Deacon and Monismith (1967), which found that frequencies of 0.05 Hz to 0.3 Hz had no effect on fatigue life, although higher frequencies in the range of 0.5 Hz to 1.6 Hz decreased the fatigue life by approximately 20%. As the previous work was performed using lower frequencies and controlled stress testing, the possibility of different conclusions is unsurprising and results may also be complicated by the small sample set used for this evaluation.

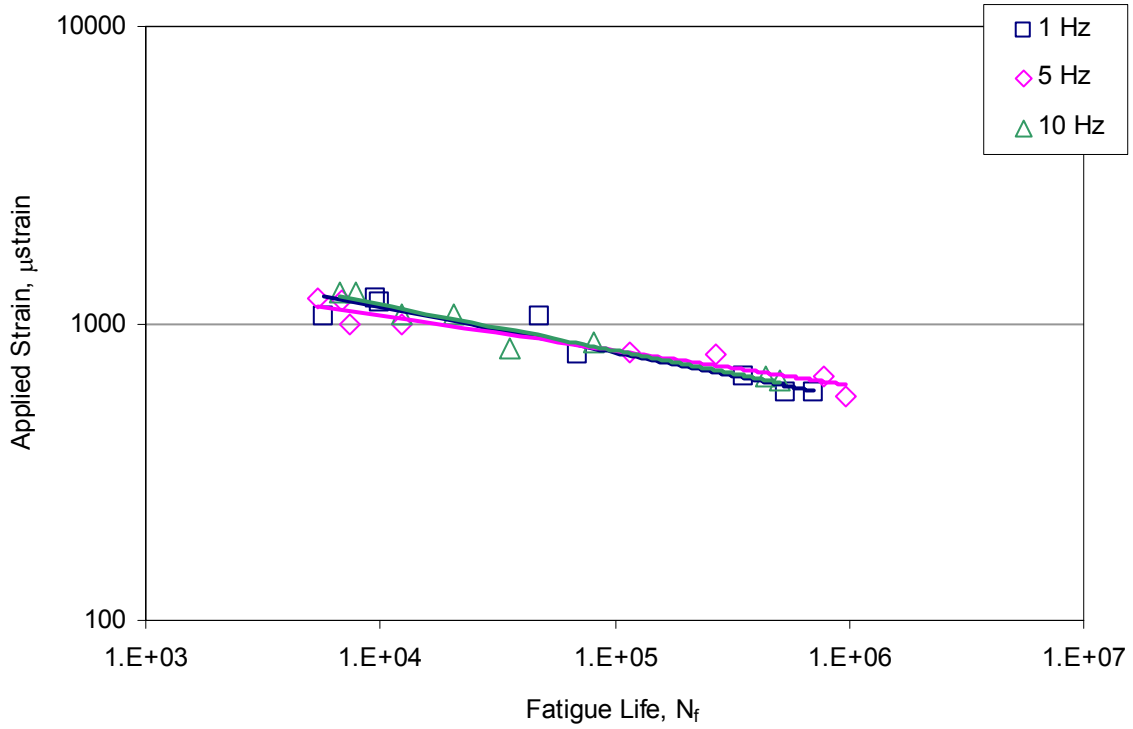

Figure 4.8 Applied strain versus fatigue life for varying loading frequencies.

Equation 4.2 was included in this analysis to investigate the combined effects of the cumulative dissipated energy and initial stiffness on the fatigue life prediction model. As can be seen in Table 4.21, in general, the inclusion of both lowered the RMSE values and increased the adjusted R^2 values over those of the other investigated models and did not render any of the coefficients insignificant. Trends with increasing test frequency may be seen in the K_0, K_1, and K_3 coefficients; however, it was again found that the differences in the coefficients attributable to differences in test frequency were not significant, and a single model may capture the fatigue performance at test frequencies of 10Hz and below.

Conclusions about the necessity of separate equations for each test frequency and the validity of proposed model forms resulted in the creation of three fatigue life prediction models that may be used without regard to test frequency. However, further testing on additional HMA mixtures should be conducted, as additional data may contradict the use of a single model for fatigue life prediction utilizing testing frequencies below 10Hz. The models resulting from this portion of the study on the SM-9.5E mixture are summarized as follows:

$$N_f = 9.1756 \times 10^{23} \times \varepsilon^{-6.5313} \quad (4.9)$$

$$N_f = 1.9565 \times 10^{10} \times \varepsilon^{-2.4686} \times CDE^{0.87924} \quad (4.10)$$

$$N_f = 8.8565 \times 10^{10} \times \varepsilon^{-1.9931} \times CDE^{0.9854} \times S_0^{-0.6802} \quad (4.11)$$

The RMSE and adjusted R^2 values for these three models are, respectively, 0.5939 and 90.06%; 0.2373 and 98.41%; and 0.0383 and 99.96%. It can clearly be seen that the inclusion of additional variables improved the model. The improvement shown by the inclusion of stiffness in equation 4.11 is interesting, as it may be recalled that the equations containing only strain and

stiffness terms showed that stiffness was not significant; this indicates that when present with both the strain and energy terms, the stiffness term captures a significant effect related to fatigue life.

4.2.4 Rest Periods

The effects of rest periods during loading on fatigue life were evaluated as part of this study. Design-lab specimens of the SM-9.5E mixture were tested using 10 Hz sinusoidal loading with no rest period, a 0.4 sec rest period, or a 0.9 sec rest period following each load application. Test results were expressed in terms of applied stress and strain, stiffness, cumulative dissipated energy, and fatigue life. A summary of the test results for the 24 specimens in this portion of the study is shown in Table 4.22.

Table 4.22 Summary of fatigue response with inclusion of rest periods.

Mixture	Loading	Measured Strain, μstrain	Fatigue Life	Initial Stiffness, kN/mm	Cumulative Dissipated Energy, kN-m/mm^2
SM-9.5E section C	Sine Waveform 10Hz frequency no rest period	1277	6686	2347	25.53
		1269	7879	2705	32.27
		1069	12233	2632	33.29
		1064	20463	2705	60.14
		862	81970	2802	152.06
		820	35888	2619	58.76
		664	437513	3123	545.92
		639	502838	2815	512.30
	Sine Waveform 10Hz frequency 0.4sec rest period	1478	8733	2923	33.85
		1418	13023	2900	48.29
		1196	19053	2993	43.30
		1078	31264	2846	72.28
		932	88633	2729	145.22
		876	87523	3165	147.66
		746	148623	3021	156.29
		706	112543	3075	119.60
	Sine Waveform 10Hz frequency 0.9sec rest period	1424	10219	2769	36.06
		1206	21069	2846	49.18
		1128	27809	3043	60.79
		1056	33179	2719	66.00
		884	80600	2470	126.51
		870	187199	3063	266.63
		800	247119	2579	289.56
		762	257189	2991	281.21

An initial evaluation was performed to determine if correlations existed between test frequency, fatigue life, applied strain, cumulative dissipated energy, and initial stiffness. Table 4.23 summarizes the correlation analysis and indicates that significant correlations existed for several relationships using a sensitivity of α=0.05. Applied strain was highly correlated with cumulative dissipated energy, shown graphically in Figure 4.9. Correlations were also seen between the initial stiffness and both the rest period and cumulative dissipated energy, although these were not as strong.

Table 4.23 Pearson correlation coefficients for significant effects between variables.

Pearson Correlation *p*-value (α = 0.05)	Rest Period	Applied Strain	Cumulative Dissipated Energy	Initial Stiffness
Rest Period	1	0.17836 0.5087	-0.04791 0.8601	0.57208 0.0206
Applied Strain		1	-0.86546 <0.0001	-0.36497 0.1645
Cumulative Dissipated Energy			1	0.52811 0.0355
Initial Stiffness				1

Note: Shaded cells indicate significant effect between variables.

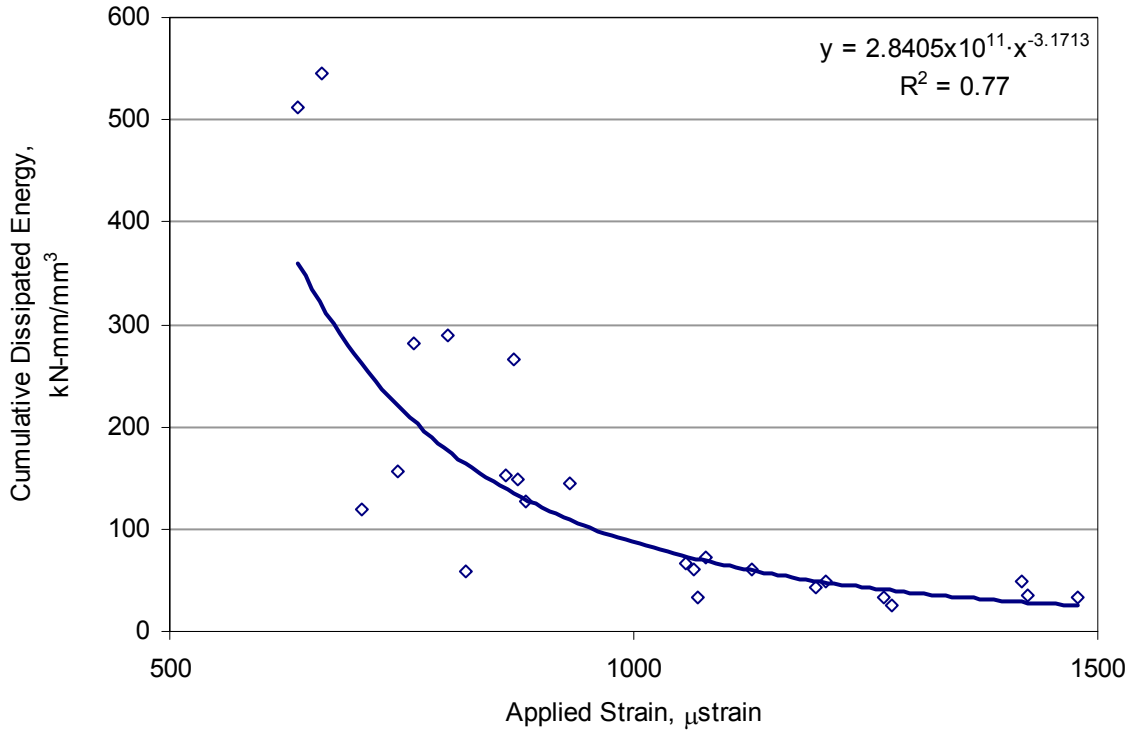

Figure 4.9 Relationship between applied strain and cumulative dissipated energy found for frequency evaluation specimens.

Modeling of the fatigue performance is presented in Table 4.24 and an evaluation of the coincidence of slopes and intercepts is shown in Table 4.25. The first model considered, equation 2.2, was the relationship between applied strain and resulting fatigue life. Results of the evaluation did not indicate any trends in the values of the coefficients with respect to the length of the rest period. An investigation of the coincidence in the intercept and slope coefficients indicated that the regressed models used to describe the fatigue response with no rest period and with 0.9 sec rest periods were statistically similar. However, significant differences were found between the regressed model with a 0.4 sec rest period and the models having no rest period and a 0.9 sec rest period; this is shown in Figure 4.10. It can be seen, however, that the model incorporating all testing data was not found to be significantly different from any rest period treatment, and so may be used regardless of the rest period.

The second evaluated model, equation 2.2, includes the initial stiffness as a factor in addition to the applied strain. It is evident that the initial stiffness is superfluous to the model, as the stiffness coefficient was not statistically significant when included on the model. Because of this, further evaluation of this model was not pursued.

Table 4.24 Regression results for evaluation of models.

$N_f = K_0 \times \varepsilon^{K_1}$ Equation (2.2)						
Rest Period	K_0	K_1	K_2	K_3	RMSE	adjusted R^2
None	5.9337×10^{22}	-6.1179	-	-	0.4528	0.9295
0.4sec	1.1099×10^{16}	-3.7988	-	-	0.2694	0.9382
0.9sec	2.1508×10^{21}	-5.5201	-	-	0.2733	0.9510
All tests	2.2079×10^{19}	-4.9046	-	-	0.5139	0.8483
$N_f = K_0 \times \varepsilon^{K_1} \times S_0^{K_2}$ Equation (2.5)						
Rest Period	K_0	K_1	K_2	K_3	RMSE	adjusted R^2
None	1.6260×10^{7}	-5.2898	3.8171	-	0.4287	0.9368
0.4sec	1.1367×10^{26}	-3.9766	-2.7304	-	0.2606	0.9421
0.9sec	3.4320×10^{16}	-5.5668	1.4321	-	0.2685	0.9527
All tests	5.9410×10^{9}	-4.7136	2.6080	-	0.4856	0.8645
$N_f = K_0 \times \varepsilon^{K_1} \times CDE^{K_3}$ Equation (4.1)						
Rest Period	K_0	K_1	K_2	K_3	RMSE	adjusted R^2
None	1.9473×10^{9}	-2.1865	-	0.9305	0.0482	0.9992
0.4sec	8.5183×10^{8}	-1.9985	-	0.8879	0.0892	0.9932
0.9sec	7.7392×10^{7}	-1.7241	-	1.0138	0.0564	0.9979
All tests	5.5493×10^{6}	-1.4160	-	1.1001	0.1530	0.9866
$N_f = K_0 \times \varepsilon^{K_1} \times S_0^{K_2} \times CDE^{K_3}$ Equation (4.2)						
Rest Period	K_0	K_1	K_2	K_3	RMSE	adjusted R^2
None	3.0798×10^{11}	-2.1294	-0.7186	0.9809	0.0323	0.9996
0.4sec	7.5494×10^{11}	-2.1329	-0.7088	0.8443	0.0926	0.9927
0.9sec	2.5191×10^{7}	-1.8570	0.2766	0.9807	0.0574	0.9979
All tests	1.3113×10^{5}	-1.4710	0.5361	1.0704	0.1515	0.9868

Note: Shaded cells indicate that the regressor is statistically not significant.

Table 4.25 Results of analysis comparing effects of rest periods using coincidence of slopes and intercepts (α=0.05).

$N_f = K_0 \times \varepsilon^{K_1}$ Equation (2.2)

Coefficient	Rest Period	All tests	None	0.4sec	Coefficient	Rest Period	All tests	None	0.4sec
K_0 intercept coefficient	None	NS			K_3 stiffness coefficient	None			
	0.4sec	NS	sig			0.4sec			
	0.9sec	NS	NS	sig		0.9sec			
K_1 strain coefficient	None	NS			K_4 CDE coefficient	None			
	0.4sec	NS	sig			0.4sec			
	0.9sec	NS	NS	sig		0.9sec			

$N_f = K_0 \times \varepsilon^{K_1} \times CDE^{K_3}$ Equation (4.1)

Coefficient	Rest Period	All tests	None	0.4sec	Coefficient	Rest Period	All tests	None	0.4sec
K_0 intercept coefficient	None	NS			K_3 stiffness coefficient	None			
	0.4sec	NS	NS			0.4sec			
	0.9sec	NS	NS	NS		0.9sec			
K_1 strain coefficient	None	NS			K_4 CDE coefficient	None	NS		
	0.4sec	NS	NS			0.4sec	NS	NS	
	0.9sec	NS	NS	NS		0.9sec	NS	NS	NS

sig = Significant difference found.
NS = No significant difference found.

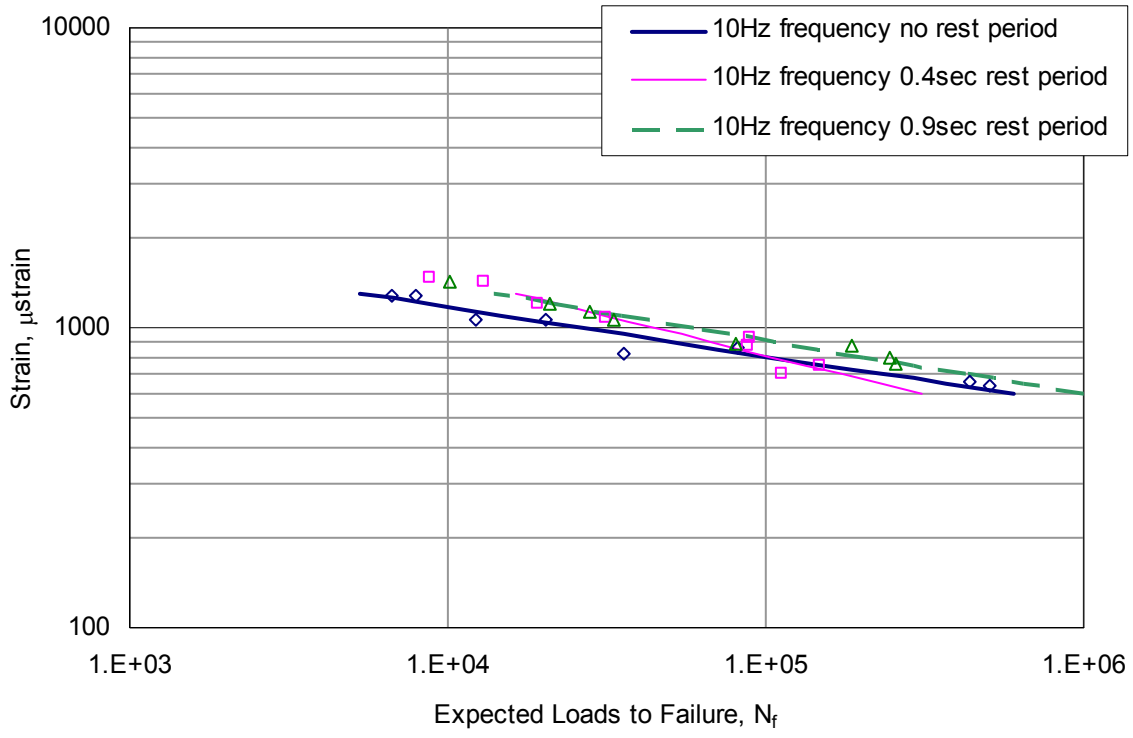

Figure 4.10 Expected fatigue response of SM-9.5E section C, design-lab mixtures with varying rest periods.

An evaluation of equation 5.1 indicated that the addition of the cumulative dissipated energy to the strain model (equation 2.2) offers improvement, as the RMSE values were reduced and the correlation coefficient (adjusted R^2) was increased. This is interesting given the strong correlation between cumulative dissipated energy and the applied strain, as it would be expected that either could be unnecessary, since the other would capture the response mechanism. Table 4.24 indicates increasing trends in the values of the intercept (K_0) and strain (K_1) coefficients with increasing rest period, although no trend is seen for the K_3 coefficient. However, Table 4.25 indicates there are no differences between the regressed models; thus, it appears that inclusion of either the 0.4 sec or 0.9 sec rest period has no effect on fatigue life when predicted from applied strain and cumulative dissipated energy. Equation 5.2 was also considered during this analysis and it was found that initial stiffness was not significant when applied strain and cumulative dissipated energy were included in the model. Due to this, no further consideration was given to the model.

The investigation of the need for unique models indicated that a summary model may be sufficient for each equation. From Table 4.25, it can be seen that no significant differences are present between the summary model coefficients and those determined for the rest period treatments for either equation 2.2 or equation 5.1, although additional testing of different mixtures is recommended to verify this conclusion. From this, it was concluded that for the tested mixture, SM-9.5E, the following summary equations may be used without concern for rest periods to predict fatigue response:

$$N_f = 2.2079 \times 10^{19} \cdot \varepsilon^{-4.9046} \quad (4.12)$$

$$N_f = 5.5493 \times 10^{6} \cdot \varepsilon^{-1.4160} \cdot CDE^{1.1001} \quad (4.13)$$

where

N_f = predicted fatigue cycles to failure,
ε = applied strain, μstrain, and
CDE = cumulative dissipated energy, kN-mm/mm^3.

The RMSE and adjusted R^2 values for these models are, respectively, 0.5139 and 84.83%; and 0.1530 and 99.56%. It can clearly be seen that the inclusion of the CDE term is improving the model; however, without extensive prior experience in fatigue testing, it is unlikely that the cumulative dissipated energy expected for a mixture is available, so equation (4.12) is preferred for practical use.

4.2.5 Location within Pavement Surface

As part of this study, the effects of location and orientation of specimens cut from the wearing surface on fatigue life were evaluated. As previously noted, field specimens were cut from large slabs removed from the pavement during installation of a weigh-in-motion facility. The slabs were left unprotected over the winter following removal from the pavement and sustained some damage that may have affected the fatigue response of the specimens. It should also be noted that these slabs only experienced light traffic prior to their removal from the pavement.

The SM-9.5E field specimens from section C were tested after being cut from the inner and outer wheelpaths and the center of the lane. Specimens cut with the longitudinal axis parallel with and perpendicular to the direction of traffic were compared with specimens cut from the outer wheelpath. Test results were expressed in terms of applied stress and strain, stiffness, cumulative dissipated energy, and fatigue life. A summary of the test results for the 29 specimens utilized in this portion of the study is shown in Table 4.26.

Table 4.26 Summary of fatigue response for field specimens from SM-9.5E section C.

Location	Measured Strain, μstrain	Fatigue Life	Initial Stiffness, kN/mm	Cumulative Dissipated Energy, kN-mm/mm^2
Center of Lane	1352	8236	3271	49.89
	1086	12384	3225	47.45
	869	33973	3085	79.35
	635	465004	1933	442.53
	1485	3222	2486	18.90
	1137	17401	2734	58.88
	813	71418	2230	108.12
	712	38615	3388	65.00
Outer Wheelpath	1230	15218	2081	55.94
	1502	6189	1881	32.94
	882	11415	2587	25.56
	798	53597	3198	122.16
	1317	8121	2871	47.88
	1104	11892	3504	57.72
	534	230079	4178	270.11
	486	866194	4144	840.12
Inner Wheelpath Perpendicular to Traffic	1121	2933	2246	9.70
	802	17121	2298	30.42
	612	71552	2110	66.19
	1210	1366	2098	5.63
	777	64498	2000	90.72
	708	39058	1828	43.62
	515	365937	1836	208.81
Inner Wheelpath Parallel to Traffic	1068	5395	2879	19.07
	867	17022	2705	38.01
	635	68522	2592	77.35
	550	518677	2450	382.83
	426	493043	2550	249.99
	528	328415	1671	221.82

An evaluation was performed to determine if correlations existed between location in the pavement, fatigue life, applied strain, cumulative dissipated energy, and initial stiffness. Results are presented in Table 4.27 and show significant correlations for several relationships using a sensitivity of α=0.05. Applied strain was highly correlated with the cumulative dissipated energy, as expected, since the dissipated energy is a function of the applied strain. Correlations were also seen between the location in the pavement and both applied strain and initial stiffness.

Results of the regressions are presented in Table 4.28. The models were found to describe the observed data very well, as determined by the adjusted R^2 values. However, the results of the regressions using equation 4.1 indicated that the initial stiffness was not a significant contributor to the model when applied strain was used in the model. Interestingly, the initial stiffness was found to be a significant factor when both applied strain and cumulative dissipated energy were included in the model.

The results from the regression analysis, with the exception of those for equation 2.5, were used in the comparison of location and orientation within the pavement through the analysis of intercepts and slopes methodology. The model expressed in equation 2.5 was removed from consideration since for this data set it contains non-significant regressors. A summary of the results obtained by evaluating the differences between the K_0, K_1, K_3, and K_4 terms in each model is shown in Table 4.29.

The model expressed by equation 2.2 indicates significant differences in the slope and intercept coefficients for the inner and outer wheelpath specimens that were oriented perpendicular to the direction of traffic. This was likely influenced by the difference in the air void content between the two specimen sets, shown in Table 4.30, although is it not clear why the higher air void content of the inner wheelpath specimens oriented perpendicular to the direction of traffic (IWP-PP) specimens would not also lead to significant differences when

Table 4.27 Pearson correlation coefficients for significant effects between variables.

Pearson Correlation *p*-value (α = 0.05)	Location in Pavement	Applied Strain	Cumulative Dissipated Energy	Initial Stiffness
Location in Pavement	1.00	-0.37969 0.0422	-0.08153 0.6742	-0.44155 0.0165
Applied Strain		1.00	-0.58188 0.0009	-0.03839 0.8432
Cumulative Dissipated Energy			1.00	0.29968 0.1143
Initial Stiffness				1.00

Note: Shaded cells indicate significant effects between variables.

Table 4.28 Results of analysis comparing location effects using coincidence of slopes and intercepts.

$N_f = K_0 \times \varepsilon^{K_1}$ Equation (2.2)						
Location	K_0	K_1	K_2	K_3	RMSE	adjusted R^2
center of lane	1.3194×10^{18}	-4.5846	-	-	0.6239	0.8292
outer wheelpath	3.0676×10^{16}	-4.0459	-	-	0.6299	0.8749
iwp - perpendicular to traffic	1.6084×10^{22}	-6.1547	-	-	0.4853	0.9374
iwp - parallel to traffic	1.7161×10^{20}	-5.4374	-	-	0.5634	0.9138
all locations	2.7098×10^{17}	-4.4111	-	-	0.7384	0.8228
$N_f = K_0 \times \varepsilon^{K_1} \times S_0^{K_2}$ Equation (2.5)						
Location	K_0	K_1	K_2	K_3	RMSE	adjusted R^2
center of lane	1.8736×10^{24}	-4.1056	2.2053	-	0.4630	0.9060
outer wheelpath	2.2266×10^{17}	-4.4130	0.1652	-	0.6893	0.8503
iwp - perpendicular to traffic	7.3176×10^{26}	-5.8729	1.6527	-	0.5220	0.9276
iwp - parallel to traffic	6.5892×10^{22}	-5.1417	1.0083	-	0.6138	0.8977
all locations	1.1638×10^{17}	-4.4124	0.1089	-	0.7520	0.8162
$N_f = K_0 \times \varepsilon^{K_1} \times CDE^{K_3}$ Equation (4.1)						
Location	K_0	K_1	K_2	K_3	RMSE	adjusted R^2
center of lane	2.3437×10^{8}	-1.7958	-	1.1358	0.1566	0.9892
outer wheelpath	2.7894×10^{8}	-1.7563	-	0.9394	0.1841	0.9893
iwp - perpendicular to traffic	1.2093×10^{9}	-1.9812	-	1.0744	0.0720	0.9886
iwp - parallel to traffic	2.0316×10^{8}	-1.7644	-	1.1375	0.0503	0.9993
all locations	4.0866×10^{9}	-2.1382	-	0.9530	0.1883	0.9885
$N_f = K_0 \times \varepsilon^{K_1} \times S_0^{K_2} \times CDE^{K_3}$ Equation (4.2)						
Location	K_0	K_1	K_2	K_3	RMSE	adjusted R^2
center of lane	1.2356×10^{12}	-2.0578	0.7906	0.9592	0.0586	0.9985
outer wheelpath	7.6904×10^{12}	-2.1720	0.9477	0.9975	0.0214	0.9999
iwp - perpendicular to traffic	2.0896×10^{11}	-1.9400	0.7056	1.0540	0.0412	0.9995
iwp - parallel to traffic	1.2841×10^{9}	-1.7704	0.2223	1.1155	0.0252	0.9998
all locations	3.0896×10^{11}	-1.9760	0.7141	1.0173	0.06984	0.9984

iwp = inner wheelpath

Note: Shaded cells indicate that regressor is statistically not significant.

compared to the other specimen sets. In addition, significant differences were not found between any of the specimen sets and the summary model fitted from the combined data. Figure 4.11 corroborates the statistical finding of a difference in the fitted models for the inner and outer wheelpath specimens that were oriented perpendicular to the direction of traffic; however, it appears that there should also be a difference between the center of lane model and that for the inner wheelpath oriented parallel to the direction of traffic.

An evaluation of equation 2.5 indicated that the inclusion of the initial stiffness does not significantly improve the model for any specimen set, as the stiffness coefficient was found to be non-significant in the model. Further assessment of the model for this data set was halted upon this conclusion.

Table 4.29 Location effect comparison using coincidence of slopes and intercepts (α=0.05).

$N_f = K_0 \times \varepsilon^{K_1}$ Equation (2.2)

Coeff.	Location	All	CL	OWP	IWP-PP	Coeff.	Location	All	CL	OWP	IWP-PP
K_0	CL	NS				K_2	CL				
	OWP	NS	NS				OWP				
	IWP-PP	NS	NS	sig			IWP-PP				
	IWP-PL	NS	NS	NS	NS		IWP-PL				
K_1	CL	NS				K_3	CL				
	OWP	NS	NS				OWP				
	IWP-PP	NS	NS	sig			IWP-PP				
	IWP-PL	NS	NS	NS	NS		IWP-PL				

$N_f = K_0 \times \varepsilon^{K_1} \times CDE^{K_3}$ Equation (4.1)

Coeff.	Location	All	CL	OWP	IWP-PP	Coeff.	Location	All	CL	OWP	IWP-PP
K_0	CL	NS				K_2	CL				
	OWP	NS	NS				OWP				
	IWP-PP	NS	NS	NS			IWP-PP				
	IWP-PL	NS	NS	NS	NS		IWP-PL				
K_1	CL	NS				K_3	CL	NS			
	OWP	NS	NS				OWP	NS	NS		
	IWP-PP	NS	NS	NS			IWP-PP	NS	NS	NS	
	IWP-PL	NS	NS	NS	NS		IWP-PL	NS	NS	NS	NS

sig = Significant difference found.
NS = No significant difference found.

Table 4.30 Average asphalt and air void contents for SM-9.5E section C specimens.

Mixture	Location	Asphalt (%)	VTM (%)
SM-9.5E section C	All	5.80%	8.6%
	CL-PP		7.4%
	OWP-PP		7.5%
	IWP-PP		12.9%
	IWP-PL		6.8%

Table 4.28 also offers results of regression using equation 4.1, and Table 4.29 includes a summary of the differences in coefficients. The addition of cumulative dissipated energy improved the model fit over that seen from equation 2.2. In addition, no significant differences between the coefficients were attributable to location or orientation of the specimen sets. Thus, the summary model was sufficient to use for this modeling process, as no significant differences were found for coefficients between it and any of the location/orientation-differentiated models.

The evaluation of equation 4.2 indicated that, for the inner wheelpath specimens, the initial stiffness was unnecessary to the model. This finding shed doubt upon the integrity of using the model for all specimen sets, so the model was discarded from further evaluation.

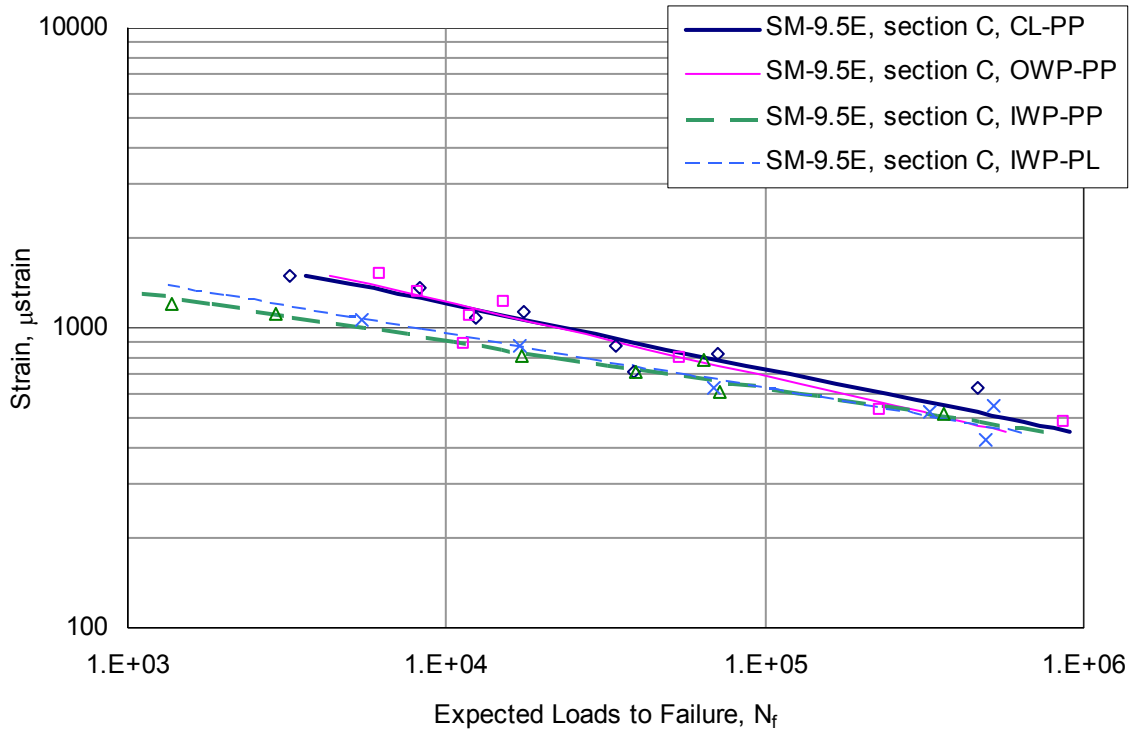

Figure 4.11 Comparison of expected fatigue response, modeled by equation 2.2, for SM-9.5E section C specimen sets with varying locations and orientations.

4.2.6 Performance of Mixtures

The coefficients seen in Table 4 for equation 2.2 were used to predict the fatigue life for each tested mixture under each production/compaction scenario at five strains ranging from 200 to 1000 µstrain. These strains were representative of the testing range used in the laboratory. The resulting comparisons are shown in Figure 4.12 through Figure 4.14.

Figure 4.12 shows the predicted fatigue lives for the field-mixed, laboratory-compacted mixtures. This figure indicates that some field-lab mixtures may have different rankings in terms of fatigue response at different applied strains. At all strains, the SM-9.5E mixture showed the best resistance to fatigue, followed by the SMA-12.5; however, the rankings of the SM-9.5A, SM-9,5D, and SM-12.5D mixtures varied with different strains.

The predicted fatigue lives for the lab-lab mixtures are shown in Figure 4.13. It can be seen that the SM-9.5A mixture produced with high-laboratory compaction exhibits considerably improved fatigue performance as compared to the other mixtures. The SM-9.5D mixture located in sections E-H showed poor fatigue performance as compared to the other mixtures. The remaining five mixtures had relatively similar predicted fatigue performance.

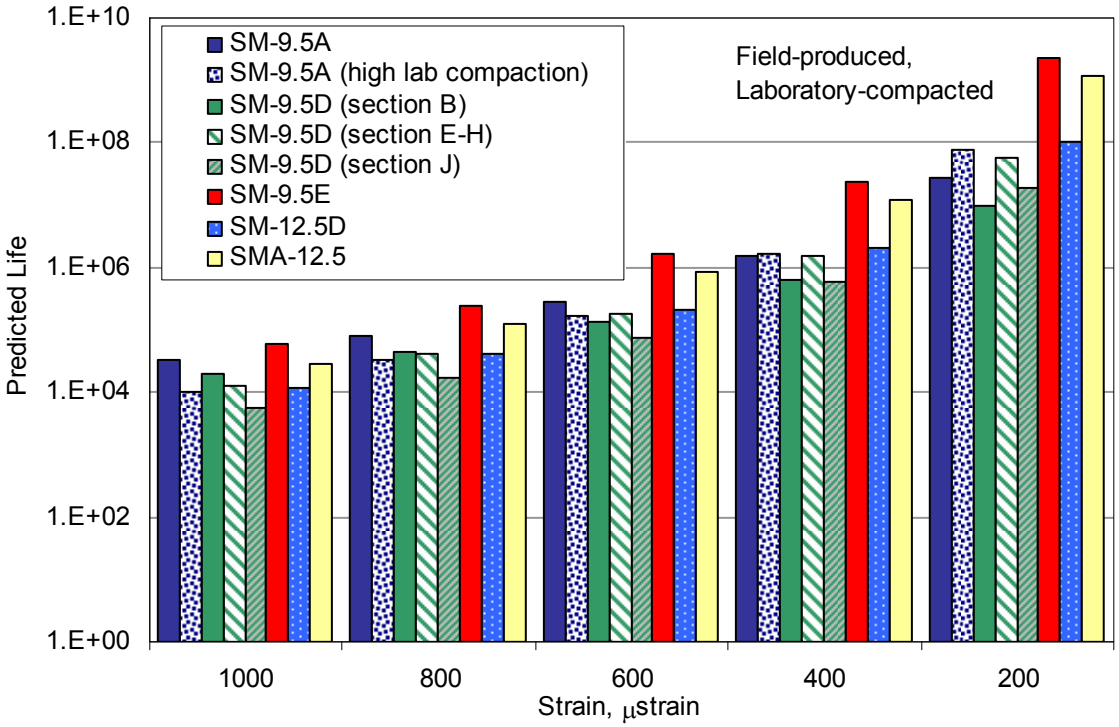

Figure 4.12. Effect of binder type on predicted fatigue life, field-lab mixtures.

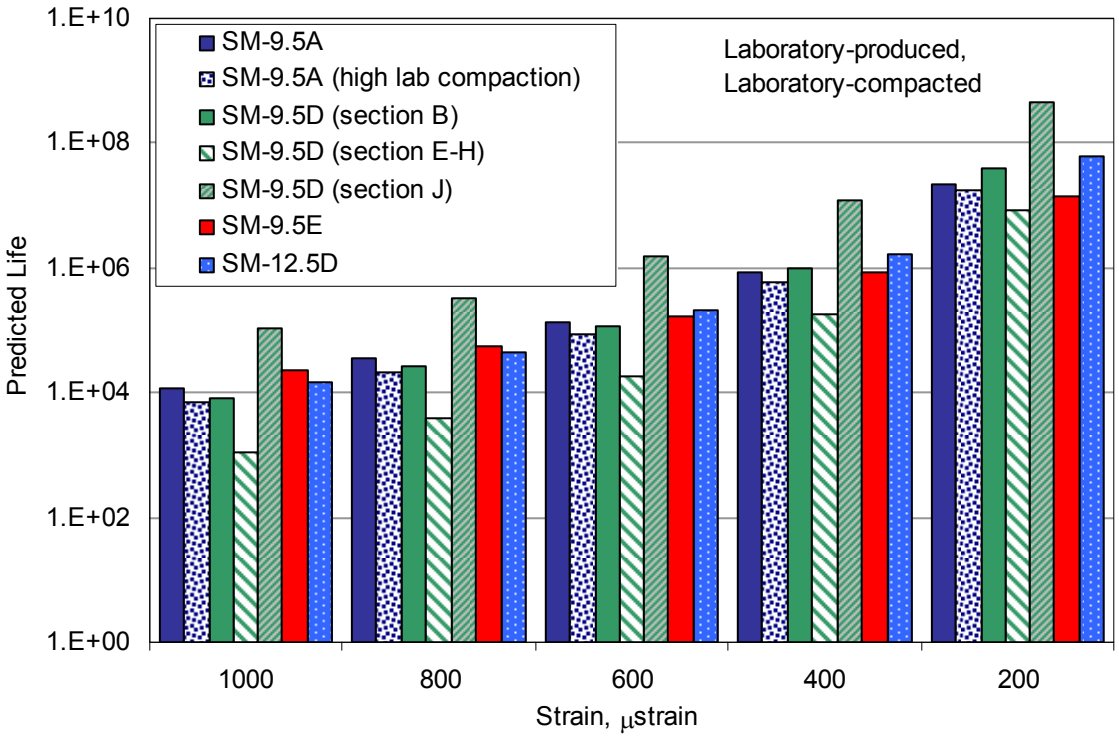

Figure 4.13 Effect of binder type on predicted fatigue life, lab-lab mixtures.

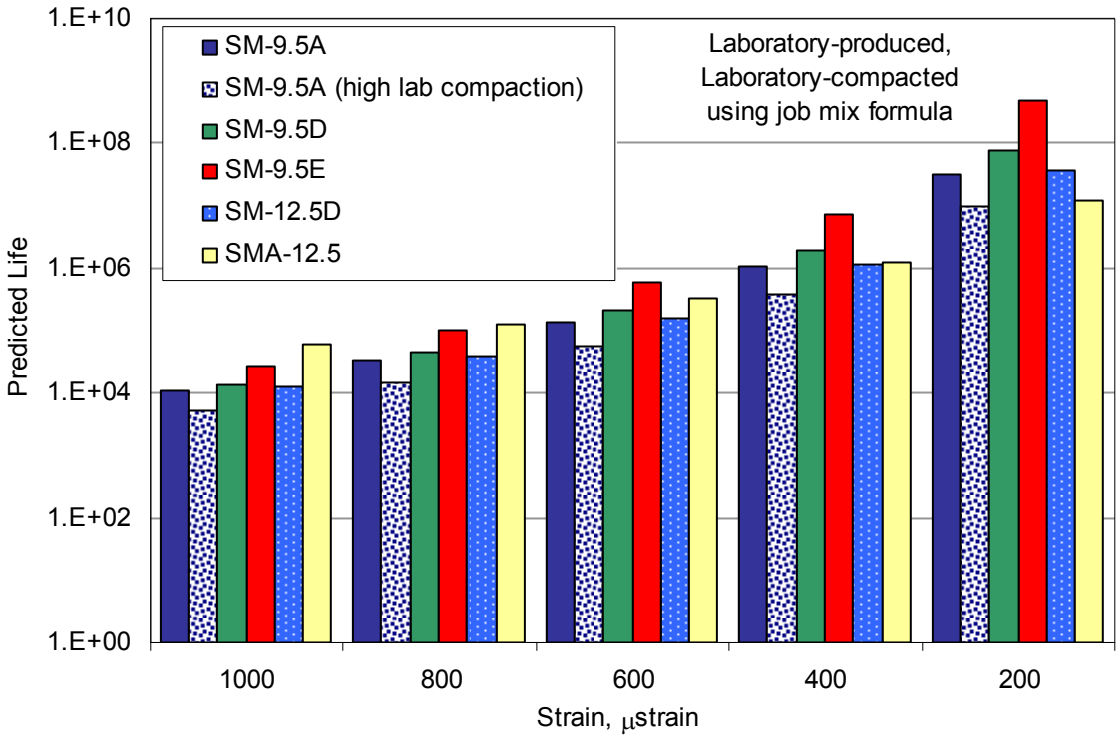

Figure 4.14 Effect of binder type on predicted fatigue life, design-lab mixtures.

Design-lab mixture predicted fatigue lives are compared in Figure 4.14. This figure indicates that SM-9,5E mixture may have the better overall fatigue resistance, based on laboratory design mixtures. The next best performance is shown by the SMA-12.5 mixture at strains of 600 microstrain and above; at lower strains, the predicted life of the SMA-12.5 was less than that of most other mixtures. These results indicate the benefits to fatigue life that can be seen through the use of fiber-modification of mixes or polymer modification of binders; however, the improved performance of these mixes was not apparent across all combinations of production and compaction. This may indicate issues in the production of the mixtures, or other discrepancies.

Evaluation of Aggregate and Binder Effects

Comparisons were performed to evaluate the effects of aggregate size and binder type on fatigue performance during laboratory testing. Figure 4.15 shows the results of the aggregate analysis. The two mixtures shown, SM-12.5D and SM9.5D, were produced using the same PG70-22 binder and having maximum nominal aggregate sizes of 12.5mm and 9.5mm respectively. However, examination of the mixture gradations indicated that the 12.5mm mixtures were fine (nearly meeting the specification for a 9.5mm mixture). Thus the effect of the differing aggregate sizes on the fatigue performance was not able to be appropriately evaluated.

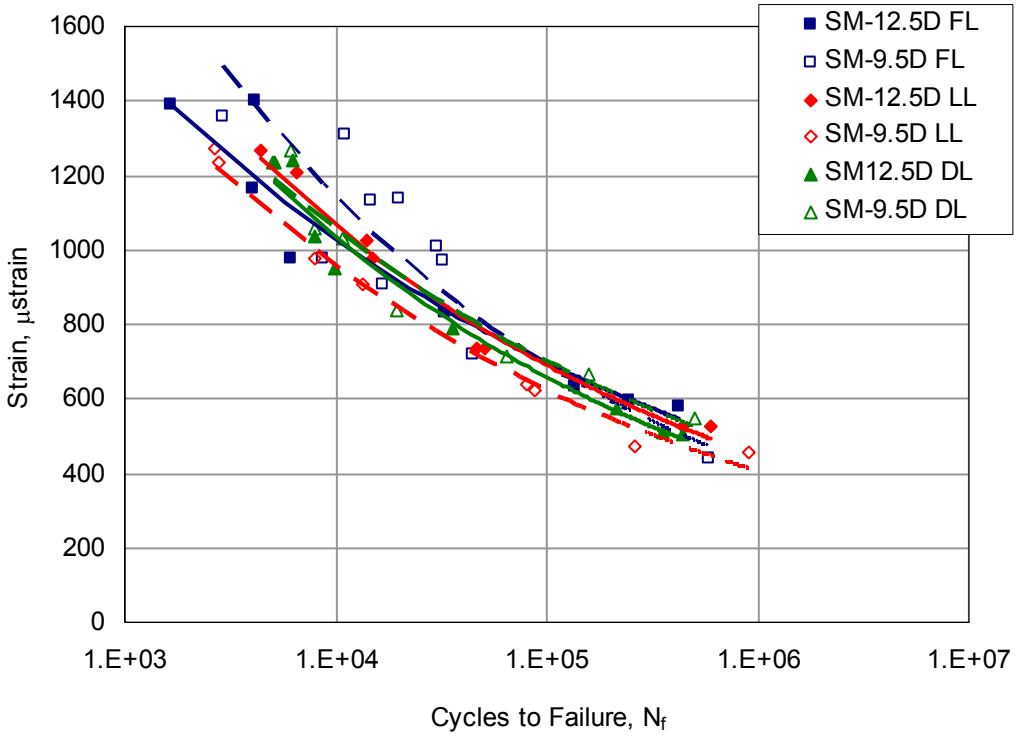

Figure 4.15 Comparison of aggregate effects.

Figure 4.16 through Figure 4.18 show the fatigue response of mixtures containing the three binders used in this study. The binders used included PG64-22, PG70-22, and PG76-22 polymer-modified. It can be seen in Figure 4.16 through Figure 4.18 that the ranking of performance changes for differing production and compaction scenarios. The results indicate that, for the field-lab and lab-lab mixtures, the PG70-22 mixture performs less well than the other mixtures; however for the design-lab samples produced according to the JMF, the PG70-22 showed performance characteristics between the that of the PG64-22 andPG 70-22 mixtures. The mixed responses are likely influenced by the differing binder contents and volumetric properties of the mixes: in every case the PG64-22 binder content is greater than the PG70-22 content. The effects of the PG76-22 polymer-modified binder on fatigue life appear great enough that they are observed even though the binder content of the SM9.5E mixes is, in all cases other than the field-lab, less than that of either the SM9.5A or SM-9.5D mixtures.

4.2.7 Endurance Limit

Comparisons between mixtures were also considered on the basis of the predicted fatigue endurance limit using two methodologies of prediction. It must be noted that there were no means available to validate these predictions, as fatigue testing was not carried out for enough cycles to approach a true endurance limit. However, the predictive comparisons are the most practical and likely means for highway agencies to compare mixtures, as full fatigue testing and advanced analysis are usually beyond the scope of reasonable effort used during the design process.

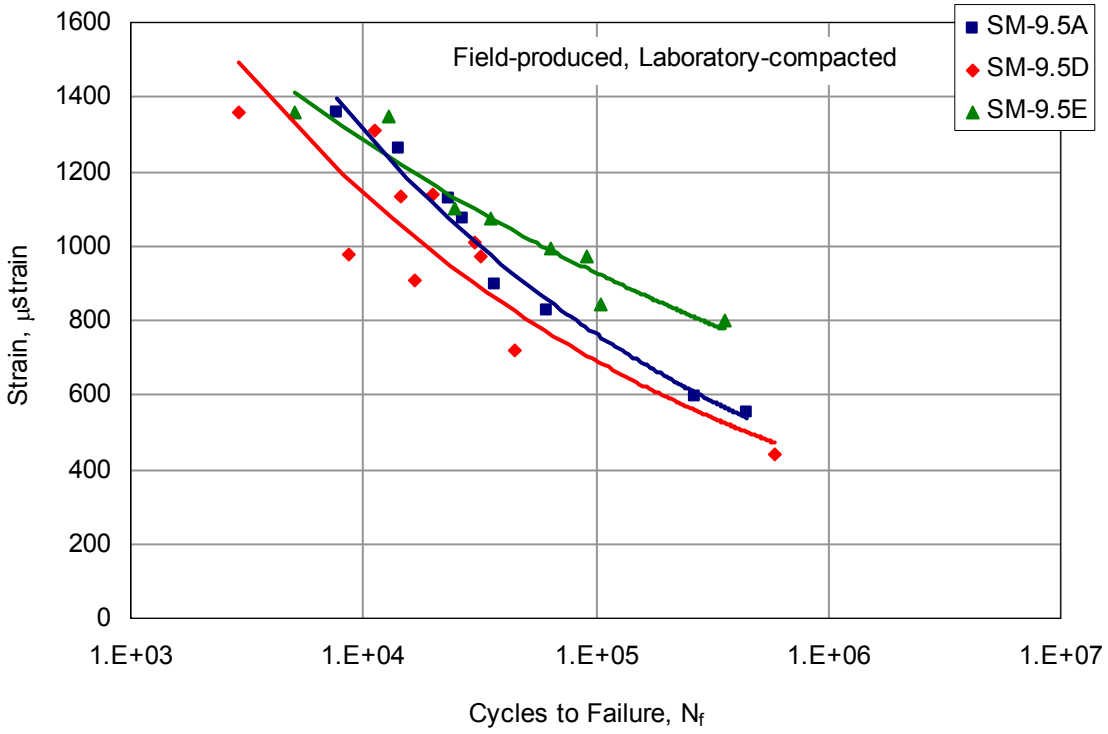

Figure 4.16 Comparison of binder effects on fatigue life, field-lab mixtures.

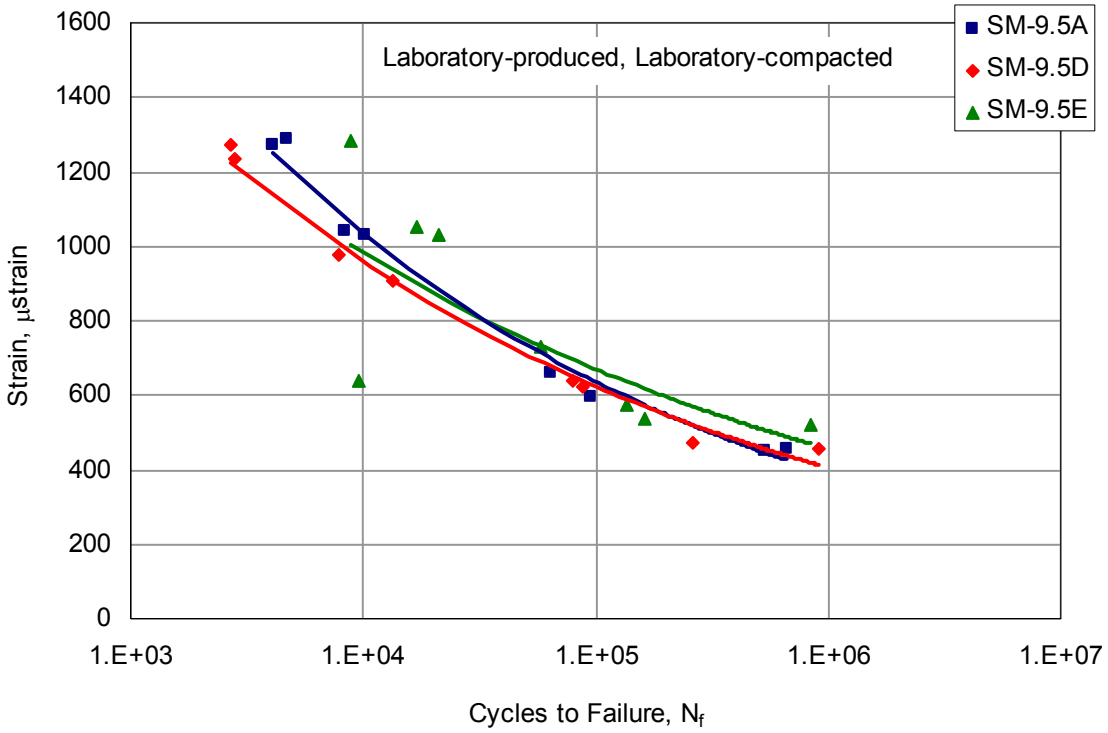

Figure 4.17 Comparison of binder effects on fatigue life, lab-lab mixtures.

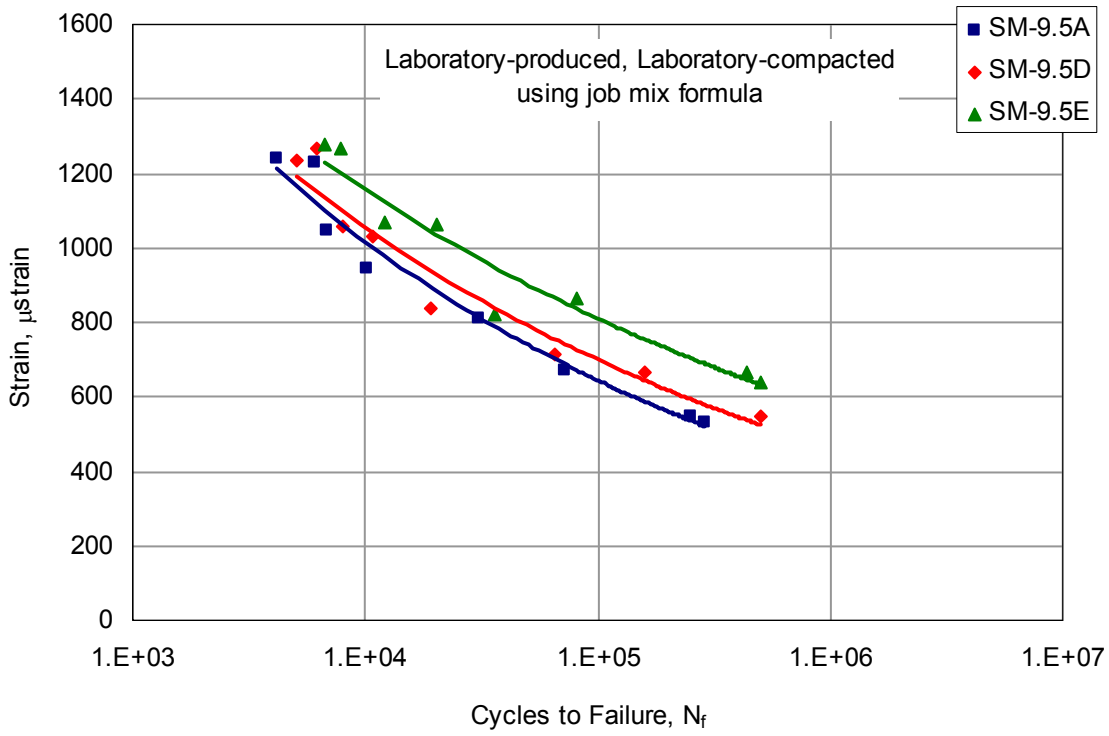

Figure 4.18 Comparison of binder effects on fatigue life, design-lab mixtures.

Two methods of prediction were used in this study. The first is an empirical predictive method that estimates the endurance limit from the lower 95% predictive interval of the expected strain when the fatigue life is extrapolated to 50,000,000 cycles. This method was used by Maupin et al. (2008). The second is an energy method proposed by Shen and Carpenter (2007) based on the ratio of dissipated energy change per cycle.

Empirical Endurance Limit Prediction

The empirical endurance limit prediction uses a regression of the fatigue life versus the applied strain. The regression line is extrapolated to determine the expected applied strain for a fatigue life of 50,000,000 cycles. Then, the value of the applied strain at the lower 95% predictive interval is determined and considered to be the fatigue endurance limit.

Energy Method for Endurance Limit Prediction

Shen and Carpenter (2007) propose an energy based fatigue model based on the ratio of dissipated energy change per cycle (RDEC). During testing, the RDEC becomes constant before dramatically increasing at the onset of true fatigue failure. The constant value of the RDEC, called the plateau value (PV), has been shown by Shen and Carpenter (2005) to be a unique parameter for damage and failure regardless of differing test conditions. From extensive testing, a PV value of 6.74×10^{-9} is recommended as the limiting plateau value to determine the fatigue endurance limit (Shen and Carpenter, 2007). Based on this plateau value, they propose a model for the prediction of the endurance limit:

$$PV = 44.422\,\varepsilon^{5.140}\,S^{2.993}\,VP^{1.850}\,GP^{-0.4063}$$

$$VP = \frac{AV}{AV + V_b}$$

$$V_b = 100 \times \frac{G_{mb}\,P_b}{G_b}$$

$$GP = \frac{P_{NMAS} - P_{PCS}}{P_{200}} \qquad (2.63)$$

where

PV = plateau value,
ε = tensile strain, in/in,
S = flexural stiffness of the mixture from the laboratory fatigue test, MPa,
VP = volumetric parameter,
GP = gradation parameter,
AV = mixture air voids, %,
V_b = mixture asphalt content by volume, %,
G_{mb} = mixture bulk specific gravity,
P_b = mixture asphalt content by total weight of mix, %,
G_b = asphalt binder specific gravity (generally assumed 1.03),
P_{NMAS} = aggregate percent passing the nominal maximum sieve size,
P_{PCS} = aggregate percentage passing the primary control sieve (PCS = NMAS × 0.22), and
P_{200} = aggregate percentage passing the No. 200 (0.075mm) sieve.

This method was applied to the fatigue data collected in this study to predict the fatigue endurance limit for each mixture. The results are summarized in Table 4.31. A paired t-test was performed using all data to determine if the results from each method of determination were statistically equivalent. The two-sided p-value from the test was found to be 0.00001, indicating that the endurance limits determined using the two methods are significantly different. The correlation coefficient for the data sets was also calculated and found to be 0.1442, indicating little correlation between the results using the two methods. The lack of equivalence and correlation brings forth the question of which method is most appropriate for use. This should be determined with additional testing performed for durations of cycles much closer to the endurance limit than the testing performed in this study.

4.3 SUMMARY

Fatigue testing using the third point beam fatigue test was performed on five mixtures under four sets of production and compaction conditions. Test results were analyzed to determine characteristic strain-life curves for each mixture. The fatigue responses of the mixtures were evaluated to identify mixture characteristics having significant effects upon the fatigue service life of HMA. Additionally, the plateau values and fatigue strain endurance limits of the mixtures were calculated and compared.

Table 4.31 Fatigue strain endurance limits for all mixtures using the energy and empirical prediction methods.

Mixture	Section	Preparation Method	Energy Method		Empirical Prediction
			Average ε_L	Std. Deviation	ε_L
SM-9.5A	D	field-lab	0.000177	0.000011	0.000138
		lab-lab	0.000227	0.000012	0.000135
		design-lab	0.000315	0.000045	0.000146
	I[a]	field-lab	0.000176	0.000013	0.000186
		lab-lab	0.000408	0.000096	0.000135
		design-lab	0.000221	0.000015	0.000101
SM-9.5D	B	field-lab	0.000172	0.000025	0.000091
		lab-lab	0.000240	0.000013	0.000151
		design-lab	0.000262	0.000015	0.000164
	E	field-lab	0.000173	0.000004	0.000160
	F	field-lab	0.000160	0.000006	0.000174
	G	field-lab	0.000162	0.000009	0.000111
	H	field-lab	0.000168	0.000012	0.000111
	E - H	lab-lab	0.000195	0.000013	0.000167
	J	field-lab	0.000162	0.000007	0.000121
		lab-lab	0.000194	0.000016	0.000174
SM-9.5E	C	field-lab	0.000212	0.000020	0.000283
		lab-lab	0.000195	0.000017	0.000094
		design-lab	0.000292	0.000037	0.000224
		field-field (OWP)	0.000197	0.000029	0.000092
		field-field (CL)	0.000209	0.000020	0.000123
		field-field (IWP PP)	0.000213	0.000017	0.000166
		field-field (IWP PL)	0.000224	0.000020	0.000132
SM-12.5D	A	field-lab	0.000197	0.000015	0.000167
		lab-lab	0.000206	0.000012	0.000167
		design-lab	0.000252	0.000013	0.000151
SMA-12.5	L	field-lab	0.000437	0.000087	0.000210
		design-lab	0.000349	0.000043	0.000076

[a]Designed with high laboratory compaction.
OWP - outer wheelpath; CL- center of lane; IWP PP - inner wheelpath, perpendicular to direction of traffic; IWP PL - inner wheelpath, parallel to direction of traffic.

Comparisons of expected fatigue performance for mixtures produced using different methods were made using the traditional strain-life relationship. Comparisons between the field-lab and lab-lab specimens sets showed no significant differences between production at the plant and in the laboratory. No differences were seen when the lab-lab and design-lab specimen sets were compared. For the field-lab and design-lab comparison, only two mixtures indicated significant differences in the strain-life relationship. One mixture was found to have considerable differences in the specimen air void content between the two production methods, which explained the difference in fatigue performance; however the second mixture did not show any clear reason for the difference in expected performance. Overall, this portion of the study indicated that small differences in mixture volumetrics due to the production method (at the plant

or in the laboratory) or due to the accuracy in replicating the job mix formula do not appear to have significant impact on the laboratory fatigue performance of HMA.

Comparisons of expected fatigue performance for mixture compacted in the field and compacted in the laboratory were also made using the traditional strain-life relationship. The differences that were seen in two of the three comparisons indicated a shift in the strain-life curve resulting in predictions of shorter fatigue lives (under the same strain conditions) for laboratory-compacted specimens when compared to field-compacted specimens. Interestingly, this result was found despite the visual observation of surface cracking in the field-compacted specimens, which were assumed to have sustained some damage during the collection process.

Analysis of testing performed on one mixture (SM-9.5E) to determine the influence of different loading frequencies indicated that fatigue life was independent of the frequencies tested (1Hz, 5 Hz, and 10Hz) for the strain ranges investigated. An investigation of the effect of rest periods was also performed on the SM-9.5E mixture and indicated that no differences in fatigue life were expected for loading conducted at 10 Hz frequency and no rest period, 0.4sec rest period, or 0.9sec rest period. Examination of the data from the SM-9.5E field-field specimens cut from different locations and in different orientations indicated that location and orientation did not significantly affect the laboratory fatigue performance.

The effect of aggregate size on fatigue performance was also considered in this study; however, due to the limited number of mixtures, results were inconclusive. The effect of binder type on fatigue performance was also investigated. Overall, the mixtures containing PG76-22 showed improved fatigue life over those containing PG70-22 and PG64-22 binders.

Using the predictive fatigue equations developed for each mixture, the benefits of polymer-modification of binders and use of SMA were seen for the field-lab and design-lab mixtures. In all production and compaction scenarios, the ranking of mixtures were shown to change when varying the applied strain.

The plateau value analysis indicated that the values determined from regression of the data did not agree with those determined using equation (4.8). Values determined from the equation were considered to be less biased due to user calculation, and were thus used for further comparisons of the mixture performance. These comparisons showed no difference in plateau value between the field-lab specimens for sections E, F, G, and H, indicating that production variability is not expected to significantly affect fatigue life. Additionally, significant differences in plateau value indicating differences in fatigue performance due to production and compaction methods were only found for four of forty cases.

Evaluation of the predicted fatigue strain endurance limit was performed using two methods, an energy-based method and an empirical method. The energy method was shown to estimate significantly higher endurance limit strains for mixtures than the empirical method. The lack of equivalence and correlation brings forth the question of which method is most appropriate for use. This should be determined with additional testing performed for durations of cycles much closer to the endurance limit than the testing performed in this study.

5 SUMMARY, FINDINGS, AND CONCLUSIONS

5.1 SUMMARY

Fatigue testing of Superpave surface mixtures in use at the Virginia Smart Road was performed for mixture characterization and evaluation purposes. The response of the mixtures in fatigue testing and equations relating applied strain and resulting fatigue life were presented. Evaluation of the effects on laboratory fatigue life of specimen location and orientation within the pavement surface was performed. Differences between field and laboratory production and compaction were discussed and their effect on mixture fatigue resistance was considered. The effects of aggregate size and binder type on fatigue life were determined. Finally, the fatigue responses of the tested mixtures were compared and differences in the predicted fatigue life were evaluated.

It should be noted that the results and conclusions of this study are applicable only to the surface mixtures tested and should not be carelessly generalized to other VDOT or Superpave mixtures without verification.

5.2 FINDINGS

Results from the fatigue evaluation indicated several findings related to mixture production and compaction and fatigue performance with respect to the mixtures evaluated in this study. The following findings are presented:

Comparisons of the expected fatigue performance for mixtures produced using different methods were made using the traditional strain-life relationship. Comparisons between the field-lab and lab-lab specimen sets and between the design-lab and lab-lab specimen sets showed no significant differences between the production and compaction scenarios. For the field-lab and design-lab comparison, only two mixtures indicated significant differences in the strain-life relationship. The SMA-12.5 mixture was found to have considerable differences in the specimen air voids content between the two production methods, which explained the difference in fatigue performance; however the SM-9.5D section B mixture did not show any clear reason for the discrepancy in expected performance. Overall, this portion of the study indicated that small differences in mixture volumetrics due to the production method (at the plant or in the laboratory) or due to the accuracy in replicating the job mix formula appear to have little significant impact on the laboratory fatigue performance of HMA as measured by the traditional strain-life relationship.

Comparisons of expected fatigue performance for the SM-9.5E mixture compacted in the field and compacted in the laboratory were also made using the traditional strain-life relationship. The differences that were seen in two of the three production-compaction comparisons indicated a shift in the strain-life curve resulting in predictions of shorter fatigue lives (under the same strain conditions) for laboratory-compacted specimens when compared to field-compacted specimens. Interestingly, this result was found despite the visual observation of

surface cracking in the field-compacted specimens, which were assumed to have sustained some damage during the collection process.

Analysis of testing performed on design-lab specimens of the SM-9.5E mixture to determine the influence of different loading frequencies indicated that fatigue life was independent of the frequencies tested (1Hz, 5 Hz, and 10Hz). An investigation of the effect of rest periods was also performed on the same design-lab SM-9.5E mixture and suggested that no differences in fatigue life were expected for loading conducted at 10 Hz frequency and no rest period, 0.4sec rest period, or 0.9sec rest period. Examination of the data from the SM-9.5E field-field specimens cut from different locations and in different orientations indicated that location and orientation did not significantly affect the laboratory fatigue performance.

The effect of aggregate size on fatigue performance was considered in this study; however, as the 12.5mm mixture gradation was very fine and nearly met the specification for a 9.5mm gradation, results were inconclusive.

The effect of binder type on fatigue performance was investigated. Overall, the mixtures containing PG76-22 binder showed improved fatigue life over those containing PG70-22 and PG64-22 binders. One influence on this finding was the inclusion of the SMA-12.5 mixture in the study as SMA is considered to have improved performance due to the interlock provided by the mixture aggregate structure.

Using predictive fatigue equations developed for each mixture, the benefits of polymer-modification of binders and use of SMA were generally seen for the field-lab and design-lab mixtures. The rankings of all other mixtures changed dependent on the production and compaction scenario and the applied strain.

The plateau value analysis indicated that the values determined from regression of the data did not agree with those determined using equation 4.8. Values determined from the equation were considered to be less biased and were thus used for further comparisons of the mixture performance. These comparisons showed no difference in plateau value between the SM-9.5D field-lab specimens for sections E, F, G, and H, indicating that production variability is not expected to significantly affect fatigue life. Additionally, significant differences in plateau value indicating differences in fatigue performance due to production and compaction methods were only found for four of forty cases.

Evaluation of the predicted fatigue strain endurance limit was performed using two methods, an energy-based method and an empirical method. The energy method was shown to estimate significantly higher endurance limit strains for mixtures; further testing and analysis is necessary to determine which method is most appropriate for use.

5.3 CONCLUSIONS

Considering the responses from the mixtures evaluated in this study, it can be concluded that laboratory fatigue life is not significantly impacted by whether a mixture is produced in the laboratory or plant. Any impact is most likely due to differences in variability inherent in a

large-batch process as compared to the lesser volumes produced in laboratory batches. Out of the 31 comparisons performed, only two indicated significant differences due to production or compaction method, and these did not indicate trends in the same direction. Of these, one appeared to be directly attributable to a difference in air void content; the other failed to indicate a material reason for the difference.

Compaction appeared to have a mixed influence on fatigue life as well. Two of the three comparisons between the SM-9.5E mixture sampled from the field and those compacted in the laboratory indicated that the in-situ mixture should be expected to have increased fatigue life over that predicted for the laboratory-compacted mixtures.

Based on the results of the SM-9.5E mixture tested, no significant differences in the laboratory fatigue life are expected when mixtures are tested at frequencies of 1 Hz, 5 Hz, or 10Hz. Additionally, no differences in the laboratory fatigue life should be expected due to the inclusion of rest periods of 0.4sec or 0.9sec when testing is performed at a frequency of 10 Hz.

Binder evaluation indicated that, for mixes produced in the laboratory according to the job mix formula, polymer modification resulted in improvements to fatigue life. Overall comparison of the mixtures indicated mixed performance. Predicted fatigue lives for each mixture indicated that use of polymer-modification or SMA mixtures enhanced fatigue performance when the mixtures were produced according to the job mix formula; deviations from the job mix formula affected the predicted fatigue performance.

Analysis of fatigue using the plateau value should be conducted with the equation developed by Shen and Carpenter (2007), rather than using the calculation method proposed by Shen (2006) to avoid the potential for bias inherent in the Shen calculation method. Significant differences in the plateau value indicating differences in fatigue performance due to production and compaction methods were only found for four of forty cases, further reinforcing the conclusion that production and compaction methods inconsistently affect fatigue performance.

Determination of the fatigue strain endurance limit may be accomplished by different methods. Testing to a high number of cycles to failure may be necessary to validate the appropriate method, as results were mixed from the methods investigated in this study. The energy method estimated higher endurance limit strains for mixtures than the empirical method, although there was no data available to verify which was more accurate. Ranking of mixtures between the two methods was not consistent.

6 RECOMMENDATIONS

Testing was performed on variations of six Superpave mixtures having specific properties. Additional testing using controlled changes in mixture properties such as gradation, asphalt content, and air voids for each mixture should be performed to fully quantify the effects of these variables and to evaluate the dependence of fatigue life on volumetric properties. Additional testing on samples from the in-situ pavement should be evaluated to verify the results obtained herein regarding in-situ mixture variability and specimen orientation.

Fatigue evaluation of mixtures at different temperatures should be performed to characterize and quantify the temperature susceptibility of these mixtures under fatigue loading. Testing should also be performed on the asphalt base mixtures to evaluate their fatigue properties and contributions to the overall pavement fatigue response. Consideration should also be given to the development of relationships between fatigue performance and dynamic modulus to provide another means of validation during pavement design.

Additional analysis should be performed to further evaluate the ability of the vibratory compactor to replicate in-situ material volumetric properties. The consideration of differing mold capacities and the effects on the resulting volumetric properties should be considered, as should the effect of using un-cut as-compacted specimens versus specimens cut from larger slabs. Since specimens cut from the in-situ pavement have different surface conditions from the specimens utilized in this study, assessment should be made of the significance of such effects.

Additional work is necessary to further pursue quantification of the fatigue endurance limit and determine the limits of its use in quantifying mixture performance. Care should be taken in this work to provide useful outcomes that may be used by pavement designers to choose the best-performing mixture at the design stage of projects.

Finally, application of the presented fatigue life models to pavement designs should be performed by comparing the fatigue response from the laboratory testing with observed fatigue development in in-situ pavements. This should result in quantifiable response model to explain the discrepancies seen between laboratory fatigue and in-situ pavement fatigue.

REFERENCES

Adedimila, A. S. and T. W. Kennedy. (1976) “Repeated-Load Indirect Tensile Fatigue Characteristics of Asphalt Mixtures.” Transportation Research Record, no. 595, Transportation Research Board, Washington, DC, pp. 25-33.

Asphalt Institute. (1981) Thickness Design Manual. 9th edition, The Asphalt Institute, College Park, MD.

Asphalt Institute. (1996) Superpave Mix Design. Superpave Series No. 2, Asphalt Institute, Lexington, KY, 117p.

Baladi, G. Y., R. S. Harichandran, and R. W. Lyles. (1988) “New Relationship between Structural Properties and Asphalt Mix Parameters.” Transportation Research Record, no. 1171, Transportation Research Board, Washington, DC, pp. 168-177.

Balbissi, A. H. (1983) A Comparative Analysis of the Fracture and Fatigue Properties of Asphalt Concrete and Sulphlex. PhD thesis, Texas A&M University, College Station, TX.

Bazin, P. and J. B. Saunier. (1967) “Deformability, Fatigue, and Healing Properties of Asphalt Mixes.” Proceedings of the Second International Conference on the Structural Design of Asphalt Pavements, Ann Arbor, MI, pp. 553-569.

Bell, C. A., R. G. Hicks, and J. E. Wilson. (1984) “Effect of Percent Compaction on Asphalt Mixture Life.” ASTM Special Technical Publication, no. 829, ASTM, Philadelphia, Pa, pp. 107-130.

Bonnaure, F., A. Gravois, and J. Udron. (1980) “A New Method for Predicting the Fatigue Life of Bituminous Mixes.” Journal of the Association of Asphalt Paving Technologists, vol. 49, pp. 499-529.

Bonnaure, F. P., A. H. J. J. Huibers, and A. Boonders. (1982) “A Laboratory Investigation of the Influence of Rest Periods on the Fatigue Characteristics of Bituminous Mixes.” Proceedings of the Association of Asphalt Paving Technologists, vol. 51, pp. 104-128.

Brennan, M. J., J. Meade, M. Hynes, D. J. Murphy, and C. Lycett. (1996) "A Piot Study of the Performance of Porous Asphalt in Static Creep and Repeated Loading." Proceedings of the Eurasphalt and Eurobitume Congress, Strasbourg, France.

Buttlar, W. G. and R. Roque. (1994) “Development and Evaluation of the Strategic Highway Research Program Measurement and Analysis System for Indirect Tensile Testing at Low Temperatures.” Transportation Research Record, no. 1454, Transportation Research Board, Washington, DC, pp. 163-171.

Button, J. W., D. N. Little, V. Jagadam, and O. J. Pendleton. (1994) “Correlation of Selected Laboratory Compaction Methods with Field Compaction.” Transportation Research Record, no. 1454, Transportation Research Board, Washington, DC, pp. 193-201.

Carpenter, S. H., K. A. Ghuzlan, and S. Shen. (2003) “A Fatigue Endurance Limit for Highway and Airport Pavement.” Transportation Research Record, no. 1832, Transportation Research Board, Washington, DC, pp. 131-138.

Carpenter, S. H. and S. Shen. (2006) “Dissiated Energy Approach to Study Hot-Mix Asphalt Healing in Fatigue.” Transportation Research Record, no. 1970, Transportation Research Board, Washington, DC, pp. 178-185.

Christensen, D. W. (1998) "Analysis of Creep Data from Indirect Tension Test on Asphalt Concrete." Journal of the Association of Asphalt Paving Technologists, vol. 67, pp. 458-492.

Collop, A. C. and D. Cebon. (1996) “Stiffness Reduction of Flexible Pavement due to Cumulative Fatigue Damage.” Journal of Transportation Engineering, vol. 122, no. 2, 131-139.

Consuegra, A., D. N. Little, H. Von Quintus, and J. Burati. (1989) “Comparative Evaluation of Laboratory Compaction Devices Based on Their Ability to Produce Mixtures with Engineering Properties Similar to Those Produced in the Field.” Transportation Research Record, no. 1228, Transportation Research Board, Washington DC, pp. 80-87.

Daniel, J.S., W. M. Bisirri, and Y. R. Kim. (2004) Fatigue Evaluation of Asphalt Mixtures Using Dissipated Energy and Viscoelastic Continuum Damage Approach.” Journal of the Association of Asphalt Paving Technologists, vol. 73, pp. 557-583.

Daniel, J. S. and W. M. Bisirri. (2005) “Characterizing Fatigue in Pavement Materials Using a Dissipated Energy Parameter.” Soil Constitutive Models: Evaluation Selection and Calibration, Geotechnical Special Publication no. 128, American Society of Civil Engineers, Reston, VA pp. 199-208.

Deacon, J. A. and C. L. Monismith. (1967) “Laboratory Flexural-Fatigue Testing of Asphalt-Concrete With an Emphasis on Compound-Loading Tests.” Highway Research Record, no. 158, Highway Research Board, Washington, DC, pp. 1-32.

Deacon, J. A., J. S. Coplantz, A. A. Tayebali, and C. L. Monismith. (1994) “Temperature Considerations in Asphalt-Aggregate Mixture Analysis and Design.” Transportation Research Record, no. 1454, pp. 97-112.

Deacon, J. A., A. A. Tayebali, G. M. Rowe, and C. L. Monismith. (1995a) “Validation of SHRP A-003A flexural beam fatigue test.” ASTM Special Technical Publication, no. 1265, ASTM, Philadelphia, PA, pp. 21-36.

Deacon, J. A., R. B. Leahy, and C. L. Monismith. (1995b) “Mix Testing and Analysis Systems Resulting from SHRP Contract A-003A.” Transportation Congress, Proceedings, vol. 1, ASCE, New York, NY, 691-711.

Federal Highway Administration. (2007) “Highway Statistics 2007.” http://www.fhwa.dot.gov/policyinformation/statistics/2007/ (accessed 11/11/09).

Francken, L. (1979) “Fatigue Performance of a Bituminous Road Mix Under Realistic Test Conditions.” Transportation Research Record, no. 712, Transportation Research Board, Washington, DC, pp. 30-37.

Francken, L. and J. Verstraeten. (1974) “Methods for Predicting Moduli and Fatigue laws of Bituminous Road Mixtures under Repeated Bending.” Transportation Research Record, no. 515, Transportation Research Board, Washington, DC, pp. 114-123.

Francken, L. and J. Verstraeten. (1998) “Interlaboratory Test Program on Complex Modulus and Fatigue”. RILEM Report 17, Bituminous Binders and Mixes, London, pp. 182-215.

Ghuzlan, K. and S. H. Carpenter. (2000) “An Energy-Derived / Damage-Based Failure Criteria for Fatigue Testing.” Transportation Research Record, no. 1723, Transportation Research Board, Washington, DC, pp. 141-149.

Ghuzlan, K. (2001) “Fatigue Damage Analysis in Asphalt Concrete Mixtures Based Upon Dissipated Energy Concepts.” Ph.D. Thesis, Universotu of Illinois at Urbana-Champaign, Urbana, IL, 282p.

Hadley, W. O. and H. Vahida. (1983) "Fundamental Comparison of the Flexural and Indirect Tension Tests." Transportation Research Record, no. 911, Transportation Research Board, Washington, DC, pp. 42-51.

Harvey, J. and C. L. Monismith. (1993) “Effects of Laboratory Asphalt Concrete Specimen Preparation Variables on Fatigue and Permanent Deformation Test Results Using Strategic Highway Research Program A-003A Proposed Testing Equipment.” Transportation Research Record, no. 1417, Transportation Research Board, Washington, DC, pp. 38-48.

Harvey, J., T. Lee, J. Sousa, J. Pak, and C. L. Monismith. (1994) “Evaluation of Fatigue and Permanent Deformation Properties of Several Asphalt-aggregate Field Mixes Using Strategic Highway Research Program A-003A Equipment.” Transportation Research Record, no. 1454, Transportation Research Board, Washington, DC, pp. 123-133.

Harvey, J. T. and B. Tsai. (1996) “Effects of Asphalt Content and Air Void Content on Mix Fatigue and Stiffness.” Transportation Research Record, no. 1543, Transportation Research Board, Washington, DC, pp. 38-45.

Hveem, F. N. and R. M. Carmany. (1948) "The Factors Underlying the Rational Design of Pavements." Proceedings of Highway Research Board, vol. 28, Highway Research Board, Washington, DC, pp. 101-136.

Irwin, L. H. and B. M. Gallaway. (1974) "Influence of Laboratory Test Method on Fatigue Test Results for Asphaltic Concrete." ASTM Special Technical Publication 561, American Society for Testing and Materials, Philadelphia, PA, pp. 12-46.

Jacobs, M. M. J., P. C. Hopman, and A. A. A. Molenaar. (1996) "The Crack Growth Mechnaism in Asphalt Mixes." Proceedings of the Eurasphalt and Eurobitume Congress, Strasbourg, France.

Khalid, H. A. (2000a) “Comparison Between Bending and Diametral Fatigue Tests for Bituminous Materials.” Materials & Structures, vol. 33, no. 231, pp. 457-465.

Khalid, H A. (2000b) “Evaluation of Asphalt Fatigue Properties in the Laboratory.” roceedings of the Institution of Civil Engineers-Transport, vol. 141, no. 4, pp. 171-178.

Khan, Z. A., H. I. Al-Abdul, I. Asi, R. Ramadhan. (1998) “Comparative Study of Asphalt Concrete Laboratory Compaction Methods to Simulate Field Compaction.” Construction and Building Materials, vol. 12, no. 6-7, pp. 373-384.

Khedaywi, T. S. and T. D. White. (1996) “Effect of Segregation on Fatigue Performance of Asphalt Paving Mixtures.” Transportation Research Record, no. 1543, Transportation Research Board, Washington, DC, pp. 63-70.

Kim, Y. R. (1988) "Evaluation of Healing and Constitutive Modeling of Asphalt Concrete by Means of the Theory of Nonlinear Viscoelasticity and Damage Mechanics." PhD Dissertation, Texas A&M University.

Kim, Y.R., D. N. Little, and F. Benson. (1990) “Chemical and Mechanical Evaluation on Healing Mechanism of Asphalt Concrete.” Journal of the Association of Asphalt Paving Technologists, vol. 59, pp. 240-276.

Kim, Y. R., N. Kim, and N. P. Khosla. (1992) “Effects of Aggregate Type and Gradation on Fatigue and Permanent Deformation of Asphalt Concrete.” ASTM Special Technical Publication, no. 1147, ASTM, Philadelphia, PA, pp. 310-328.

Kim, Y. R., H.-J. Lee, and D. N. Little. (1997) "Fatigue Characterization of Asphalt Concrete Using Viscoelasticity and Continuum Damage Theory." Journal of the Association of Asphalt Paving Technologists, vol. 66, pp. 521-569.

Kim, Y. R., D. N. Little, and F. C. Benson. (1998) "Fundamental Properties of Asphalts and Modified Asphalts." Volume 4, Final Report, Texas A&M University.

Leahy, R. B., C. L. Monismith, and J. R. Lundy. (1995) “Performance-Based Properties of Asphalt Concrete Mixes.” ASTM Special Technical Publication, no. 1265, ASTM, Philadelphia, PA, pp. 37-54.

Lee, H-J. (1996) Uniaxial Constitutive Modeling of Asphalt Concrete Using Viscoelasticity and Continuum Damage Theory. Ph.D. Thesis, North Carolina State University, Raleigh, NC.

Lee, H.-J., J. S. Daniel, and Y. R. Kim. (2000) “Continuum Damage Mechanics-Based Fatigue Model of Asphalt Concrete.” Journal of Materials in Civil Engineering, vol. 12, no. 2, pp. 105-112.

Liang, R. Y. and J. Zhou. (1997) “Prediction of Fatigue Life of Asphalt Concrete Beams.” International Journal of Fatigue, vol. 19, no. 2, pp. 117-124.

Little, D. N., R. L. Lytton, D. Williams, and Y. R. Kim. (1999) “An Analysis of the Mechanism of Microdamage Healing Based on the Application of Micromechanics First Principles of Fracture and Healing.” Journal of the Association of Asphalt Paving Technologists, vol. 68, 501-542.

Little, D.N., R. L. Lytton, D. Williams, and C. W. Chen. (2001) “Microdamage Healing in Asphalt and Asphalt Concrete, Volume I: Microdamage and Microdamage Healing, Project Summary Report.” Report FHWA-RD-98-141, Federal Highway Administration, McLean, VA, 76p.

Lytton, R. L., J. Uzan, E. G. Fernando, R. Roque, D. Hiltunen, and S. M. Stoffels. (1993) Development and Validation of Performance Prediction Models and Specifications for Asphalt Binders and Paving Mixes. Report SHRP-A-357, Strategic Highway Research Program, National Research Council, Washington, DC, 294p.

Lytton, R. L., C. W. Chen, and D. N. Little. (1998) “A Micromechanics Fracture and Healing Model for Asphalt Concrete.” Final Report Project 7229, Volume 3, Task K - Microdamage Healing in Asphalt and Asphalt Concrete, Texas A&M University.

Lytton, R. L. (2000) “Characterizing Asphalt Pavements for Performance.” Transportation Research Record, no. 1723, Transportation Research Board, Washington, DC, pp. 5-16.

Majidzadeh, K., E. M. Kauffmann, and D. V. Ramsamooj. (1971) “Application of Fracture Mechanics in the Analysis of Pavement Fatigue.” Proceedings of the Association of Asphalt Paving Technologists, vol. 40, pp. 227-246.

Majidzadeh, K., E. M. Kauffman, and C. W. Chang. (1973) Verification of Fracture MechanicsConcepts ot Predict Fatigue Cracking in Pavements. Report No. FHWA-RD-73-91, Federal Highway Administration, Washington, DC.

Masad, E., S. Muhunthan, N Shashidhar, and T. Harman. (1999) "Quantifying Laboratory Compaction Effects on the Internal Structure of Asphalt Concrete." Transportation Research Record, no. 1681, Transportation Research Board, Washington, DC, pp. 179-185.

Matthews, J. M. and C. L. Monismith. (1993) “Direct Tension and Simple Stiffness Tests. Tools for the Fatigue Design of Asphalt Concrete Layers.” Transportation Research Record, no. 1388, Transportation Research Board, Washington, DC, pp. 182-199.

Matthews, J. M., C. L Monismith, and J. Craus. (1993) “Investigation of Laboratory Fatigue Testing Procedures for Asphalt Aggregate Mixtures.” Journal of Transportation Engineering, vol. 119, no. 4, pp. 634-654.

Maupin, G. W. (1972) "Results of Indirect Tensile Tests Related to Asphalt Fatigue." Highway Research Record, no. 404, Highway Research Board, Washington, DC, pp. 1-7.

Maupin, G. W. and J. R. Freeman. (1976) “Simple Procedure for Fatigue Characterization of Bituminous Concrete.” Final Report No. FHWA-RD-76-102, Federal Highway Administration, Washington, DC.

Maupin, G. W. (1977) "Test for Predicting Fatigue Life of Bituminous Concrete." Transportation Research Record, no. 659, Transportation Research Board, Washington, DC, pp. 32-37.

Maupin, G. W., S. D. Diefenderfer, and J. S. Gillespie. (2008) “Evaluation of Using Higher Percentages of Recycled Asphalt Pavement in Asphalt Mixes in Virginia.” Report VTRC 08-R22. Virginia Transportation Research Council, Charlottesville, VA, 29p.

Medani, T. O. and A. A. A. Molenaar. (2000) “Estimation of fatigue characteristics of asphaltic mixes using simple tests.” Heron, vol. 45, no. 3, pp. 155-165.

Monismith, C. L., K. E. Secor, and E. W. Blackner. (1961) “Asphalt Mixture Behavior in Repeated Flexure.” Proceedings of the Association of Asphalt Paving Technologists, vol. 30, pp. 188-222.

Monismith, C. L. and J. A. Deacon. (1969) "Fatigue of Asphalt Paving Mixtures." ASCE Transportation Engineering Journal, vol. 95, no. 2, pp. 317-346.

Monismith, C. L., J. A. Epps, D. A. Kasianchuk, and D. B. McLean. (1970) Asphalt Mixture Behavior in Repeated Flexure. Report TE 70-5, Institute of Transportation and Traffic Engineering, University of California, Berkeley, CA, 303p.

Monismith C. L. and D. B. McLean. (1972) “Technology of Thick Lift Construction: Structural Design Considerations.” Proceedings of the Association of Asphalt Paving Technologists, vol. 41, pp. 258-304.

Monismith, C. L. and Y. M. Salam. (1973) “Distress Characteristics of Asphalt Concrete Mixes.” Proceedings of the Association of Asphalt Paving Technologists, vol. 42, pp. 320-350.

Monismith, C. L., K. Inkabi, D. B. McLean, and C. R. Freeme. (1977) Design Considerations for Asphalt Pavements. Report TE-77-1. University of California, Office of Research Services, Berkeley, CA, March, 138pp.

Monismith, C. L. (1981) “Fatigue Characteristics of Asphalt Paving Mixtures and Their Use in Pavement Design.” Proceedings of the 18th Paving Conference, University of NM, Albuquerque, NM, 1-43.

Monismith, C. L., J. A. Epps, and F. N. Finn. (1985) “Improved Asphalt Mix Design.” Journal of the Association of Asphalt Paving Technologists, vol. 54, pp. 347-406.

Pell, P. S. (1967) “Fatigue of Asphalt Pavement Mixes.” Proceedings of the Second International Conference on the Structural Design of Asphalt Pavements, Ann Arbor, MI, pp. 577-593.

Pell, P. S. (1973) "Characterization of Fatigue Behavior." Structural Design of Asphalt Concrete Pavements to Prevent Fatigue Cracking, Highway Research Report Special Report 140, Highway Research Board, Washington, DC, pp. 49-64.

Pell, P. S. and K. E. Cooper. (1975) "The Effect of Testing and Mix Variables on the Fatigue Performance of Bituminous Materials." Proceedings of the Association of Asphalt Paving Technologists, vol. 44, pp. 1-37.

Pronk, A. C. (1997) "Comparison of 2 and 4 Point Fatigue Tests and Healing in a 4 Point Dynamic Bending Test Based on the Dissipated Energy Concept." Proceedings, Eighth International Conference on Asphalt Pavements, vol. 2, Seatte, WA, 986-994.

Pronk, A. C. and P. C. Hopman. (1991) “Energy Dissipation: The Leading Factor of Fatigue.” Proceedings of the Conference of the United States Strategic Highway Research Program, pp. 255-267.

Prowell, B. D. and E. R. Brown. (2006) “Methods for Determining the Endurance Limit Using Beam Fatigue Tests.” Proceedings of the 2006 International Conference on Perpetual Pavement, Columbus, OH, http://www.ohio.edu/icpp/Cnference-Proceedings.cfm, accessed 3/24/2009.

Radziszewski, P. (1997) “Fatigue Characteristics of Asphalt Modified Paving Mixtures and their Use in Pavement Design.” Archives of Civil Engineering, vol. 43, no. 2, pp. 199-215.

Raithby, K. D. and A. B. Sterling. (1970) “The Effect of Rest Periods on the Fatigue Performance of a Hot-Rolled Asphalt Under Reversed Axial Loading.” Proceedings of the Association of Asphalt Paving Technologists, vol. 39, pp. 134-147.

Ramsamooj, D. V. (1980) “Fatigue Cracking of Asphalt Pavements.” Transportation Research Record, no. 756, Transportation Research Record, Washington, DC, pp. 43-48.

Ramsamooj, D V. (1991) “Prediction of Fatigue Life of Asphalt Concrete Beams from Fracture Tests.” Journal of Testing & Evaluation, vol. 19, no. 3, pp. 231-239.

Rauhut, J. B. and T. W. Kennedy. (1982) “Characterizing Fatigue Life for Asphalt Concrete Pavements.” Transportation Research Record, no. 888, pp. 47-56.

Read, J. M. and S. F. Brown. (1996) “Practical Evaluation of Fatigue Strength for Bituminous Mixtures.” Proceedings of the Eurasphalt and Eurobitume Congress, Strasbourg, France.

Read, J. M. and A. C. Collop. (1997) “Practical Fatigue Characterization of Bituminous Paving Mixtures.” Journal of the Association of Asphalt Paving Technologists, vol. 66, pp. 74-108.

Roberts, F. L., P. S. Kandhal, E. R. Brown, D.-Y. Lee, and T. W. Kennedy. (1996) Hot Mix Asphalt Materials, Mixture Design, and Construction. NAPA Research and Education Foundation, Lanham, MD, 585p.

Roque, R. and W. G. Buttlar. (1992) “The Development of a Measurement and Analysis System to Accurately Determine Asphalt Concrete Properties Using the Indirect Tensile Mode.” Journal of the Association of Asphalt Paving Technologists, vol. 61, pp. 304-332.

Rowe, G. M. (1993) “Performance of Asphalt Mixtures in the Trapezoidal Fatigue Test.” Proceedings of the Association of Asphalt Paving Technologists, vol. 62, 344-384.

Rowe, G. M. (2003) “Performance of Asphalt Mixtures in the Trapezoidal Fatigue Test.” Journal of the Association of Asphalt Paving Technologists, vol. 62, pp. 344-384.

Schapery, R. A. (1984) “Correspondence Principles and a Generalized J Integral for Large Deformation and Fracture Analysis of Viscoelastic Media.” International Journal of Fracture, vol. 25, pp. 195-223.

Schapery, R. A. (1989) “On the Mechanics of Crack Closing and Bonding in Linear Viscoelastic Media.” International Journal of Fracture, vol. 39, pp. 163-189.

Shen, S. (2006) “Dissipated Energy Concepts for HMA Performance: Fatigue and Healing.” Ph.D. Thesis, University of Illinois and Urbana-Champaign, Urbana, IL, 227p.

Shen S. and S. H. Carpenter. (2005) “Application of the Dissipated Energy Concept in Fatigue Endurance Limit Testing.” Transportation Research Record, no. 1929, Transportation Research Board, Washington, DC, pp. 165-173.

Shen, S. and S. H. Carpenter. (2007) “Development of an Asphalt Fatigue Model Based on Energy Principles.” Journal of the Association of Asphalt Paving Technologists, vol. 76, pp. 525-573.

SHRP. (1994) Fatigue Response of Asphalt-Aggregate Mixes. Report SHRP-A-404, Strategic Highway Research Program, National Research Council, Washington, DC, 309p.

Sousa, J. B., J. C. Pais, M. Prates, R. Barros, P. Langlois, and A.-M. Leclerc. (1998) “Effect of aggregate gradation on fatigue life of asphalt concrete mixes.” Transportation Research Record, no. 1630, Transportation Research Board, Washington, DC, pp. 62-68.

Tayebali, A., G. Rowe, and J. Sousa. (1992) “Fatigue Response of Aggregate-Asphalt Mixtures.” Journal of the Association of Asphalt Paving Technologists, vol. 61, pp. 333-360.

Tayebali, A., J. Deacon, J. Coplantz, J. Harvey, and C. Monismith. (1994) “Mixture and Mode-of-Loading Effects on Fatigue Response of Asphalt-Aggregate Mixtures.” Journal of the Association of Asphalt Paving Technologists, vol. 63, pp. 118-151.

Tayebali, A. A., J. A. Deacon, and C. L. Monismith. (1996) “Development and Evaluation of Dynamic Flexural Beam Fatigue Test System.” Transportation Research Record, no. 1545, Transportation Research Board, Washington, DC, pp. 89-97.

Tseng, K. H. and R. L. Lytton. (1990) “Fatigue Damage Properties of Asphaltic Concrete Pavements.” Transportation Research Record, no. 1286, Transportation Research Board, Washington, DC, 84-97.

Van Dijk, W., H. Moreaud, A. Quedeville, and P. Uge. (1972) "The Fatigue of Bitumen and Bituminous Mixes." Proceedings of the Third International Conference on the Structural Design of Asphalt Pavements, vol. 1, London, England, pp. 354-366.

Van Dijk, W. (1975) "Practical Fatigue Characterization of Bituminous Mixes." Proceedings of the Association of Asphalt Paving Technologists, vol. 44, pp. 38-74.

Van Dijk, W. and W. Visser. (1977) "The Energy Approach to Fatigue for Pavement Design.” Proceedings of the Association of Asphalt Paving Technologists, vol. 46, pp. 1-40.

Von Quintus, H. L., J. B. Rauhut, and T. W. Kennedy. (1982) “Comparisons of Asphalt Concrete Stiffness as Measured by Various Testing Techniques.” Journal of the Association of Asphalt Paving Technologists, vol. 51, pp. 35-52.

Witczak, M. W. (1976) “Pavement Performance Models: Volume 1 Repeated Load Fracture of Pavement Systems.” US Waterways Experiment Station Contract Report S-76-15, vol. 1, 193p.

APPENDIX A MIXTURE DESIGNS

Table A.1 Mixture designs for SM-9.5A, section D.

Design – Lab Mixture		
Aggregate		
#8 Quartzite	Salem Stone Co., Sylvatus, VA	50%
#10 Quartzite	Salem Stone Co., Sylvatus, VA	30%
Concrete Sand	Wythe Stone Co., Wytheville, VA	10%
Fine RAP	Adams Construction Co., Blacksburg, VA	10%
Binder		
PG 64-22	Associated Asphalt, Inc., Roanoke, VA	5.6%

Lab – Lab Mixture		
Aggregate		
#8 Quartzite	Salem Stone Co., Sylvatus, VA	50%
#10 Quartzite	Salem Stone Co., Sylvatus, VA	30%
Concrete Sand	Wythe Stone Co., Wytheville, VA	10%
Fine RAP	Adams Construction Co., Blacksburg, VA	10%
Binder		
PG 64-22	Associated Asphalt, Inc., Roanoke, VA	5.6%

Table A.2 Mixture designs for SM-9.5A, section I.

Design – Lab Mixture		
Aggregate		
#8 Quartzite	Salem Stone Co., Sylvatus, VA	50%
#10 Quartzite	Salem Stone Co., Sylvatus, VA	30%
Concrete Sand	Wythe Stone Co., Wytheville, VA	10%
Fine RAP	Adams Construction Co., Blacksburg, VA	10%
Binder		
PG 64-22	Associated Asphalt, Inc., Roanoke, VA	4.8%

Lab – Lab Mixture		
Aggregate		
#8 Quartzite	Salem Stone Co., Sylvatus, VA	50%
#10 Quartzite	Salem Stone Co., Sylvatus, VA	30%
Concrete Sand	Wythe Stone Co., Wytheville, VA	10%
Fine RAP	Adams Construction Co., Blacksburg, VA	10%
Binder		
PG 64-22	Associated Asphalt, Inc., Roanoke, VA	5.0%

Table A.3 Mixture designs for SM-9.5D, section B.

Design – Lab Mixture		
Aggregate		
#8 Quartzite	Salem Stone Co., Sylvatus, VA	60%
#10 Limestone	ACCO Stone Co., Blacksburg, VA	20%
Concrete Sand	Wythe Stone Co., Wytheville, VA	10%
Fine RAP	Adams Construction Co., Blacksburg, VA	10%
Binder		
PG 70-22	Associated Asphalt, Inc., Roanoke, VA	5.6%

Lab – Lab Mixture		
Aggregate		
#8 Quartzite	Salem Stone Co., Sylvatus, VA	36%
#10 Limestone	ACCO Stone Co., Blacksburg, VA	20%
Concrete Sand	Wythe Stone Co., Wytheville, VA	10%
#10 Quartzite	Salem Stone Co., Sylvatus, VA	23%
#10 Quartzite (filler)	Salem Stone Co., Sylvatus, VA	1%
Fine RAP	Adams Construction Co., Blacksburg, VA	10%
Binder		
PG 70-22	Associated Asphalt, Inc., Roanoke, VA	4.7%

Table A.4 Mixture designs for SM-9.5D, sections E, F, G, and H.

Design – Lab Mixture		
Aggregate		
#8 Quartzite	Salem Stone Co., Sylvatus, VA	60%
#10 Limestone	ACCO Stone Co., Blacksburg, VA	20%
Concrete Sand	Wythe Stone Co., Wytheville, VA	10%
Fine RAP	Adams Construction Co., Blacksburg, VA	10%
Binder		
PG 70-22	Associated Asphalt, Inc., Roanoke, VA	5.4%

Lab - Lab Mixture		
Aggregate		
#8 Quartzite	Salem Stone Co., Sylvatus, VA	48%
#10 Quartzite	Salem Stone Co., Sylvatus, VA	12%
#10 Limestone	ACCO Stone Co., Blacksburg, VA	20%
Concrete Sand	Wythe Stone Co., Wytheville, VA	10%
Fine RAP	Adams Construction Co., Blacksburg, VA	10%
Binder		
PG 70-22	Associated Asphalt, Inc., Roanoke, VA	5.8%

Table A.5 Mixture design for SM-9.5D, section J.

Lab - Lab Mixture		
Aggregate		
#8 Quartzite	Salem Stone Co., Sylvatus, VA	48%
#10 Quartzite	Salem Stone Co., Sylvatus, VA	12%
#10 Limestone	ACCO Stone Co., Blacksburg, VA	20%
Concrete Sand	Wythe Stone Co., Wytheville, VA	10%
Fine RAP	Adams Construction Co., Blacksburg, VA	10%
Binder		
PG 70-22	Associated Asphalt, Inc., Roanoke, VA	4.9%

Table A.6 Mixture designs for SM-9.5E, section C.

Design - Lab Mixture		
Aggregate		
#8 Quartzite	Salem Stone Co., Sylvatus, VA	54%
#10 Quartzite	Salem Stone Co., Sylvatus, VA	21%
Concrete Sand	Wythe Stone Co., Wytheville, VA	10%
Fine RAP	Adams Construction Co., Blacksburg, VA	15%
Binder		
PG 76-22	Koch Materials Co., Pennsauken, NJ	5.8%

Lab - Lab Mixture		
Aggregate		
#8 Quartzite	Salem Stone Co., Sylvatus, VA	52%
#10 Quartzite	Salem Stone Co., Sylvatus, VA	23%
Concrete Sand	Wythe Stone Co., Wytheville, VA	10%
Fine RAP	Adams Construction Co., Blacksburg, VA	15%
Binder		
PG 76-22	Koch Materials Co., Pennsauken, NJ	5.8%

Table A.7 Mixture designs for SM-12.5D, section A.

Design - Lab Mixture		
Aggregate		
#78 Quartzite	Salem Stone Co., Sylvatus, VA	15%
#8 Quartzite	Salem Stone Co., Sylvatus, VA	30%
#9 Quartzite	Salem Stone Co., Sylvatus, VA	10%
#10 Limestone	Sisson and Ryan Quarry, Shawsville, VA	20%
Sand	Castle Sand Co., New Castle VA	10%
Fine RAP	Adams Construction Co., Blacksburg, VA	15%
Binder		
PG 70-22	Associated Asphalt, Inc., Roanoke, VA	5.6%

Lab - Lab Mixture		
Aggregate		
#78 Quartzite	Salem Stone Co., Sylvatus, VA	5%
#8 Quartzite	Salem Stone Co., Sylvatus, VA	30%
#9 Quartzite	Salem Stone Co., Sylvatus, VA	20%
#10 Limestone	Sisson and Ryan Quarry, Shawsville, VA	20%
Sand	Castle Sand Co., New Castle VA	10%
Fine RAP	Adams Construction Co., Blacksburg, VA	15%
Binder		
PG 70-22	Associated Asphalt, Inc., Roanoke, VA	5.9%

Table A.8 Mixture designs for SM-12.5A, section L.

Design - Lab Mixture		
Aggregate		
#68 Quartzite	Salem Stone Co., Sylvatus, VA	26%
#8 Quartzite	Salem Stone Co., Sylvatus, VA	55%
#10 Quartzite	Salem Stone Co., Sylvatus, VA	10%
Lime Filler	James River Lime, Buchanan, VA	9%
Binder		
PG 76-22	Koch Materials Co., Pennsauken, NJ	7.2%
Fiber		
Cellulose	Hi-Tech Asphalt Solutions, Mechanicsville, VA	0.3%

Lab - Lab Mixture		
Aggregate		
#68 Quartzite	Salem Stone Co., Sylvatus, VA	8%
#8 Quartzite	Salem Stone Co., Sylvatus, VA	71%
#10 Quartzite	Salem Stone Co., Sylvatus, VA	12%
Lime Filler	James River Lime, Buchanan, VA	9%
Binder		
PG 76-22	Koch Materials Co., Pennsauken, NJ	6.8%
Fiber		
Cellulose	Hi-Tech Asphalt Solutions, Mechanicsville, VA	0.3%

Note: Aggregate and binder percentages are by weight of mixture. Fiber percentages are by weight of binder.

APPENDIX B MIXTURE VOLUMETRIC PROPERTIES AND GRADATIONS

Table B.1 Volumetric properties for SM-9.5A mixtures, section D.

Property	Field - Field	Field - Lab	Lab - Lab	Design - Lab
% Asphalt	6.29	6.29	6.76	6.25
G_{mm}	2.440	2.440	2.455	2.468
G_{mb}	2.393	2.408	2.434	2.379
G_b	1.03	1.03	1.03	1.03
G_{se}	2.687	2.687	2.729	2.722
G_{sb}	2.653	2.653	2.695	2.688
CF	0.034	0.034	0.034	0.034
Bulk Density	149.4	150.3	151.9	148.4
Density at N_{ini}	-	138.9	140.4	135.8
% passing #200	9.20	9.20	5.72	6.26

Table B.2 VDOT volumetric specifications for SM-9.5A mixtures, section D.

Property	Specification		Field - Field		Field - Lab		Lab - Lab		Design - Lab	
	Min.	Max.								
VTM (%)	2.5	5.5	1.9	Fail	1.3	Fail	0.9	Fail	3.6	Pass
VMA (%)	12	-	15.5	Pass	14.9	Pass	15.8	Pass	17.0	Pass
VFA (%)	62	80	87.6	Fail	91.2	Fail	94.4	Fail	78.7	Pass
% Density at N_{ini}	-	89	-	-	91.2	Fail	91.6	Fail	88.1	Pass
F/A ratio	0.6	1.3	1.6	Fail	1.6	Fail	0.9	Pass	1.1	Pass

Figure B.1 Gradation of SM-9.5A, field-field and field-lab mixtures, section D.

Sieve opening (mm)	Sieve #	% Passing	Control Point LL	Control Point UL	Restricted Zone LL	Restricted Zone UL	Result
12.5	1/2	99.3	-	100			F
9.5	3/8	92.4	90	100			P
4.75	#4	54.9	-	90			P
2.36	#8	34.8	32	67	47.2	47.2	P
1.18	#16	25.7	-	-	31.6	37.6	P
0.6	#30	20.4	-	-	23.5	27.5	P
0.3	#50	15.3	-	-	18.7	18.7	P
0.15	#100	11.8	-	-			
0.075	#200	9.2	2	10			P

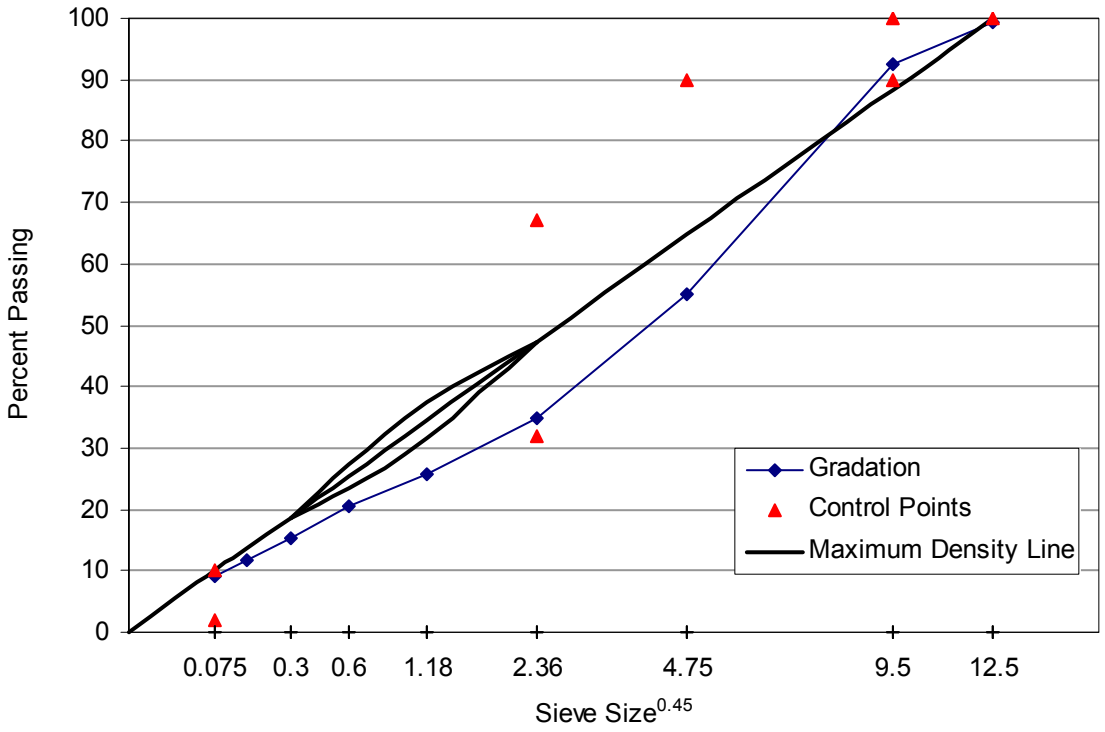

Figure B.2 Gradation of SM-9.5A, lab-lab mixture, section D.

Sieve opening (mm)	Sieve #	% Passing	Control Point LL	Control Point UL	Restricted Zone LL	Restricted Zone UL	Result
12.5	1/2	100.0	-	100			F
9.5	3/8	89.3	90	100			P
4.75	#4	50.8	-	90			P
2.36	#8	37.0	32	67	47.2	47.2	P
1.18	#16	27.7	-	-	31.6	37.6	P
0.6	#30	20.4	-	-	23.5	27.5	P
0.3	#50	12.3	-	-	18.7	18.7	P
0.15	#100	8.0	-	-			
0.075	#200	5.7	2	10			P

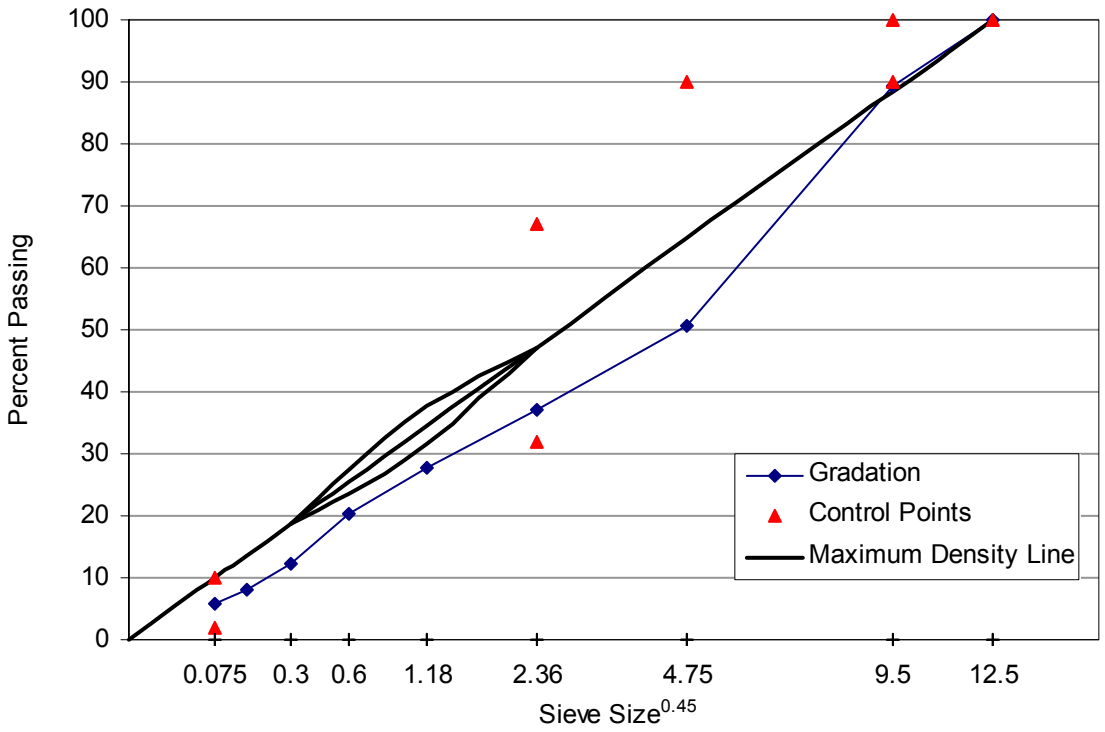

Figure B.3 Gradation of SM-9.5A, design-lab mixture, section D.

Sieve opening (mm)	Sieve #	% Passing	Control Point LL	Control Point UL	Restricted Zone LL	Restricted Zone UL	Result
12.5	1/2	99.2	-	100			F
9.5	3/8	92.3	90	100			P
4.75	#4	58.3	-	90			P
2.36	#8	41.7	32	67	47.2	47.2	P
1.18	#16	28.7	-	-	31.6	37.6	P
0.6	#30	20.3	-	-	23.5	27.5	P
0.3	#50	12.4	-	-	18.7	18.7	P
0.15	#100	8.6	-	-			
0.075	#200	6.3	2	10			P

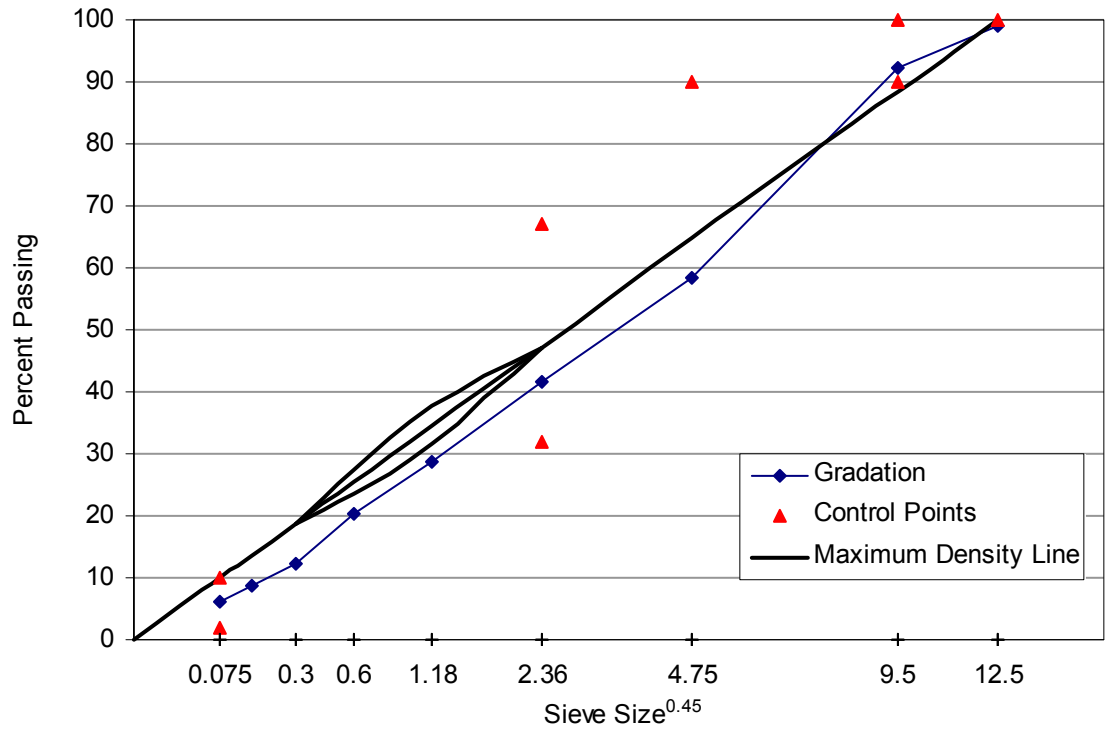

Table B.3 Volumetric properties for SM-9.5A mixtures, section I.

Property	Field - Field	Field - Lab	Lab - Lab	Design - Lab
% Asphalt	5.42	5.42	5.31	5.37
G_{mm}	2.467	2.467	2.489	2.498
G_{mb}	2.440	2.429	2.340	2.390
G_b	1.03	1.03	1.03	1.03
G_{se}	2.681	2.681	2.704	2.718
G_{sb}	2.647	2.647	2.670	2.684
CF	0.034	0.034	0.034	0.034
Bulk Density	152.3	151.6	146.0	149.1
Density at N_{ini}	-	138.1	133.4	137.0
% passing #200	7.27	7.27	6.97	7.64

Table B.4 VDOT volumetric specifications for SM-9.5A mixtures, section I.

Property	Specification		Field - Field		Field - Lab		Lab - Lab		Design - Lab	
	Min.	Max.								
VTM (%)	2.5	5.5	1.1	Fail	1.5	Fail	6.0	Fail	4.3	Pass
VMA (%)	12	-	12.8	Pass	13.2	Pass	17.0	Pass	15.7	Pass
VFA (%)	62	80	91.6	Fail	88.5	Fail	64.8	Pass	72.5	Pass
% Density at N_{ini}	-	89	-	-	89.8	Fail	85.9	Pass	87.9	Pass
F/A ratio	0.6	1.3	1.5	Fail	1.5	Fail	1.4	Fail	1.6	Fail

Figure B.4 Gradation of SM-9.5A, field-field and field-lab mixtures, section I.

Sieve opening (mm)	Sieve #	% Passing	Control Point LL	Control Point UL	Restricted Zone LL	Restricted Zone UL	Result
12.5	1/2	100.0	-	100			P
9.5	3/8	95.0	90	100			P
4.75	#4	51.8	-	90			P
2.36	#8	35.0	32	67	47.2	47.2	P
1.18	#16	27.8	-	-	31.6	37.6	P
0.6	#30	20.6	-	-	23.5	27.5	P
0.3	#50	13.9	-	-	18.7	18.7	P
0.15	#100	10.6	-	-			
0.075	#200	7.3	2	10			P

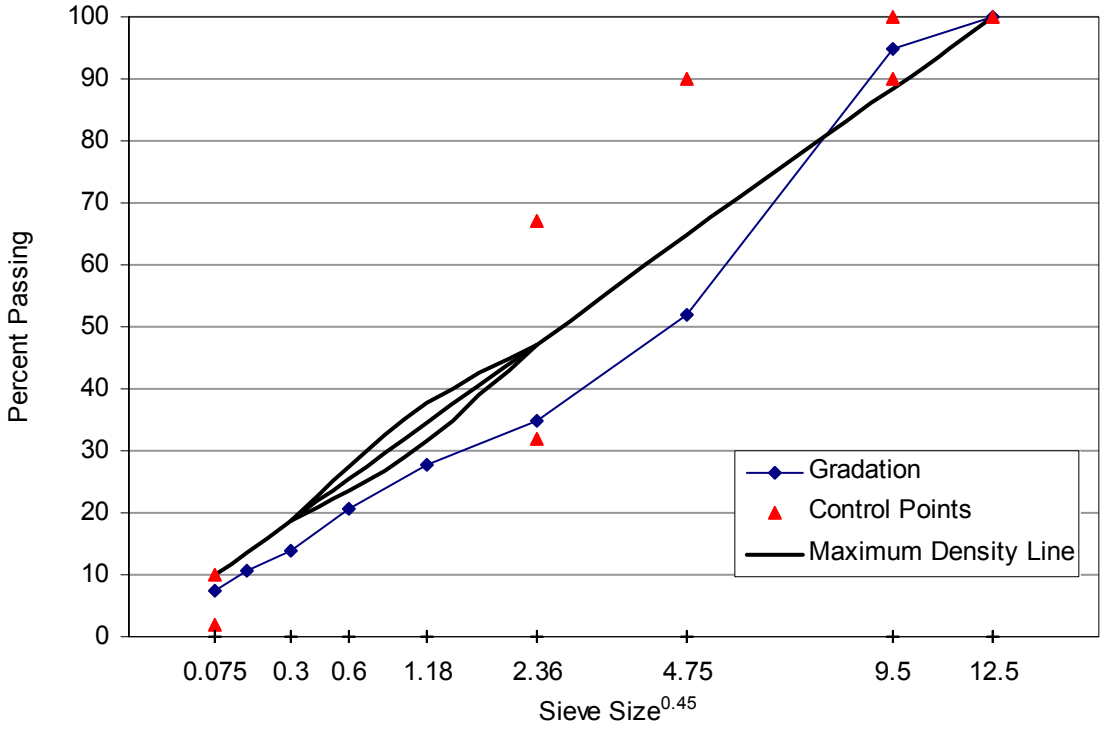

Figure B.5 Gradation of SM-9.5A, lab-lab mixture, section I.

Sieve opening (mm)	Sieve #	% Passing	Control Point LL	Control Point UL	Restricted Zone LL	Restricted Zone UL	Result
12.5	1/2	99.4	-	100			F
9.5	3/8	92.7	90	100			P
4.75	#4	54.2	-	90			P
2.36	#8	37.6	32	67	47.2	47.2	P
1.18	#16	28.4	-	-	31.6	37.6	P
0.6	#30	21.2	-	-	23.5	27.5	P
0.3	#50	13.6	-	-	18.7	18.7	P
0.15	#100	9.6	-	-			
0.075	#200	7.0	2	10			P

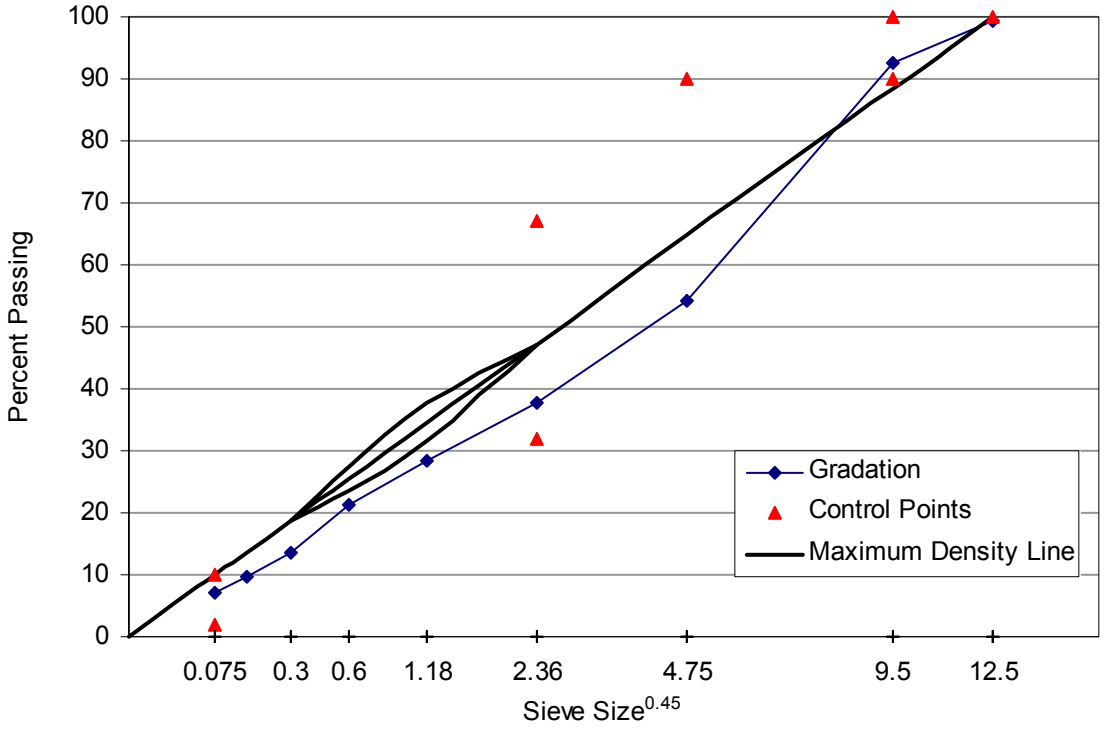

Figure B.6 Gradation of SM-9.5A, design-lab mixture, section I.

Sieve opening (mm)	Sieve #	% Passing	Control Point LL	Control Point UL	Restricted Zone LL	Restricted Zone UL	Result
12.5	1/2	98.9	-	100			F
9.5	3/8	88.6	90	100			P
4.75	#4	56.7	-	90			P
2.36	#8	43.5	32	67	47.2	47.2	P
1.18	#16	31.0	-	-	31.6	37.6	P
0.6	#30	22.1	-	-	23.5	27.5	P
0.3	#50	13.9	-	-	18.7	18.7	P
0.15	#100	10.1	-	-			
0.075	#200	7.6	2	10			P

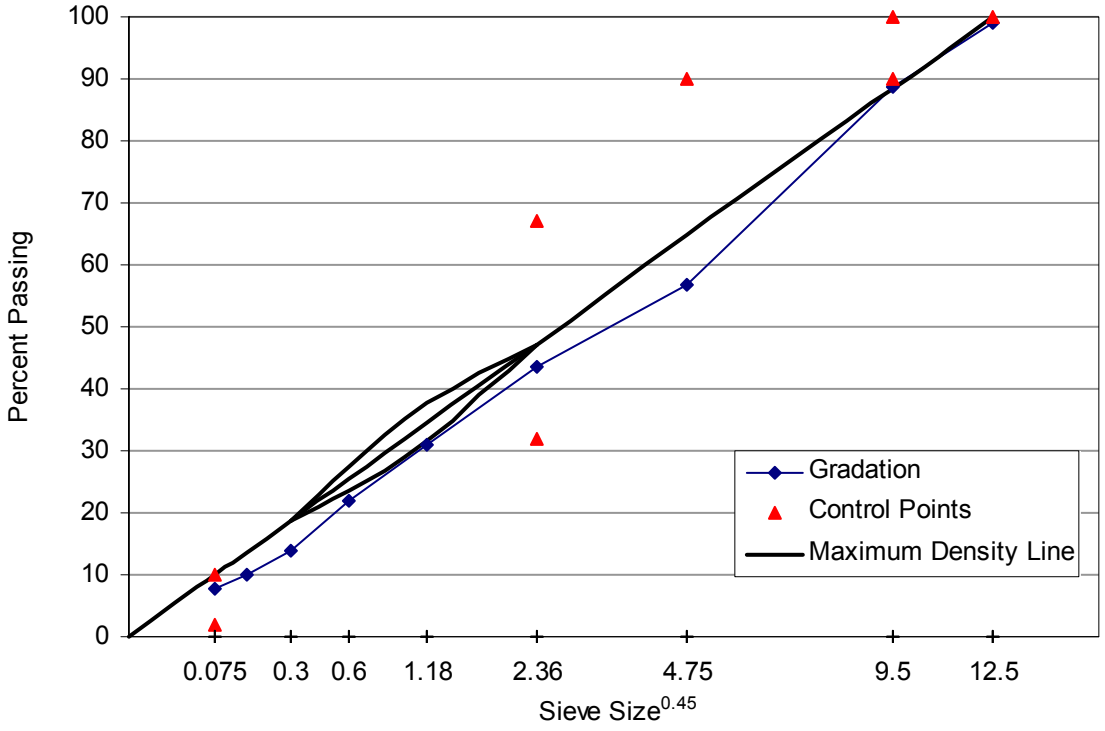

Table B.5 Volumetric properties for SM-9.5D mixtures, section B.

Property	Field - Field	Field - Lab	Lab - Lab	Design - Lab
% Asphalt	4.71	4.71	5.36	5.33
G_{mm}	2.450	2.450	2.513	2.494
G_{mb}	2.239	2.362	2.468	2.370
G_b	1.03	1.03	1.03	1.03
G_{se}	2.629	2.629	2.736	2.711
G_{sb}	2.574	2.574	2.681	2.656
CF	0.055	0.055	0.055	0.055
Bulk Density	139.7	147.4	154.0	147.9
Density at N_{ini}	-	135.1	141.7	133.1
% Passing #200	7.81	7.81	8.72	5.52

Table B.6 VDOT volumetric specifications for SM-9.5D mixtures, section B.

Property	Specification		Field - Field		Field - Lab		Lab - Lab		Design - Lab	
	Min.	Max.								
VTM (%)	2.5	5.5	8.6	Fail	3.6	Pass	1.8	Fail	5.0	Pass
VMA (%)	12	-	17.1	Pass	12.5	Pass	12.9	Pass	15.5	Pass
VFA (%)	62	80	49.7	Fail	71.6	Pass	86.0	Fail	68.0	Pass
% Density at N_{ini}	-	89	-	-	88.4	Pass	90.4	Fail	85.6	Pass
F/A ratio	0.6	1.3	2.0	Fail	2.0	Fail	1.9	Fail	1.2	Pass

Figure B.7 Gradation of SM-9.5D, field-field mixture, section B.

Sieve opening (mm)	Sieve #	% Passing	Control Point LL	Control Point UL	Restricted Zone LL	Restricted Zone UL	Result
12.5	1/2	98.5	-	100			F
9.5	3/8	90.3	90	100			P
4.75	#4	51.9	-	90			P
2.36	#8	35.4	32	67	47.2	47.2	P
1.18	#16	26.7	-	-	31.6	37.6	P
0.6	#30	18.1	-	-	23.5	27.5	P
0.3	#50	11.9	-	-	18.7	18.7	P
0.15	#100	9.4	-	-			
0.075	#200	7.8	2	10			P

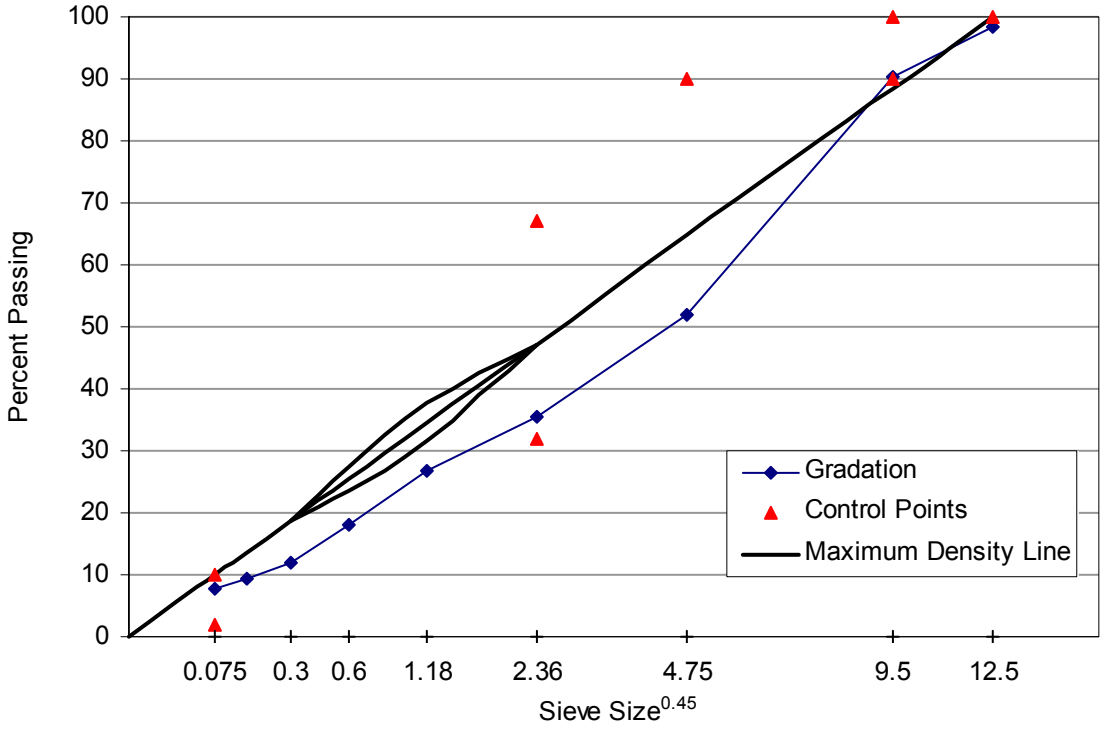

Figure B.8 Gradation of SM-9.5D, lab-lab mixture, section B.

Sieve opening (mm)	Sieve #	% Passing	Control Point LL	Control Point UL	Restricted Zone LL	Restricted Zone UL	Result
12.5	1/2	98.5	-	100			F
9.5	3/8	91.5	90	100			P
4.75	#4	58.8	-	90			P
2.36	#8	42.5	32	67	47.2	47.2	P
1.18	#16	30.8	-	-	31.6	37.6	P
0.6	#30	22.9	-	-	23.5	27.5	P
0.3	#50	15.1	-	-	18.7	18.7	P
0.15	#100	11.1	-	-			
0.075	#200	8.7	2	10			P

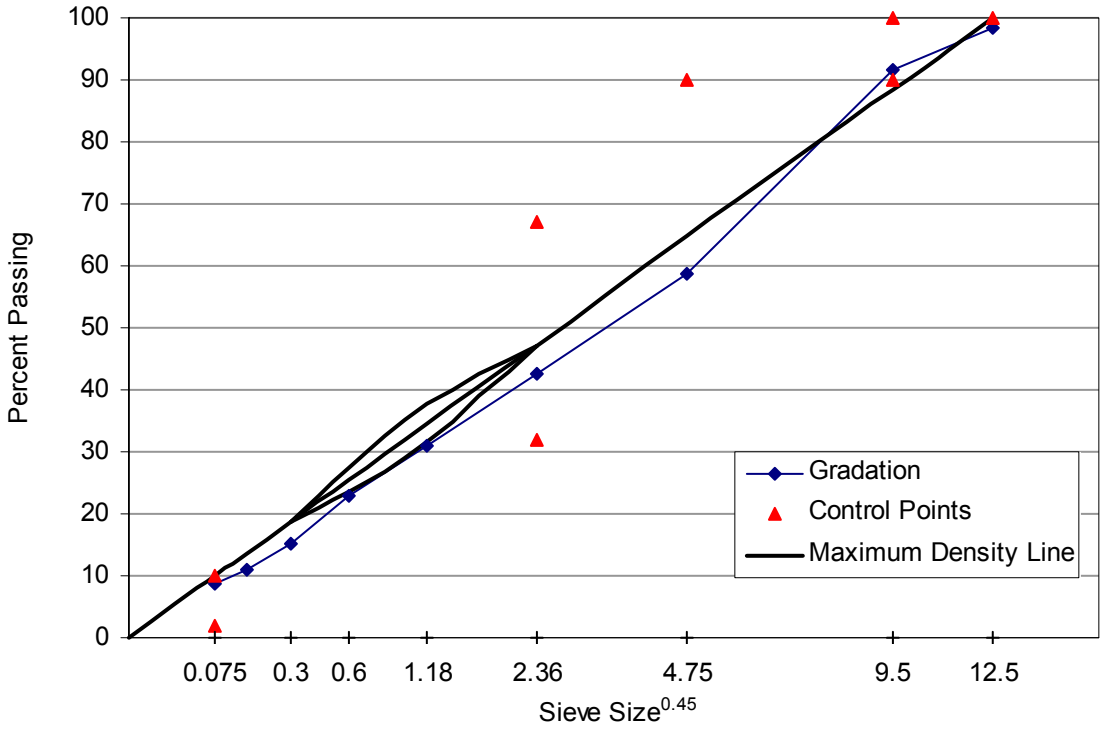

Figure B.9 Gradation of SM-9.5D, design-lab mixture, section B.

Sieve opening (mm)	Sieve #	% Passing	Control Point LL	Control Point UL	Restricted Zone LL	Restricted Zone UL	Result
12.5	1/2	99.7	-	100			F
9.5	3/8	86.1	90	100			P
4.75	#4	33.7	-	90			P
2.36	#8	22.9	32	67	47.2	47.2	F
1.18	#16	18.2	-	-	31.6	37.6	P
0.6	#30	14.0	-	-	23.5	27.5	P
0.3	#50	8.8	-	-	18.7	18.7	P
0.15	#100	6.6	-	-			
0.075	#200	5.5	2	10			P

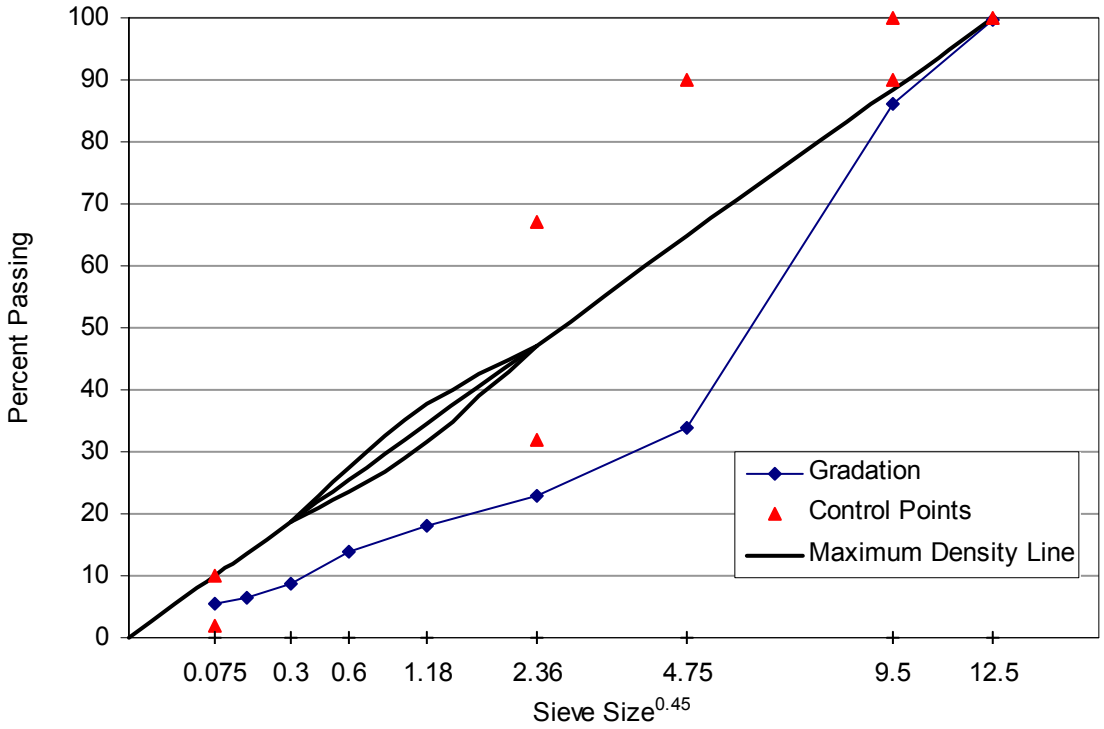

Table B.7 Volumetric properties for SM-9.5D mixtures, section E.

Property	Field - Field	Field - Lab	Lab – Lab (E, F, G, and H)
% Asphalt	5.85	5.85	6.00
Gmm	2.434	2.434	2.489
Gmb	2.317	2.400	2.442
Gb	1.03	1.03	1.03
Gse	2.659	2.659	2.737
Gsb	2.604	2.604	2.682
CF	0.055	0.055	0.055
Bulk Density	144.6	149.8	152.4
Density at Nini	-	137.3	140.2
% passing #200	7.57	7.57	8.47

Table B.8 VDOT volumetric specifications for SM-9.5D mixtures, section E.

Property	Specification		Field - Field		Field - Lab		Lab – Lab (E, F, G, and H)	
	Min.	Max.						
VTM (%)	2.5	5.5	4.8	Pass	1.4	Fail	1.9	Fail
VMA (%)	12	-	16.2	Pass	13.2	Pass	14.4	Pass
VFA (%)	62	80	70.5	Pass	89.6	Fail	86.8	Fail
% Density at N_{ini}	-	89	-	-	90.4	Fail	90.2	Fail
F/A ratio	0.6	1.3	1.5	Fail	1.5	Fail	1.6	Fail

Figure B.10 Gradation of SM-9.5D, field-field and field-lab mixtures, section E.

Sieve opening (mm)	Sieve #	% Passing	Control Point LL	Control Point UL	Restricted Zone LL	Restricted Zone UL	Result
12.5	1/2	97.6	-	100			F
9.5	3/8	92.9	90	100			P
4.75	#4	63.3	-	90			P
2.36	#8	42.6	32	67	47.2	47.2	P
1.18	#16	31.5	-	-	31.6	37.6	P
0.6	#30	20.5	-	-	23.5	27.5	P
0.3	#50	13.3	-	-	18.7	18.7	P
0.15	#100	10.4	-	-			
0.075	#200	7.6	2	10			P

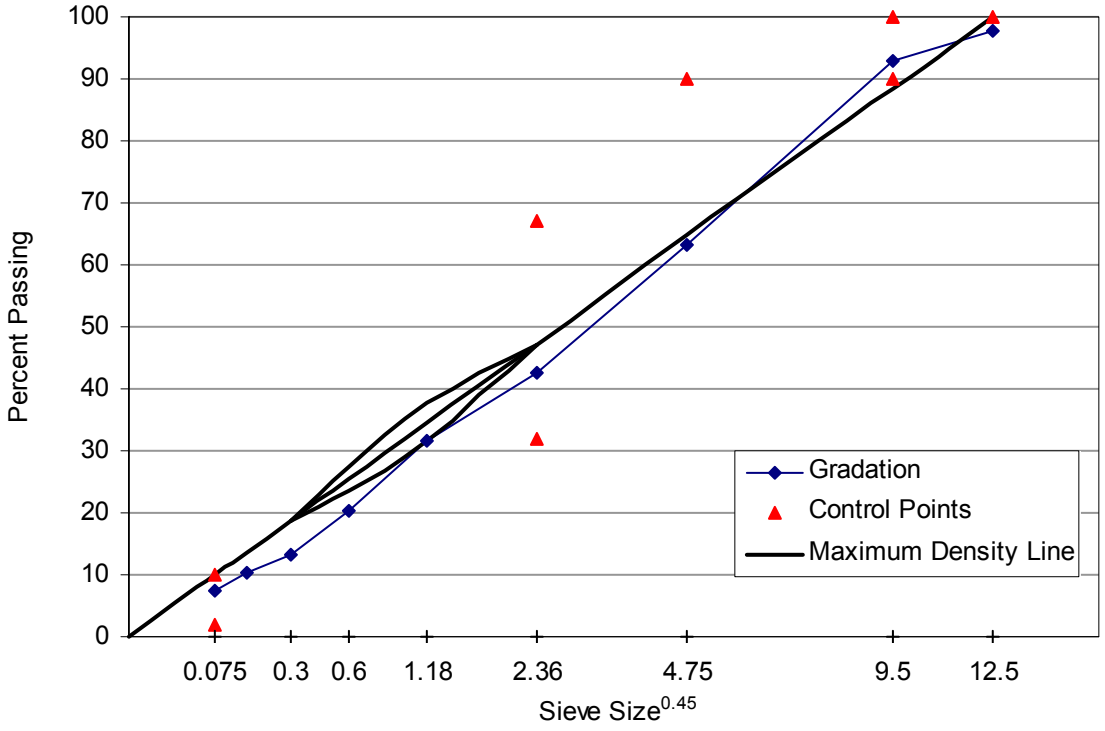

Figure B.11 Gradation of SM-9.5D, lab-lab mixture, sections E, F, G, and H.

Sieve opening (mm)	Sieve #	% Passing	Control Point LL	Control Point UL	Restricted Zone LL	Restricted Zone UL	Result
12.5	1/2	99.3	-	100			F
9.5	3/8	93.0	90	100			P
4.75	#4	61.4	-	90			P
2.36	#8	42.4	32	67	47.2	47.2	P
1.18	#16	31.0	-	-	31.6	37.6	P
0.6	#30	23.0	-	-	23.5	27.5	P
0.3	#50	15.2	-	-	18.7	18.7	P
0.15	#100	11.1	-	-			
0.075	#200	8.5	2	10			P

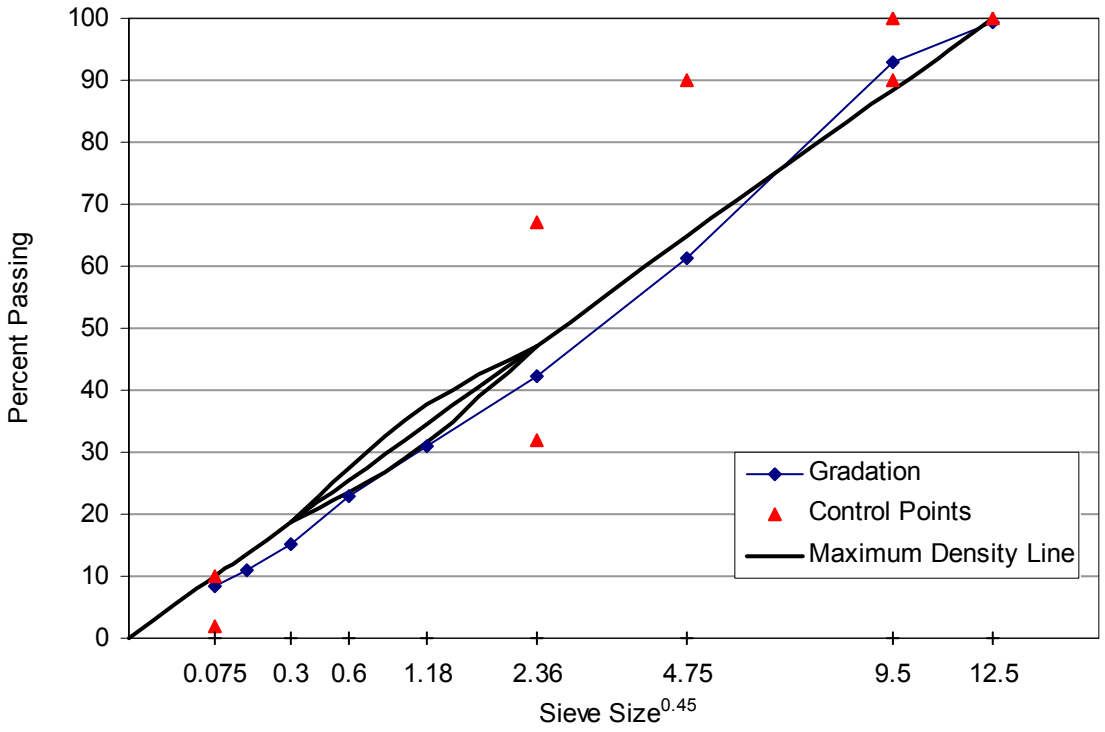

.

Table B.9 Volumetric properties for SM-9.5D mixtures, section F.

Property	Field - Field	Field - Lab
% Asphalt	5.85	5.42
Gmm	2.434	2.502
Gmb	2.317	2.412
Gb	1.03	1.03
Gse	2.659	2.725
Gsb	2.604	2.670
CF	0.055	0.055
Bulk Density	144.6	150.5
Density at Nini	-	137.5
% passing #200	7.57	6.88

Table B.10 VDOT volumetric specifications for SM-9.5D mixtures, section F.

Property	Specification		Field - Field		Field - Lab	
	Min.	Max.				
VTM (%)	2.5	5.5	4.8	Pass	3.6	Pass
VMA (%)	12	-	16.2	Pass	14.5	Pass
VFA (%)	62	80	70.5	Pass	75.4	Pass
% Density at Nini	-	89	-	-	88.1	Pass
F/A ratio	0.6	1.3	1.5	Fail	1.5	Fail

Figure B.12 Gradation of SM-9.5D, field-field and field-lab mixtures, section F.

Sieve opening (mm)	Sieve #	% Passing	Control Point LL	Control Point UL	Restricted Zone LL	Restricted Zone UL	Result
12.5	1/2	99.4	-	100			F
9.5	3/8	93.4	90	100			P
4.75	#4	56.7	-	90			P
2.36	#8	38.6	32	67	47.2	47.2	P
1.18	#16	25.7	-	-	31.6	37.6	P
0.6	#30	18.4	-	-	23.5	27.5	P
0.3	#50	12.1	-	-	18.7	18.7	P
0.15	#100	8.7	-	-			
0.075	#200	6.9	2	10			P

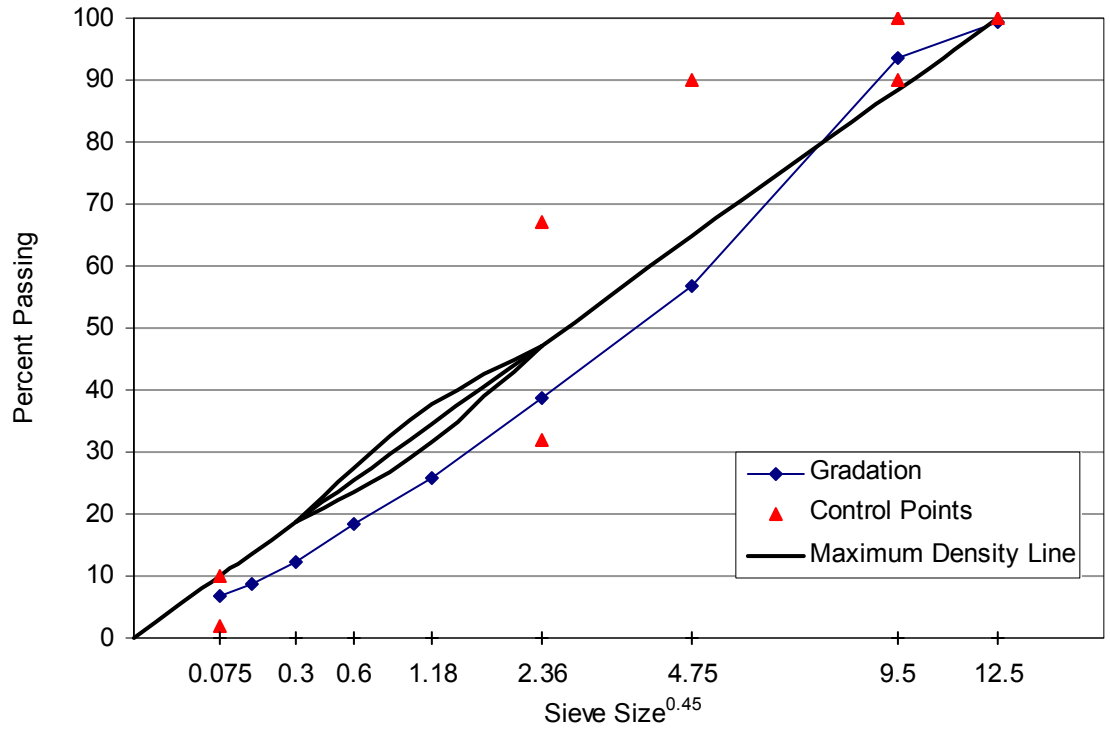

Table B.11 Volumetric properties for SM-9.5D mixtures, section G.

Property	Field - Field	Field - Lab
% Asphalt	5.85	6.29
G_{mm}	2.434	2.499
G_{mb}	2.317	2.410
G_b	1.03	1.03
G_{se}	2.659	2.763
G_{sb}	2.604	2.708
CF	0.055	0.055
Bulk Density	144.6	150.4
Density at N_{ini}	-	137.6
% passing #200	7.57	8.35

Table B.12 VDOT volumetric specifications for SM-9.5D mixtures, section G.

Property	Specification		Field - Field		Field - Lab	
	Min.	Max.				
VTM (%)	2.5	5.5	4.8	Pass	3.6	Pass
VMA (%)	12	-	16.2	Pass	16.6	Pass
VFA (%)	62	80	70.5	Pass	78.6	Pass
% Density at N_{ini}	-	89	-	-	88.2	Pass
F/A ratio	0.6	1.3	1.5	Fail	1.5	Fail

Figure B.13 Gradation of SM-9.5D, field-field and field-lab mixtures, section G.

Sieve opening (mm)	Sieve #	% Passing	Control Point LL	Control Point UL	Restricted Zone LL	Restricted Zone UL	Result
12.5	1/2	98.4	-	100			F
9.5	3/8	95.1	90	100			P
4.75	#4	62.3	-	90			P
2.36	#8	42.2	32	67	47.2	47.2	P
1.18	#16	28.9	-	-	31.6	37.6	P
0.6	#30	20.9	-	-	23.5	27.5	P
0.3	#50	13.8	-	-	18.7	18.7	P
0.15	#100	10.3	-	-			
0.075	#200	8.3	2	10			P

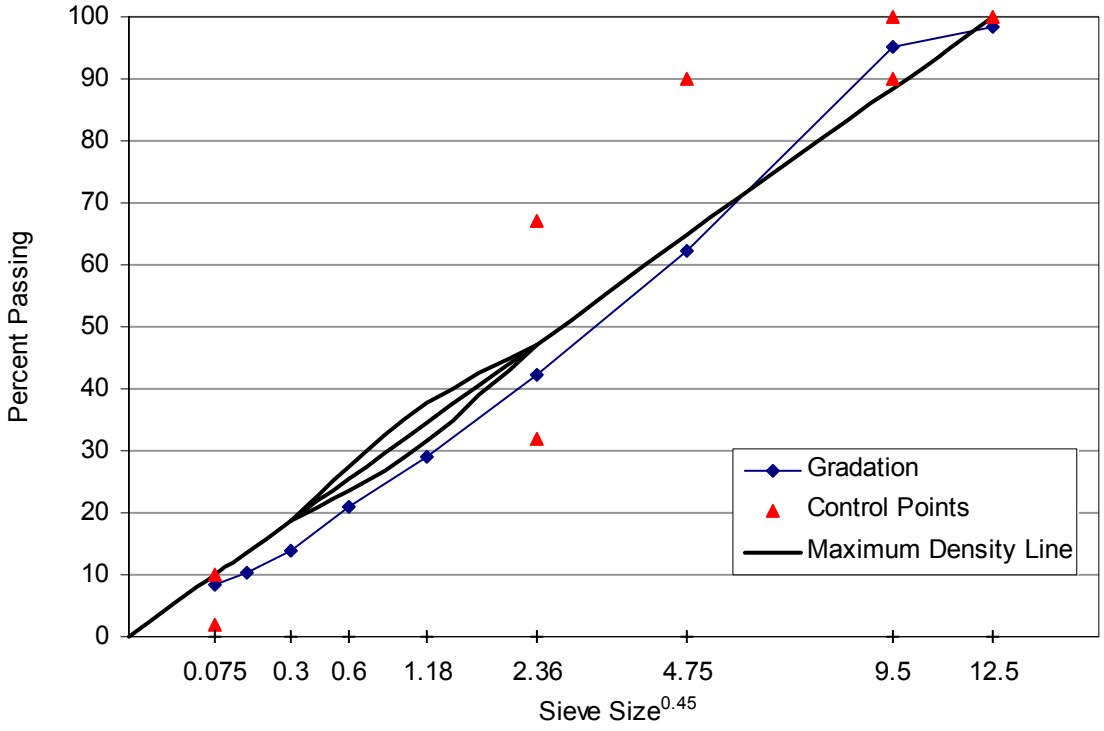

Table B.13 Volumetric properties for SM-9.5D mixtures, section H.

Property	Field - Field	Field - Lab
% Asphalt	5.85	5.63
G_{mm}	2.434	2.507
G_{mb}	2.317	2.403
G_b	1.03	1.03
G_{se}	2.659	2.741
G_{sb}	2.604	2.686
CF	0.055	0.055
Bulk Density	144.6	149.9
Density at N_{ini}	-	137.4
% passing #200	7.57	7.57

Table B.14 VDOT volumetric specifications for SM-9.5D mixtures, section H.

Property	Specification		Field - Field		Field - Lab	
	Min.	Max.				
VTM (%)	2.5	5.5	4.8	Pass	4.1	Pass
VMA (%)	12	-	16.2	Pass	15.6	Pass
VFA (%)	62	80	70.5	Pass	73.4	Pass
% Density at Nini	-	89	-	-	87.8	Pass
F/A ratio	0.6	1.3	1.5	Fail	1.5	Fail

Figure B.14 Gradation of SM-9.5D, field-field and field-lab mixtures, section H.

Sieve opening (mm)	Sieve #	% Passing	Control Point LL	Control Point UL	Restricted Zone LL	Restricted Zone UL	Result
12.5	1/2	98.3	-	100			F
9.5	3/8	94.3	90	100			P
4.75	#4	63.8	-	90			P
2.36	#8	43.1	32	67	47.2	47.2	P
1.18	#16	29.3	-	-	31.6	37.6	P
0.6	#30	20.9	-	-	23.5	27.5	P
0.3	#50	13.5	-	-	18.7	18.7	P
0.15	#100	9.6	-	-			
0.075	#200	7.6	2	10			P

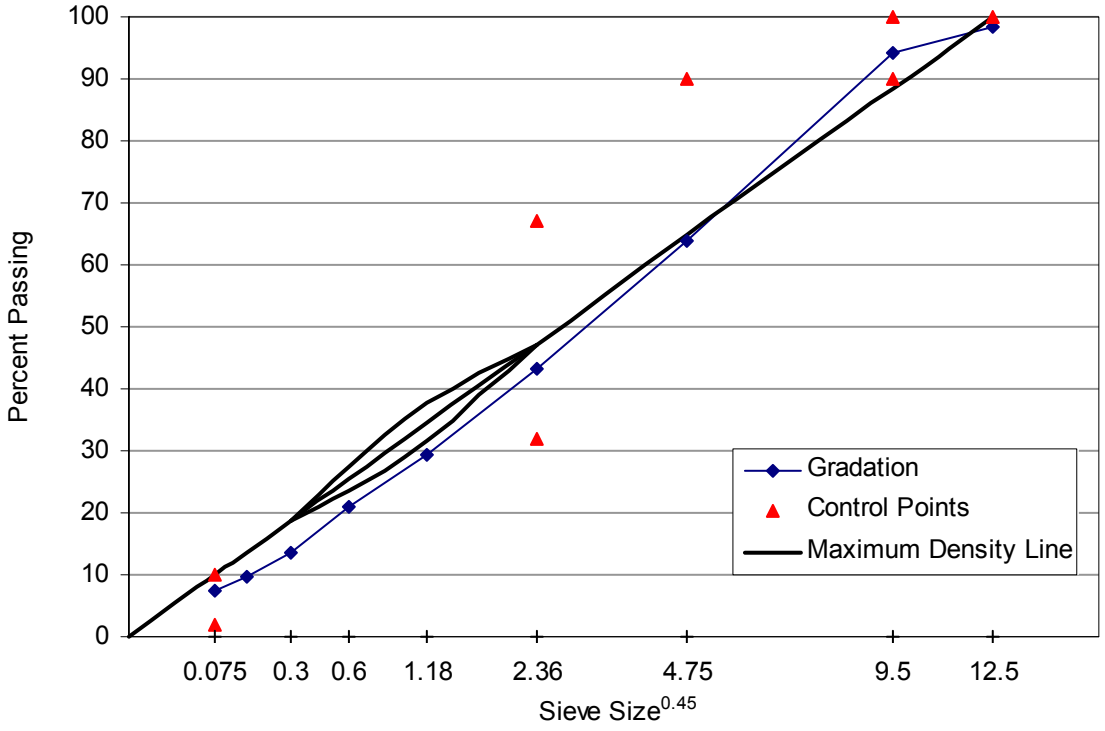

Table B.15 Volumetric properties for SM-9.5D mixtures, section J.

Property	Field - Field	Field - Lab	Lab - Lab
% Asphalt	4.90	4.90	5.06
Gmm	2.518	2.518	2.524
Gmb	2.252	2.328	2.408
Gb	1.03	1.03	1.03
Gse	2.721	2.721	2.736
Gsb	2.666	2.666	2.681
CF	0.055	0.055	0.055
Bulk Density	140.5	145.3	150.2
Density at Nini	-	133.0	137.6
% passing #200	6.31	6.31	6.72

Table B.16 VDOT volumetric specifications for SM-9.5D mixtures, section J.

Property	Specification		Field - Field		Field - Lab		Lab - Lab	
	Min.	Max.						
VTM (%)	2.5	5.5	10.6	Fail	7.5	Fail	4.6	Pass
VMA (%)	12	-	19.7	Pass	16.9	Pass	14.7	Pass
VFA (%)	62	80	46.3	Fail	55.5	Fail	68.6	Pass
% Density at N_{ini}	-	89	-	-	84.6	Pass	87.3	Pass
F/A ratio	0.6	1.3	1.5	Fail	1.5	Fail	1.6	Fail

Figure B.15 Gradation of SM-9.5D, field-field and field-lab mixtures, section J.

Sieve opening (mm)	Sieve #	% Passing	Control Point LL	Control Point UL	Restricted Zone LL	Restricted Zone UL	Result
12.5	1/2	99.2	-	100			F
9.5	3/8	91.6	90	100			P
4.75	#4	50.5	-	-			
2.36	#8	34.6	32	67	47.2	47.2	P
1.18	#16	26.2	-	-	31.6	37.6	P
0.6	#30	17.9	-	-	23.5	27.5	P
0.3	#50	11.8	-	-	18.7	18.7	P
0.15	#100	9.1	-	-			
0.075	#200	6.3	2	10			P

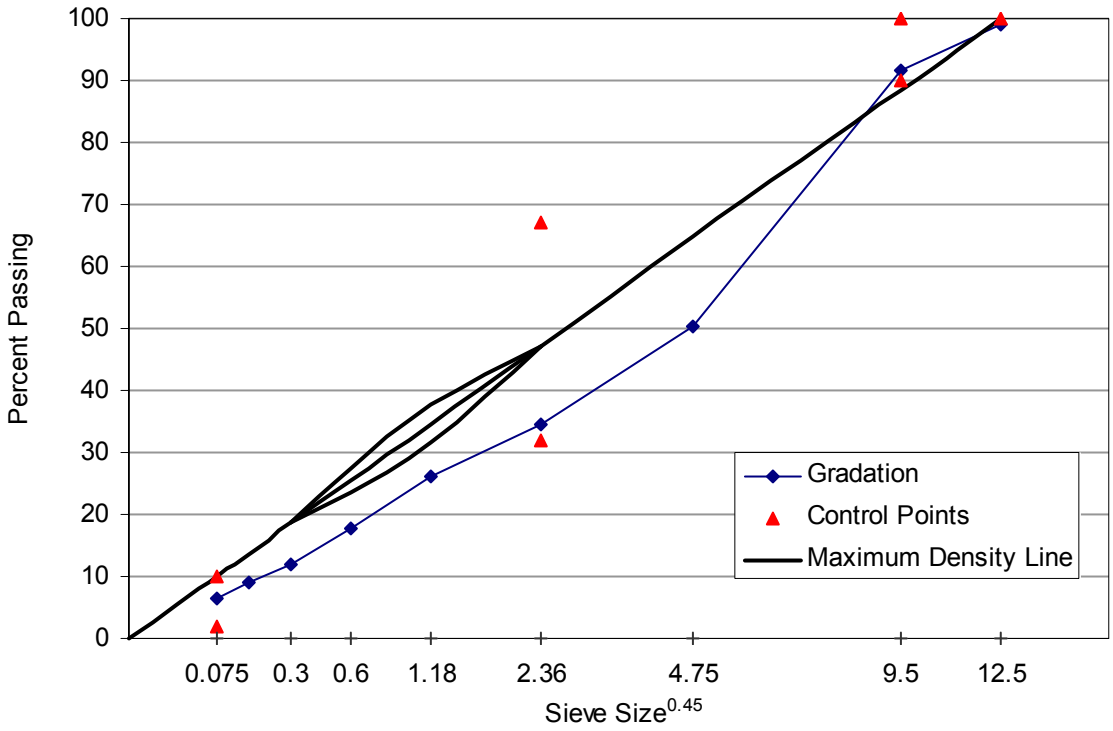

Figure B.16 Gradation of SM-9.5D, lab-lab mixture, section J.

Sieve opening (mm)	Sieve #	% Passing	Control Point LL	Control Point UL	Restricted Zone LL	Restricted Zone UL	Result
12.5	1/2	100.0	-	100			P
9.5	3/8	93.9	90	100			P
4.75	#4	52.9	-	-			
2.36	#8	31.6	32	67	47.2	47.2	F
1.18	#16	22.8	-	-	31.6	37.6	P
0.6	#30	17.4	-	-	23.5	27.5	P
0.3	#50	11.2	-	-	18.7	18.7	P
0.15	#100	8.4	-	-			
0.075	#200	6.7	2	10			P

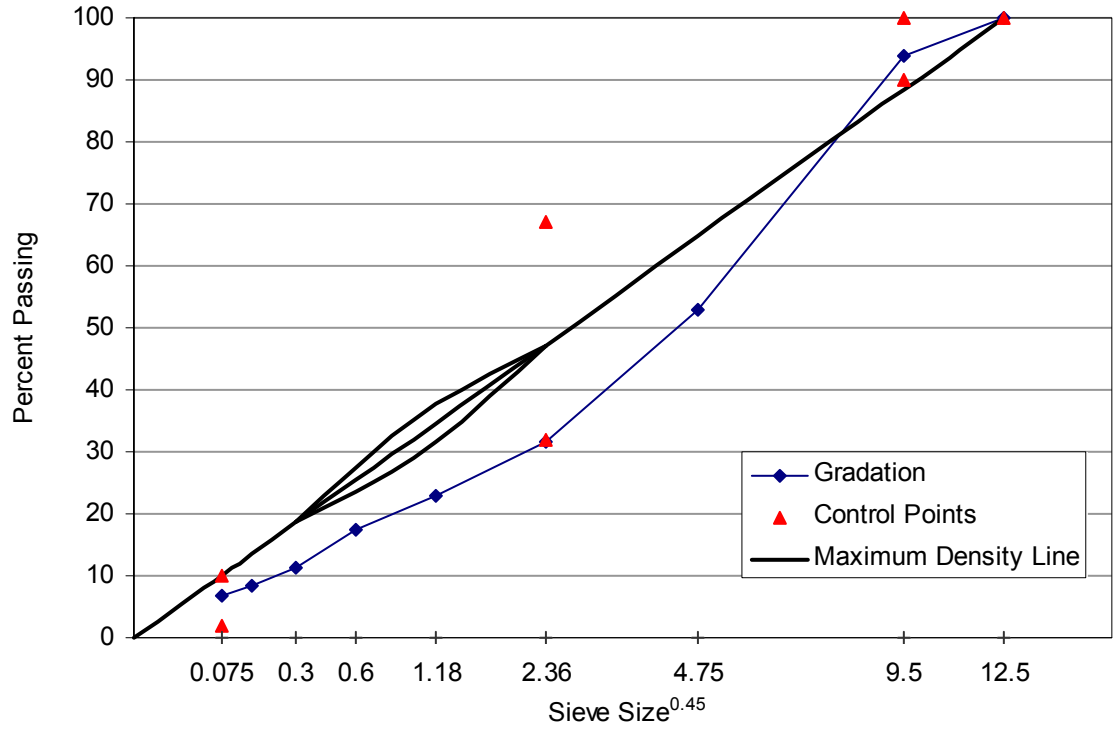

Table B.17 Volumetric properties for SM-9.5E mixtures, section C.

Property	Field - Field	Field - Lab	Lab - Lab	Design - Lab
% Asphalt	5.80	5.80	6.02	6.16
G_{mm}	2.455	2.455	2.477	2.463
G_{mb}	2.309	2.399	2.426	2.431
G_b	1.03	1.03	1.03	1.03
G_{se}	2.684	2.684	2.721	2.711
G_{sb}	2.654	2.654	2.691	2.681
CF	0.03	0.03	0.03	0.03
Bulk Density	144.1	149.7	151.4	151.7
Density at N_{ini}	-	137.5	139.0	137.4
% Passing #200	8.18	8.03	7.56	6.60

Table B.18 VDOT volumetric specifications for SM-12.5E mixtures, section C.

Property	Specification		Field - Field		Field - Lab		Lab - Lab		Design - Lab	
	Min.	Max.								
VTM (%)	2.5	5.5	6.0	Fail	2.3	Fail	2.0	Fail	1.3	Fail
VMA (%)	12	-	18.1	Pass	14.9	Pass	15.3	Pass	14.9	Pass
VFA (%)	62	80	67.0	Pass	84.6	Fail	86.6	Fail	91.4	Fail
% Density at N_{ini}	-	89	-	-	89.7	Fail	89.9	Fail	89.4	Fail
F/A ratio	0.6	1.3	1.5	Fail	1.5	Fail	1.3	Pass	1.1	Pass

Figure B.17 Gradation of SM-9.5E, field-field and field-lab mixtures, section C.

Sieve opening (mm)	Sieve #	% Passing	Control Point LL	Control Point UL	Restricted Zone LL	Restricted Zone UL	Result
12.5	1/2	98.0	-	100			F
9.5	3/8	90.9	90	100			P
4.75	#4	55.3	-	90			P
2.36	#8	34.3	32	67	47.2	47.2	P
1.18	#16	27.0	-	-	31.6	37.6	P
0.6	#30	19.7	-	-	23.5	27.5	P
0.3	#50	14.1	-	-	18.7	18.7	P
0.15	#100	11.1	-	-			
0.075	#200	8.0	2	10			P

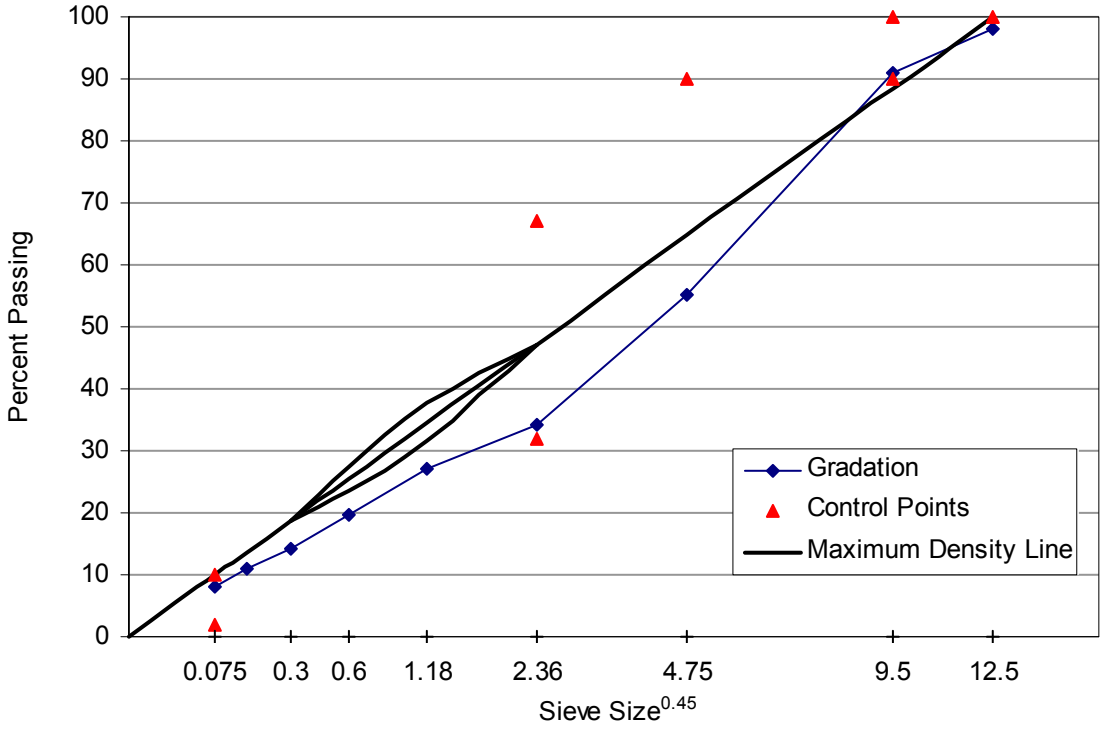

Figure B.18 Gradation of SM-9.5E, lab-lab mixture, section C.

Sieve opening (mm)	Sieve #	% Passing	Control Point LL	Control Point UL	Restricted Zone LL	Restricted Zone UL	Result
12.5	1/2	99.7	-	100			F
9.5	3/8	90.2	90	100			P
4.75	#4	44.6	-	90			P
2.36	#8	35.2	32	67	47.2	47.2	P
1.18	#16	27.3	-	-	31.6	37.6	P
0.6	#30	21.0	-	-	23.5	27.5	P
0.3	#50	13.8	-	-	18.7	18.7	P
0.15	#100	10.1	-	-			
0.075	#200	7.6	2	10			P

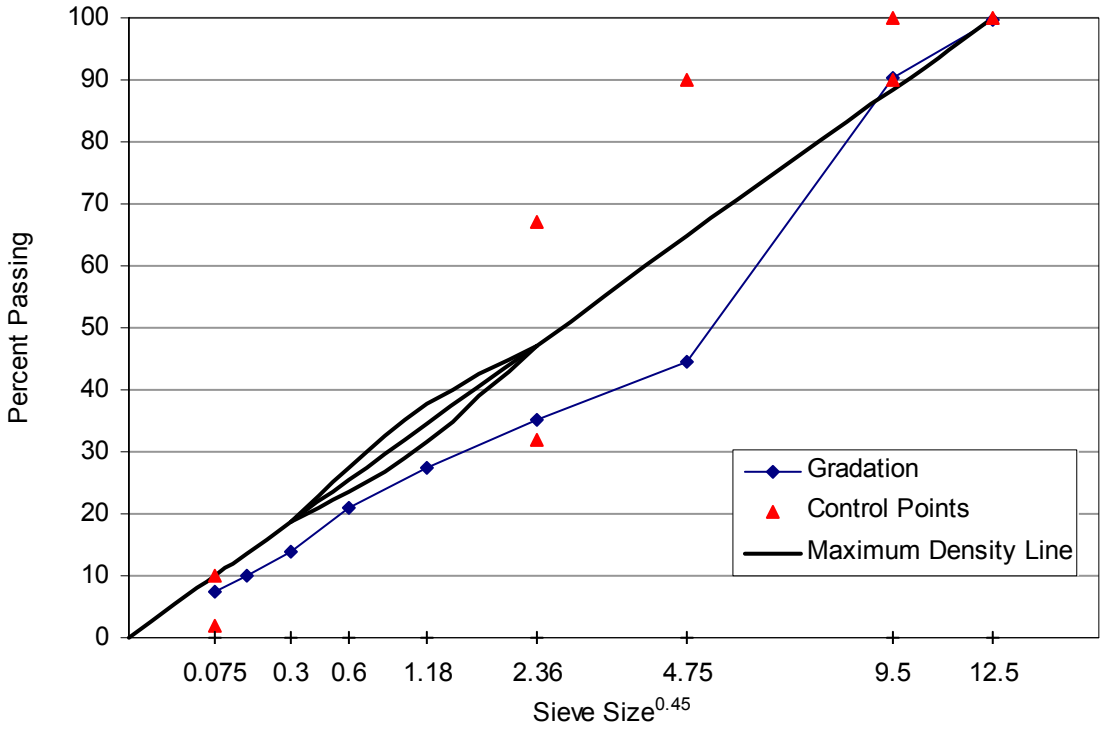

Figure B.19 Gradation of SM-9.5E, design-lab mixture, section C.

Sieve opening (mm)	Sieve #	% Passing	Control Point LL	Control Point UL	Restricted Zone LL	Restricted Zone UL	Result
12.5	1/2	99.4	-	100			F
9.5	3/8	86.5	90	100			F
4.75	#4	44.9	-	90			P
2.36	#8	32.8	32	67	47.2	47.2	P
1.18	#16	25.2	-	-	31.6	37.6	P
0.6	#30	19.3	-	-	23.5	27.5	P
0.3	#50	12.5	-	-	18.7	18.7	P
0.15	#100	8.9	-	-			
0.075	#200	6.6	2	10			P

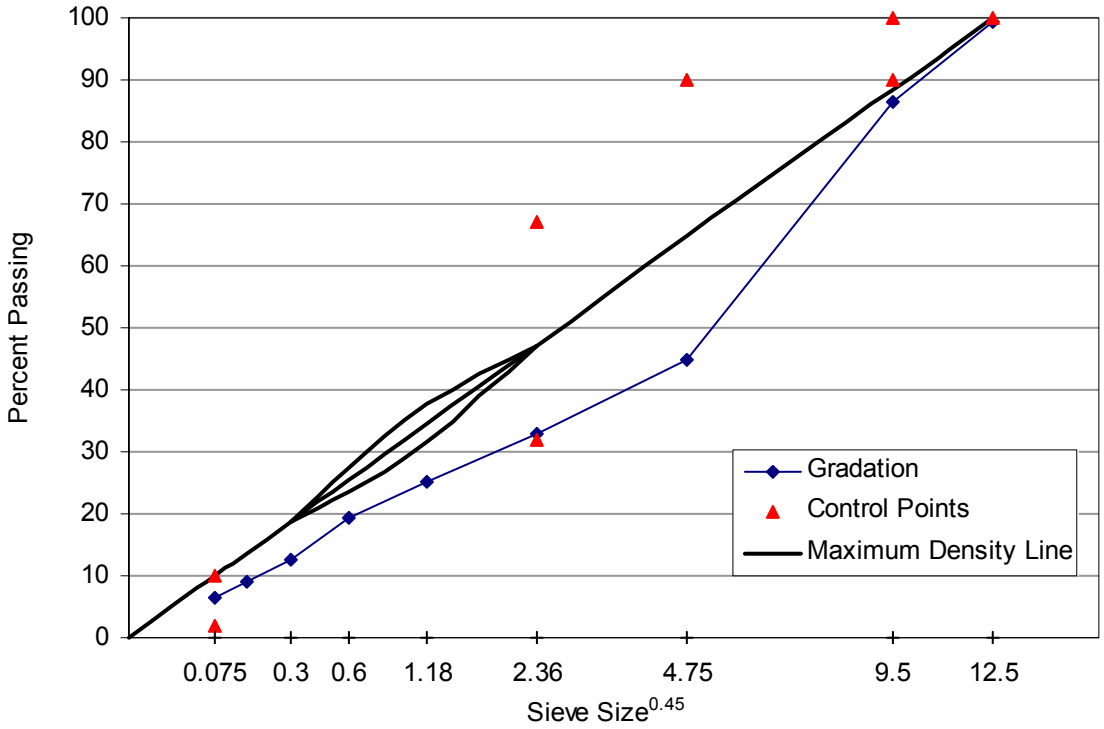

Table B.19 Volumetric properties for SM-12.5D mixtures, section A.

Property	Field - Field	Field - Lab	Lab - Lab	Design - Lab
% Asphalt	5.86	5.86	5.93	5.55
G_{mm}	2.422	2.422	2.510	2.497
G_{mb}	2.282	2.345	2.380	2.376
G_b	1.03	1.03	1.03	1.03
G_{se}	2.644	2.644	2.760	2.725
G_{sb}	2.618	2.618	2.734	2.699
CF	0.026	0.026	0.026	0.026
Bulk Density	142.4	146.3	148.5	148.3
Density at N_{ini}	-	134.2	134.0	133.1
% passing #200	5.64	5.64	12.28	5.96

Table B.20 VDOT volumetric specifications for SM-12.5D mixtures, section A.

Property	Specification		Field - Field		Field - Lab		Lab - Lab		Design - Lab	
	Min.	Max.								
VTM (%)	2.5	5.5	5.8	Fail	3.2	Pass	5.2	Pass	4.8	Pass
VMA (%)	12	-	18.0	Pass	15.7	Pass	18.1	Pass	16.8	Pass
VFA (%)	62	80	67.8	Pass	79.8	Pass	71.4	Pass	71.4	Pass
% Density at N_{ini}	-	89	-	-	88.8	Pass	85.6	Pass	85.5	Pass
F/A ratio	0.6	1.3	1.0	Pass	1.0	Pass	2.2	Fail	1.1	Pass

Figure B.20 Gradation of SM-12.5D, field-field and field-lab mixtures, section A.

Sieve opening (mm)	Sieve #	% Passing	Control Point LL	Control Point UL	Restricted Zone LL	Restricted Zone UL	Result
19	3/4	100.0		100			P
12.5	1/2	99.6	90	100			P
9.5	3/8	98.5	-	90			F
4.75	#4	84.2	-	-			
2.36	#8	47.7	28	58	39.1	39.1	P
1.18	#16	37.3	-	-	25.6	31.6	P
0.6	#30	27.0	-	-	19.1	23.1	P
0.3	#50	14.7	-	-	15.5	15.5	P
0.15	#100	10.2	-	-			
0.075	#200	5.6	2	10			P

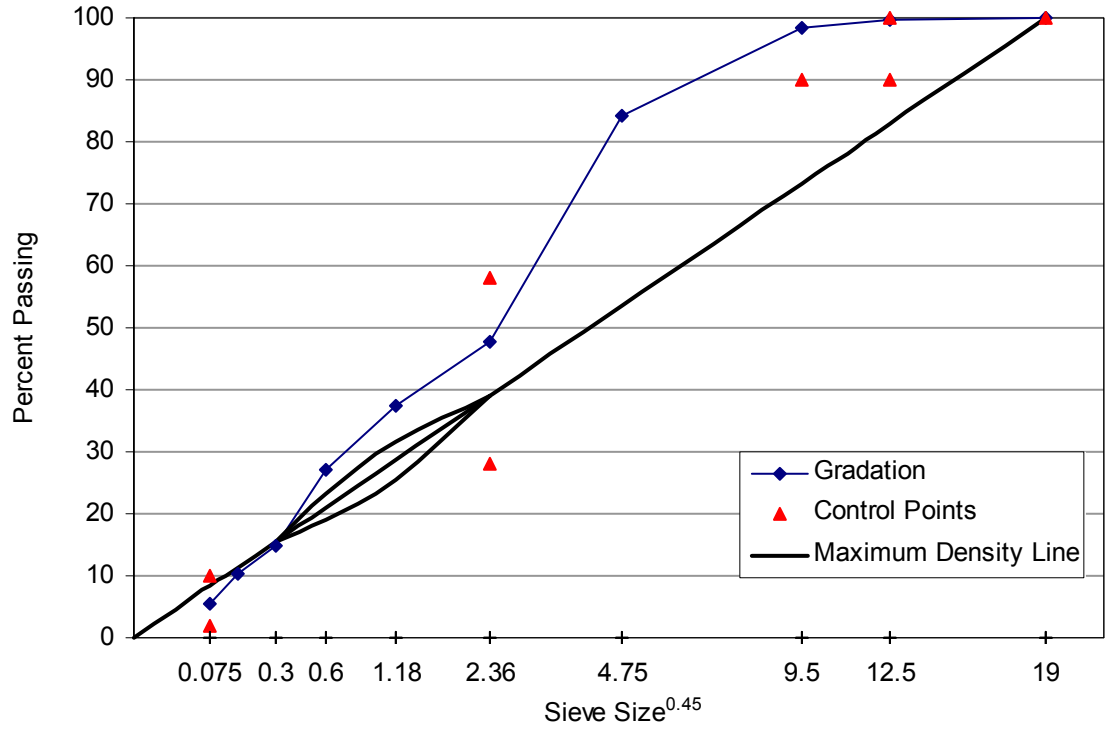

Figure B.21 Gradation of SM-12.5D, lab-lab mixture, section A.

Sieve opening (mm)	Sieve #	% Passing	Control Point LL	Control Point UL	Restricted Zone LL	Restricted Zone UL	Result
19	3/4	100.0		100			P
12.5	1/2	99.5	90	100			P
9.5	3/8	98.9	-	90			F
4.75	#4	91.3	-	-			
2.36	#8	58.3	28	58	39.1	39.1	F
1.18	#16	38.8	-	-	25.6	31.6	P
0.6	#30	28.7	-	-	19.1	23.1	P
0.3	#50	20.1	-	-	15.5	15.5	P
0.15	#100	15.6	-	-			
0.075	#200	12.3	2	10			F

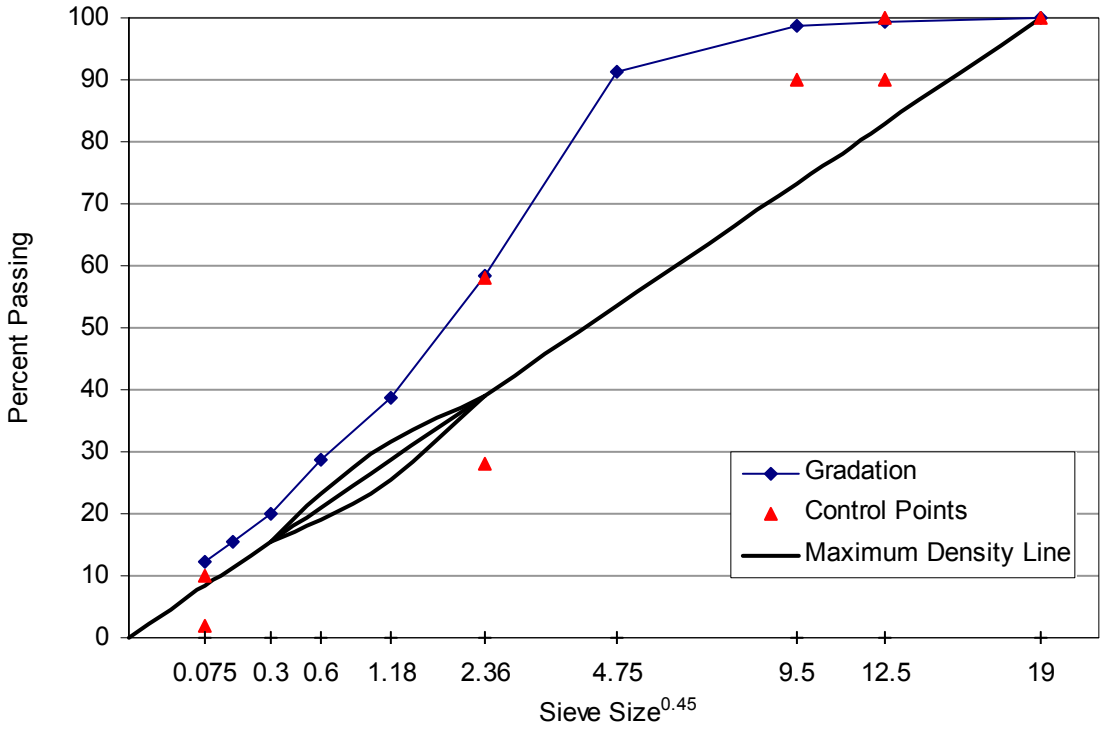

Figure B.22 Gradation of SM-12.5D, design-lab mixture, section A.

Sieve #	% Passing	Control Point LL	Control Point UL	Restricted Zone LL	Restricted Zone UL	Result
3/4	100.0		100			P
1/2	98.4	90	100			P
3/8	89.9	-	90			P
#4	50.1	-	-			
#8	27.7	28	58	39.1	39.1	F
#16	20.2	-	-	25.6	31.6	P
#30	15.3	-	-	19.1	23.1	P
#50	9.7	-	-	15.5	15.5	P
#100	7.3	-	-			
#200	6.0	2	10			P

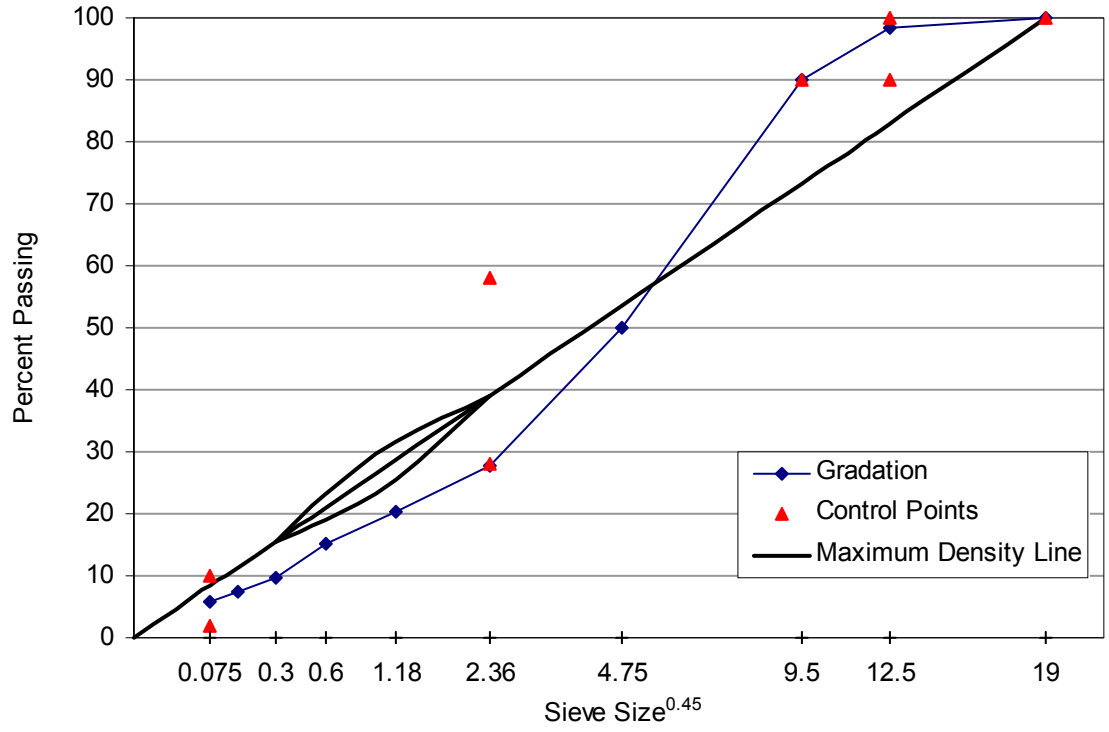

Table B.21 Volumetric properties for SMA-12.5 mixtures, section L.

Property	Field - Field	Field - Lab	Lab - Lab	Design - Lab
% Asphalt	6.80	6.80	6.44	6.33
G_{mm}	2.402	2.402	2.402	2.415
G_{mb}	2.226	2.359	2.359	2.359
G_b	1.03	1.03	1.03	1.03
G_{se}	2.661	2.661	2.644	2.657
G_{sb}	2.631	2.631	2.614	2.627
CF	0.03	0.03	0.03	0.03
Bulk Density	138.9	147.2	147.2	147.2
Density at N_{ini}	-	134.5	134.1	132.0
% passing #200	11.25	11.25	11.71	11.67

Table B.22 VDOT volumetric specifications for SMA-12.5 mixtures, section L.

Property	Specification		Field - Field		Field - Lab		Lab - Lab		Design - Lab	
	Min.	Max.								
VTM (%)	2.5	5.5	7.3	Fail	1.8	Fail	1.8	Fail	2.3	Fail
VMA (%)	12		21.1	Pass	16.4	Pass	15.6	Pass	15.9	Pass
VFA (%)	62	80	65.3	Pass	89.0	Fail	88.5	Fail	85.3	Fail
% Density at N_{ini}	-	89	-	-	89.7	Fail	89.5	Fail	87.6	Pass
F/A ratio	0.6	1.3	1.8	Fail	1.8	Fail	1.9	Fail	2.0	Fail

Figure B.23 Gradation of SMA-12.5, field-field and field-lab mixtures, section L.

Sieve opening (mm)	Sieve #	% Passing	Control Point LL	Control Point UL	Restricted Zone LL	Restricted Zone UL	Result
19	3/4	100.0		100			
12.5	1/2	99.4	90	100			P
9.5	3/8	87.7	-	90			P
4.75	#4	36.8	-	-			
2.36	#8	25.0	28	58	39.1	39.1	F
1.18	#16	21.4	-	-	25.6	31.6	P
0.6	#30	18.9	-	-	19.1	23.1	P
0.3	#50	16.1	-	-	15.5	15.5	P
0.15	#100	13.9	-	-			
0.075	#200	11.2	2	10			F

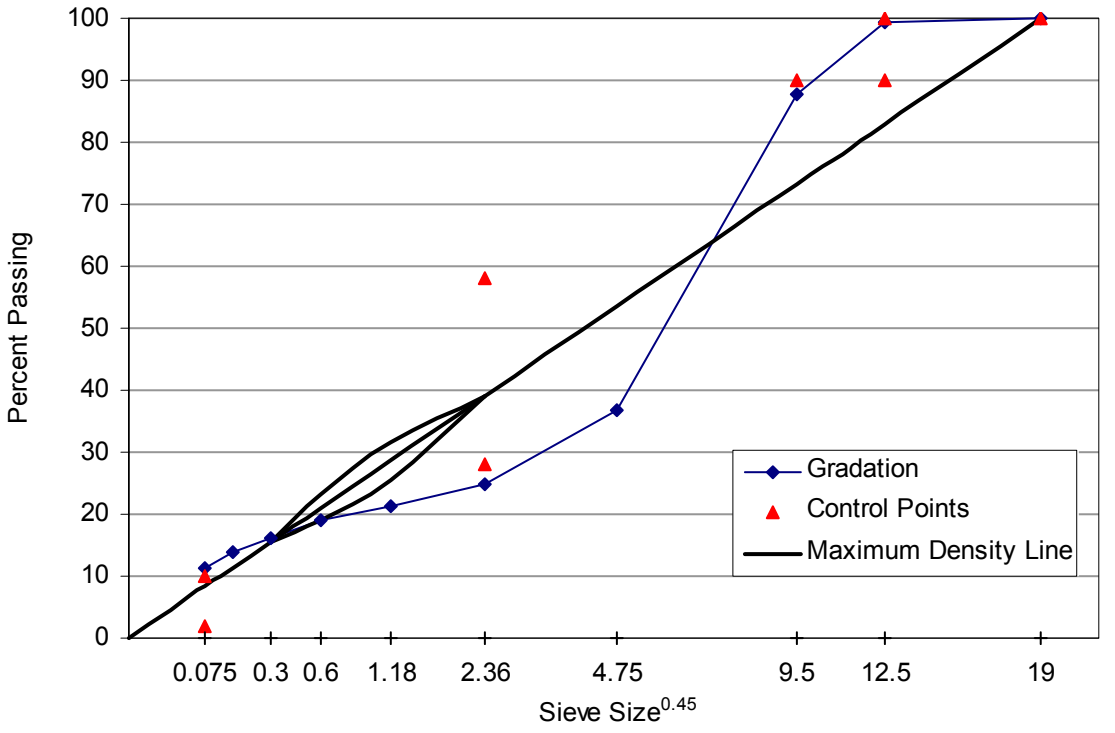

Figure B.24 Gradation of SMA-12.5, lab-lab mixture, section L.

Sieve opening (mm)	Sieve #	% Passing	Control Point LL	Control Point UL	Restricted Zone LL	Restricted Zone UL	Result
19	3/4	100.0		100			
12.5	1/2	92.8	90	100			P
9.5	3/8	76.3	-	90			P
4.75	#4	28.1	-	-			
2.36	#8	21.8	28	58	39.1	39.1	F
1.18	#16	17.9	-	-	25.6	31.6	P
0.6	#30	15.3	-	-	19.1	23.1	P
0.3	#50	14.0	-	-	15.5	15.5	P
0.15	#100	13.1	-	-			
0.075	#200	11.7	2	10			F

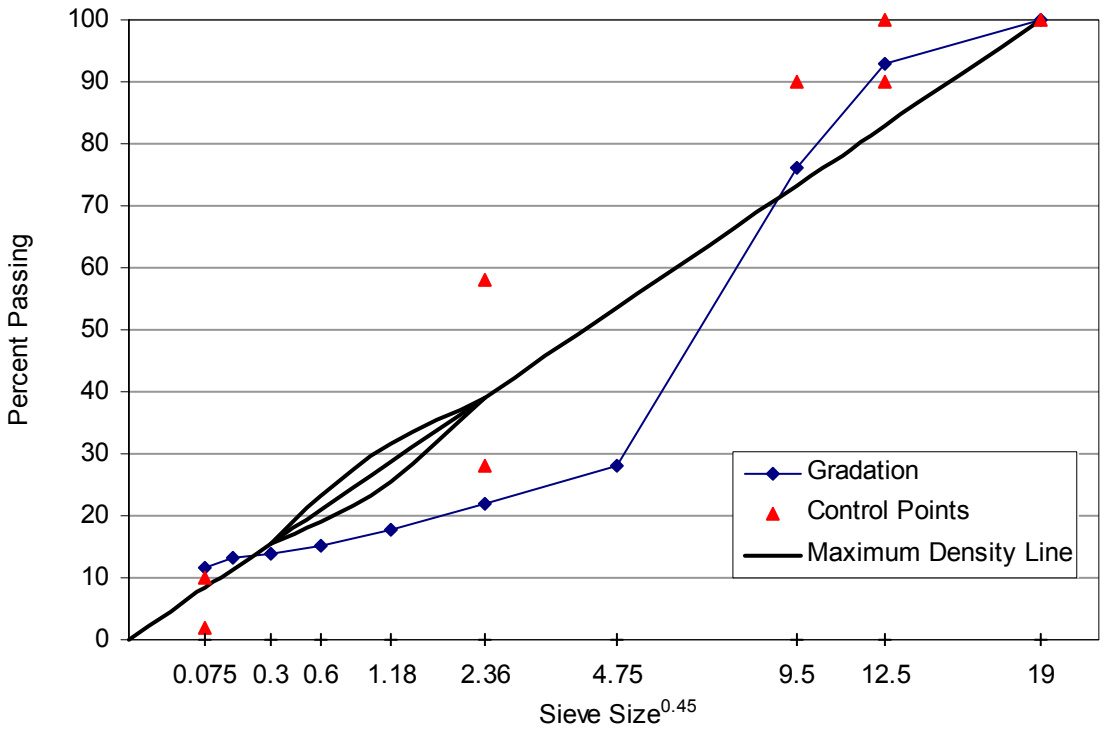

Figure B.25 Gradation of SMA-12.5, design-lab mixture, section L.

Sieve opening (mm)	Sieve #	% Passing	Control Point LL	Control Point UL	Restricted Zone LL	Restricted Zone UL	Result
19	3/4	100.0		100			
12.5	1/2	92.6	90	100			P
9.5	3/8	72.1	-	90			P
4.75	#4	27.8	-	-			
2.36	#8	19.5	28	58	39.1	39.1	F
1.18	#16	16.7	-	-	25.6	31.6	P
0.6	#30	14.8	-	-	19.1	23.1	P
0.3	#50	13.7	-	-	15.5	15.5	P
0.15	#100	12.9	-	-			
0.075	#200	11.7	2	10			F

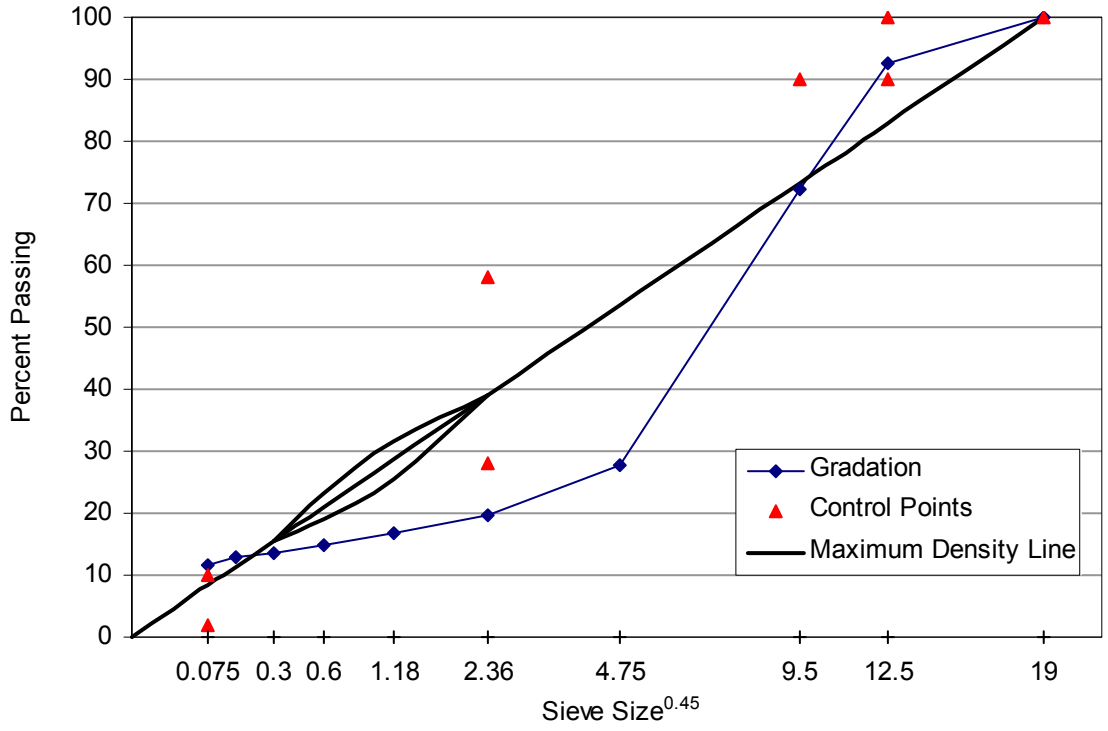

APPENDIX C FATIGUE SPECIMEN PROPERTIES

Table C.1 Average volumetric properties of fatigue specimens.

Section	Mix	Specimen	Asphalt (%)	VTM (%)	VMA (%)	VFA (%)
SM-9.5A	D	field-lab	6.3	5.3	18.4	71.3
		lab-lab	6.8	8.4	22.2	62.2
		design-lab	6.3	8.0	20.8	61.6
	I[a]	field-lab	5.4	6.4	17.5	63.8
		lab-lab	5.3	10.2	20.7	50.7
		design-lab	5.4	10.8	21.5	49.5
SM-9.5D	B	field-lab	4.7	9.0	17.4	48.6
		lab-lab	5.4	7.9	18.3	56.8
		design-lab	5.3	9.6	19.6	51.3
	E	field-lab	5.9	7.3	18.5	60.4
	F	field-lab	5.4	8.2	18.6	56.2
	G	field-lab	6.3	9.0	21.3	57.8
	H	field-lab	5.6	8.7	19.6	55.7
	EFGH	lab-lab	6.0	8.3	20.0	58.5
	J	field-lab	4.9	11.2	20.3	44.6
		lab-lab	5.1	10.7	20.2	46.9
SM-9.5E	C	field-field CL-PP	5.8	7.5	19.4	61.7
		field-field OWP-PP		7.4	19.3	62.8
		field-field IWP-PP		12.8	24.0	47.2
		field-field IWP-PL		6.8	18.8	64.1
		field-lab	5.8	7.1	19.1	62.7
		lab-lab	6.0	8.9	21.2	58.1
		design-lab	6.2	8.0	20.6	61.6
SM-12.5D	A	field-lab	5.9	7.6	19.6	61.0
		lab-lab	5.9	11.0	23.5	53.2
		design-lab	5.6	8.9	20.4	56.5
SMA-12.5	L	field-lab	6.8	7.9	21.6	65.4
		design lab	6.3	10.5	23.0	54.5

[a]Designed with high laboratory compaction.
CL – center of lane; OWP – outer wheelpath; IWP – inner wheelpath; PP – perpendicular to traffic; PL – parallel to traffic

APPENDIX D FATIGUE LIFE VERSUS APPLIED STRAIN

Figure D.1 Fatigue response of SM-9.5A, section D.

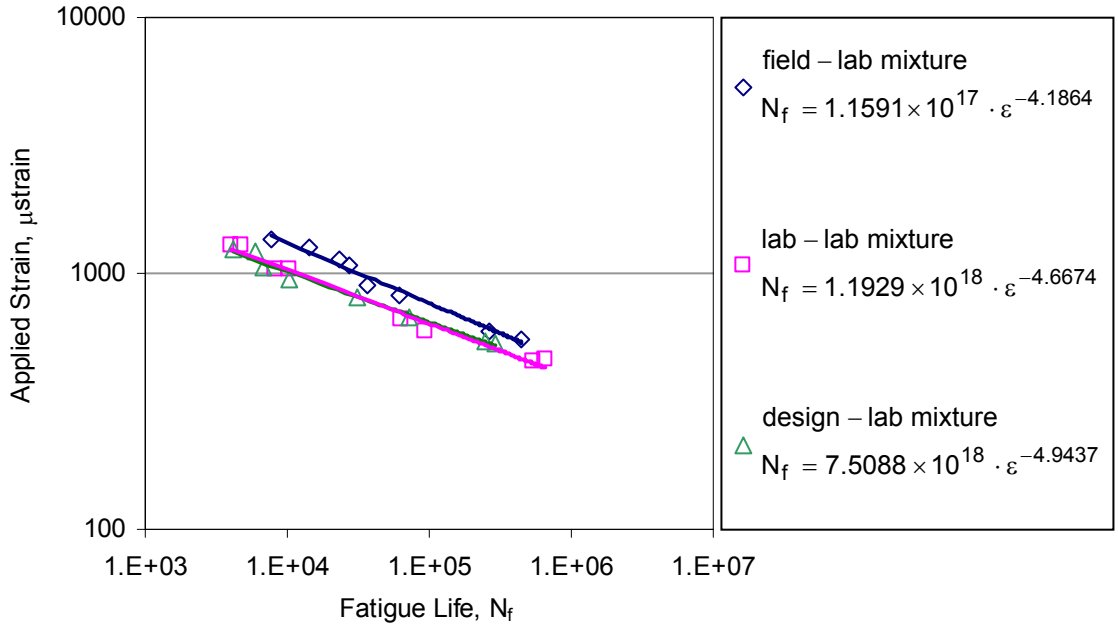

Figure D.2 Fatigue response of SM-9.5A, section I.

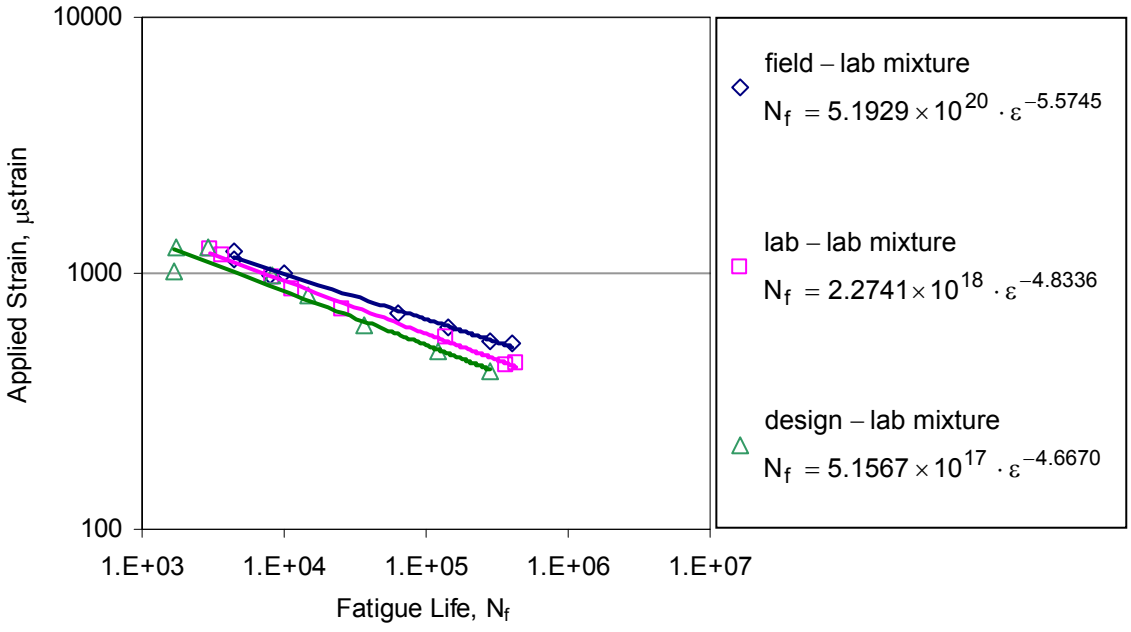

Figure D.3 Fatigue response of SM-9.5D, section B.

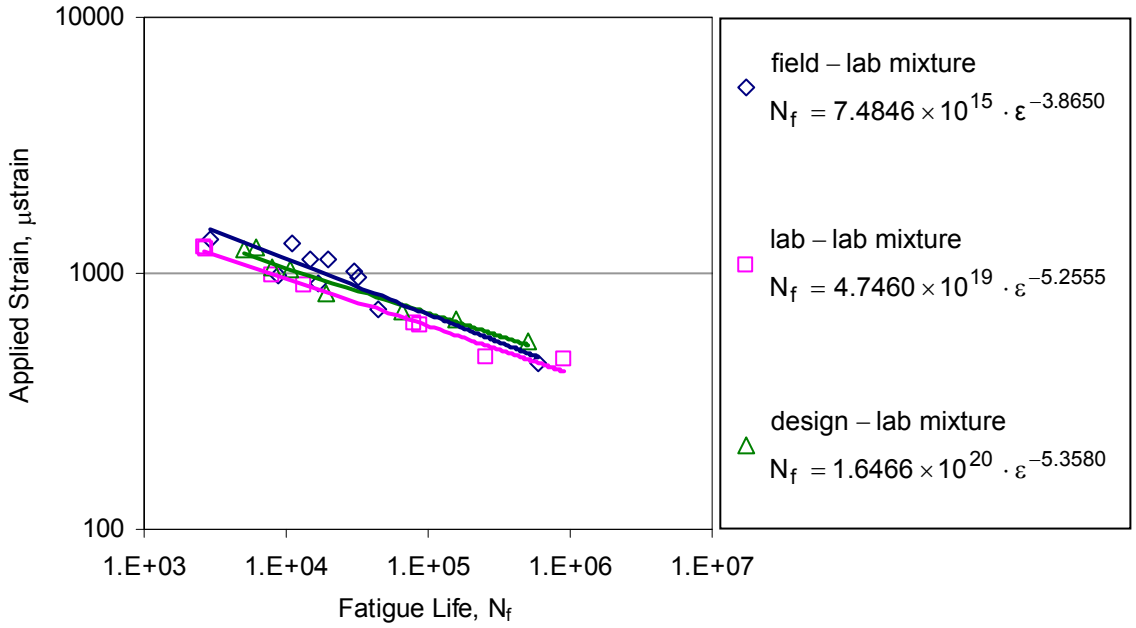

Figure D.4 Fatigue response of SM-9.5D, sections E, F, G, and H.

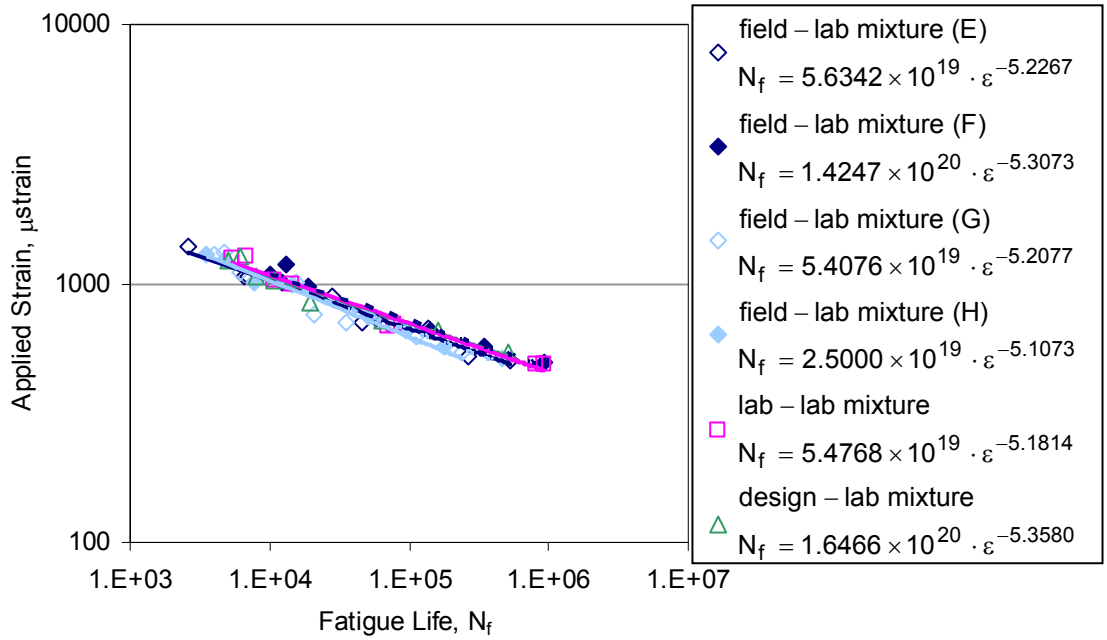

Figure D.5 Fatigue response of SM-9.5D, section J.

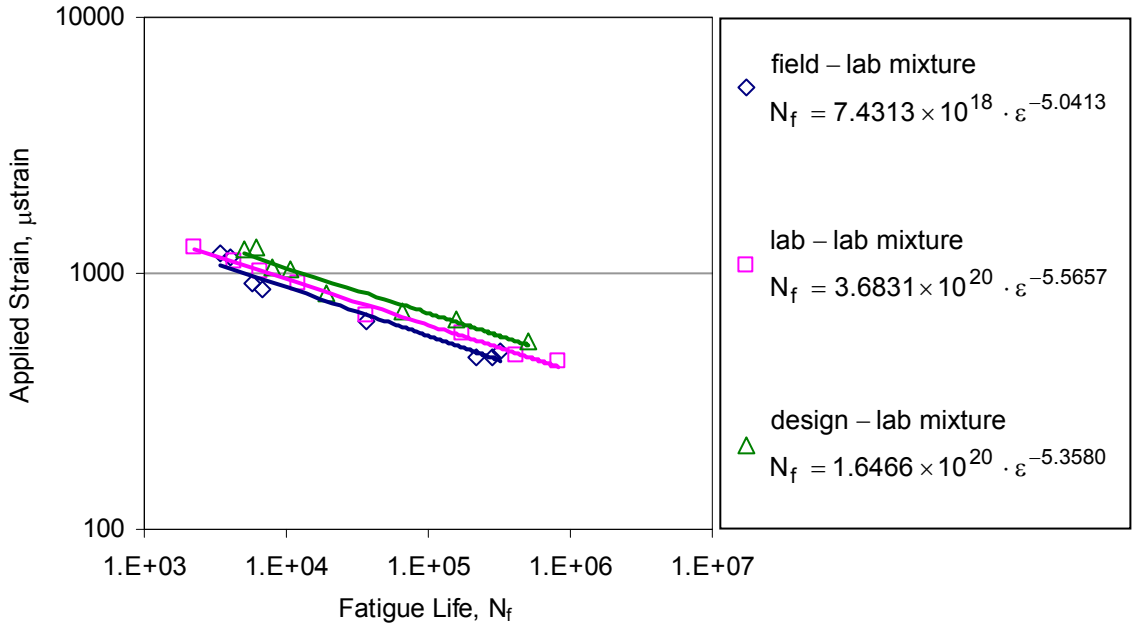

Figure D.6 Fatigue response of SM-9.5E, section C.

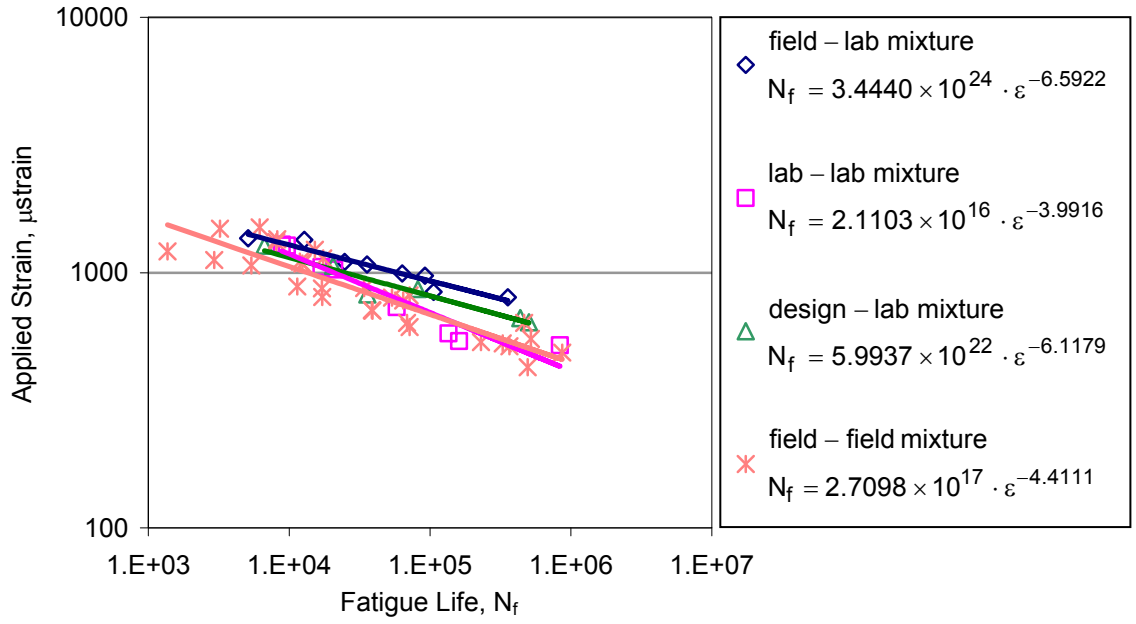

Figure D.7 Fatigue response of SM-9.5E design-lab mixtures, section C, with and without rest periods.

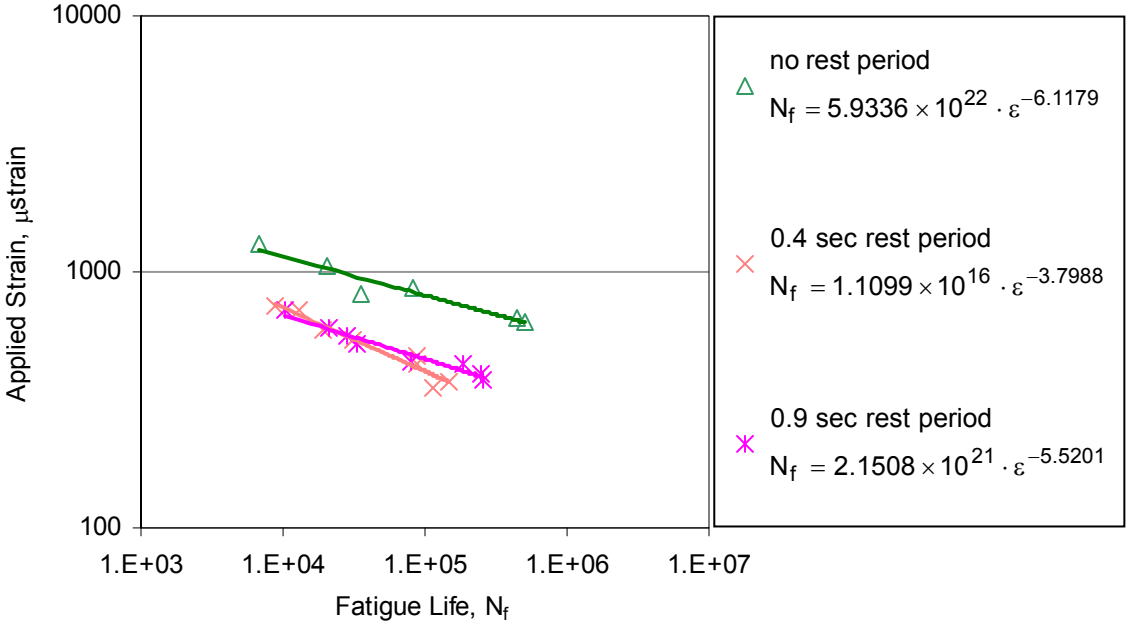

Figure D.8 Fatigue response of SM-9.5E field-field mixtures, section C, with varying locations.

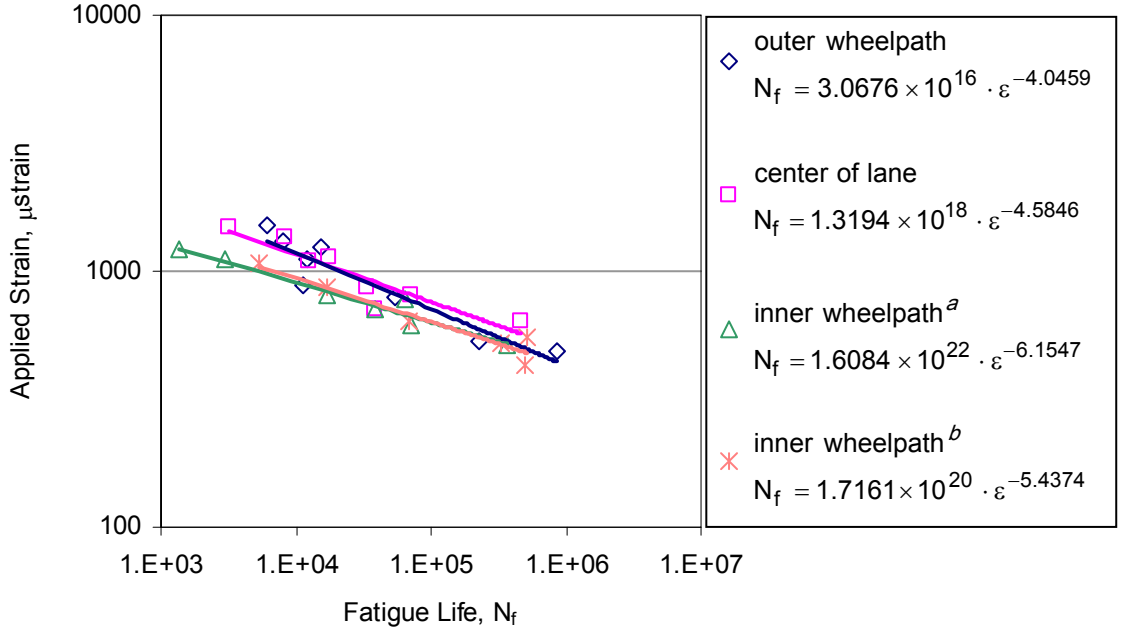

[a]Sample cut with longitudinal axis perpendicular to direction of traffic.
[b]Sample cut with longitudinal axis parallel to direction of traffic.

Figure D.9 Fatigue response of SM-12.5D, section A.

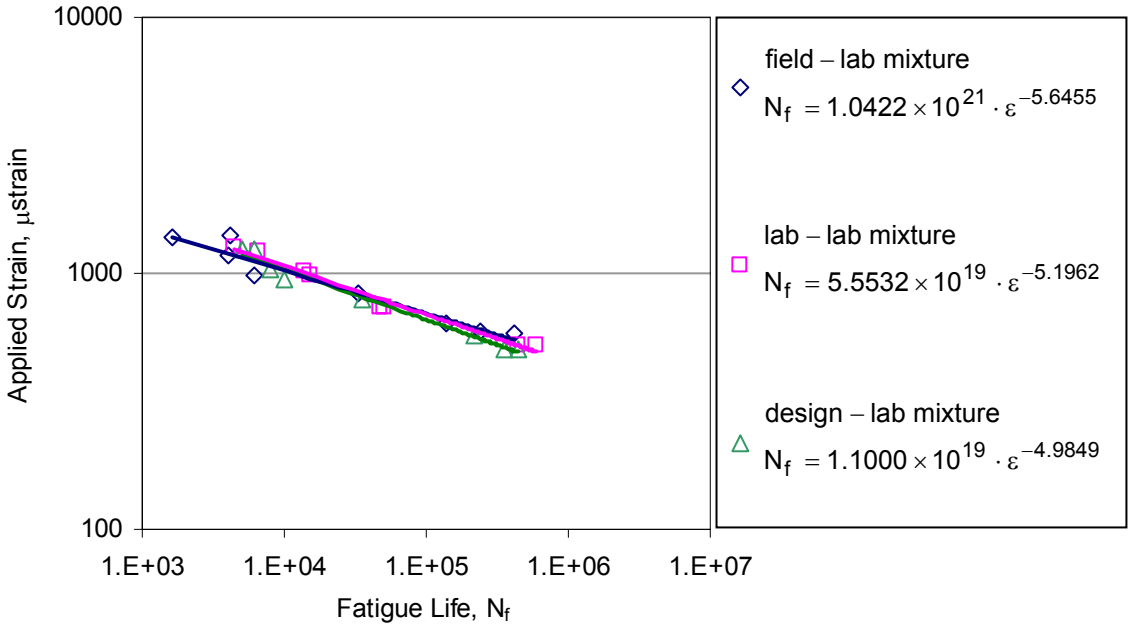

Figure D.10 Fatigue response of SMA-12.5, section L.

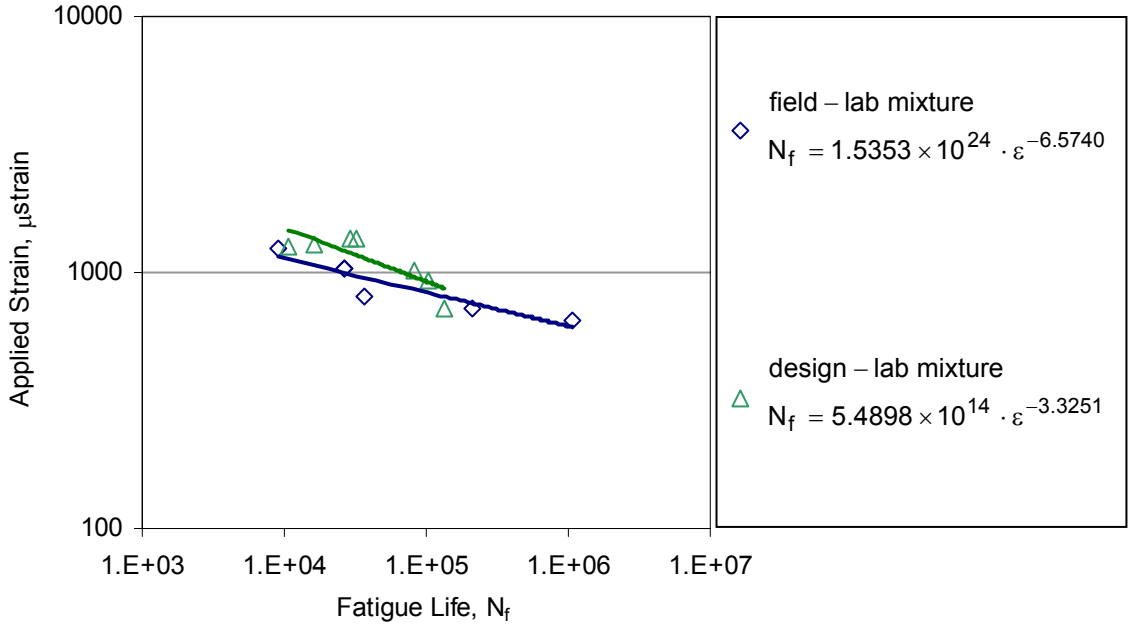

APPENDIX E FATIGUE LIFE VERSUS CUMULATIVE DISSIPATED ENERGY

Figure E.1 Fatigue life versus cumulative dissipated energy for SM-9.5A mixtures, section D.

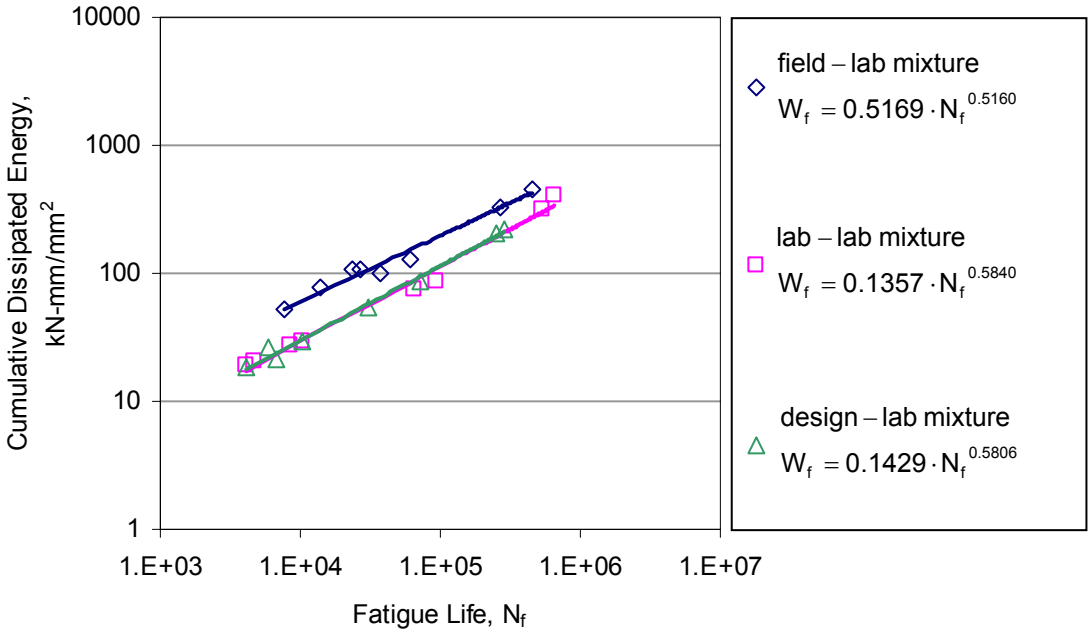

Figure E.2 Fatigue life versus cumulative dissipated energy for SM-9.5A mixtures, section I.

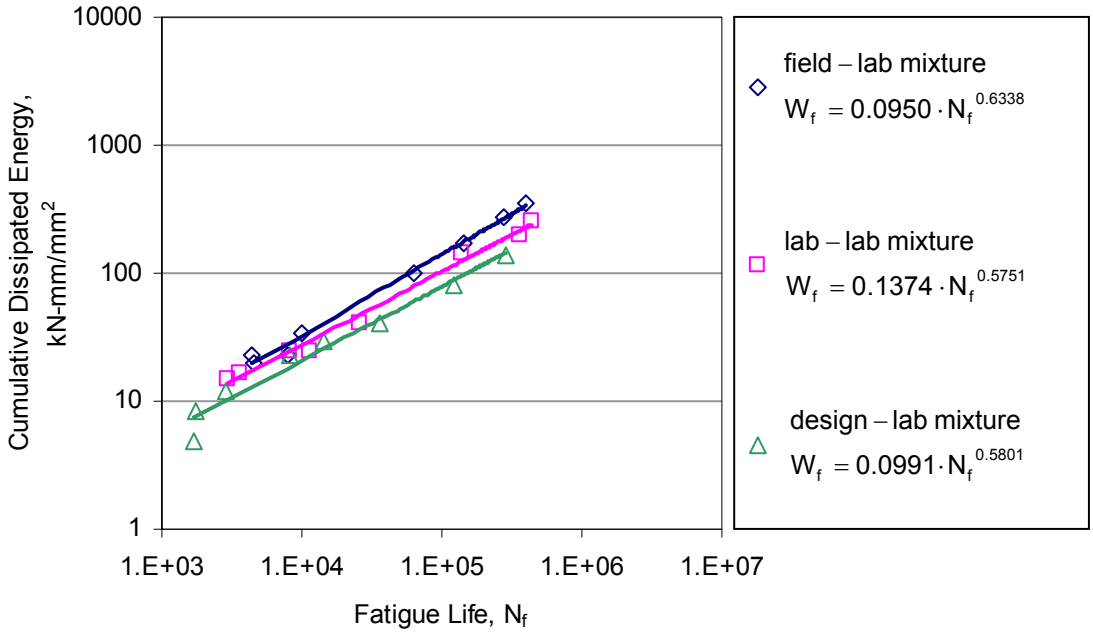

Figure E.3 Fatigue life versus cumulative dissipated energy for SM-9.5D mixtures, section B.

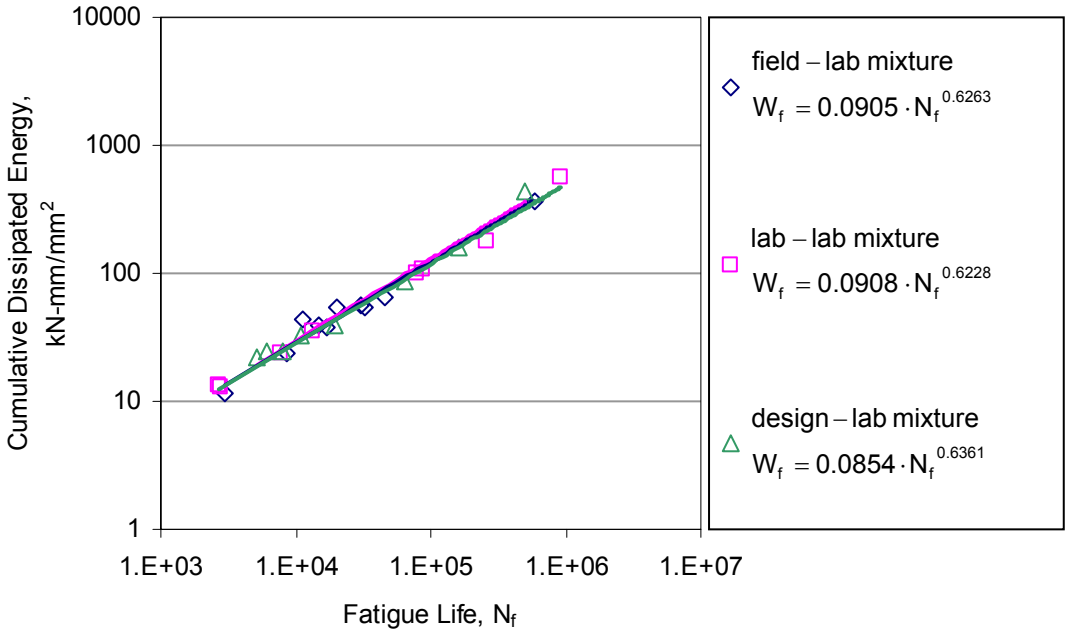

Figure E.4 Fatigue life versus cumulative dissipated energy for SM-9.5D mixtures, sections E, F, G, and H.

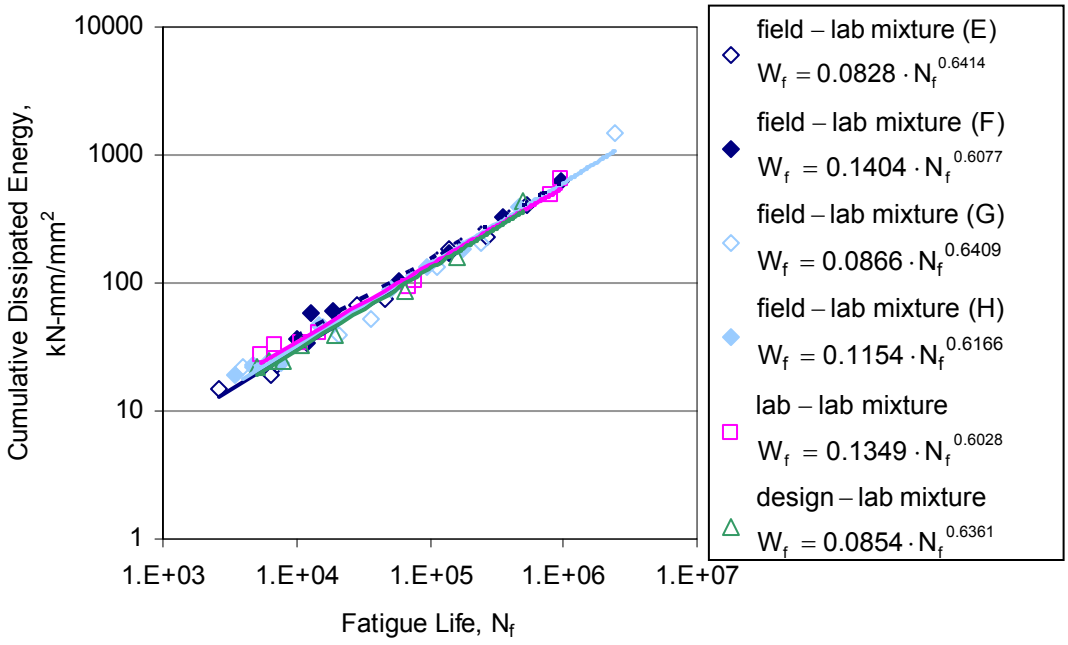

Figure E.5 Fatigue life versus cumulative dissipated energy for SM-9.5D mixtures, section J.

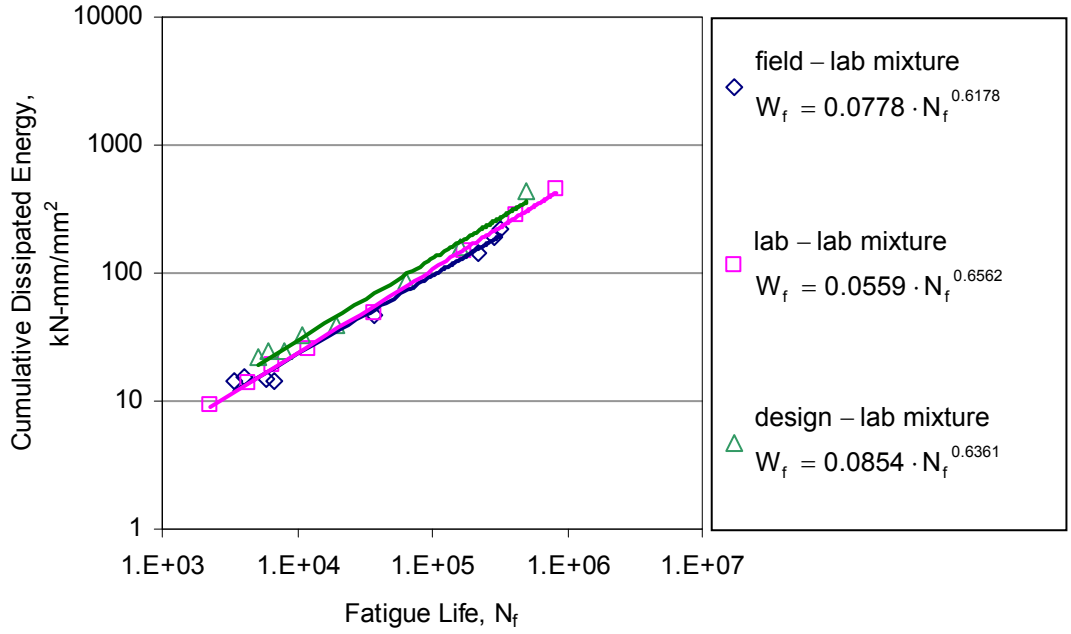

Figure E.6 Fatigue life versus cumulative dissipated energy for SM-9.5E mixtures, section C.

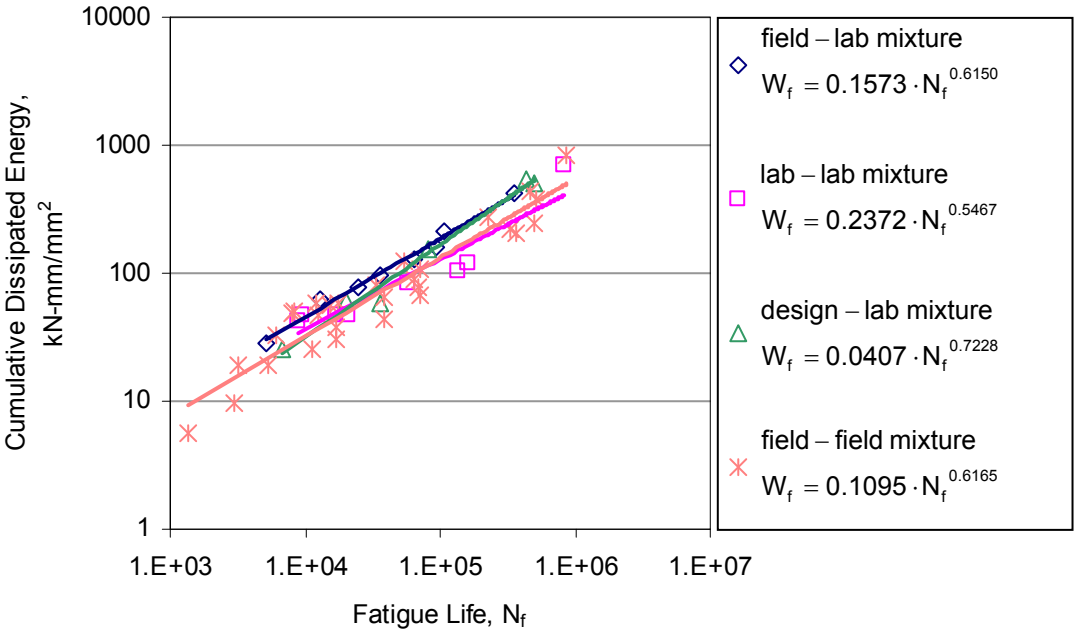

Figure E.7 Fatigue life versus cumulative dissipated energy for SM-9.5E design-lab mixtures, section C, with and without rest periods.

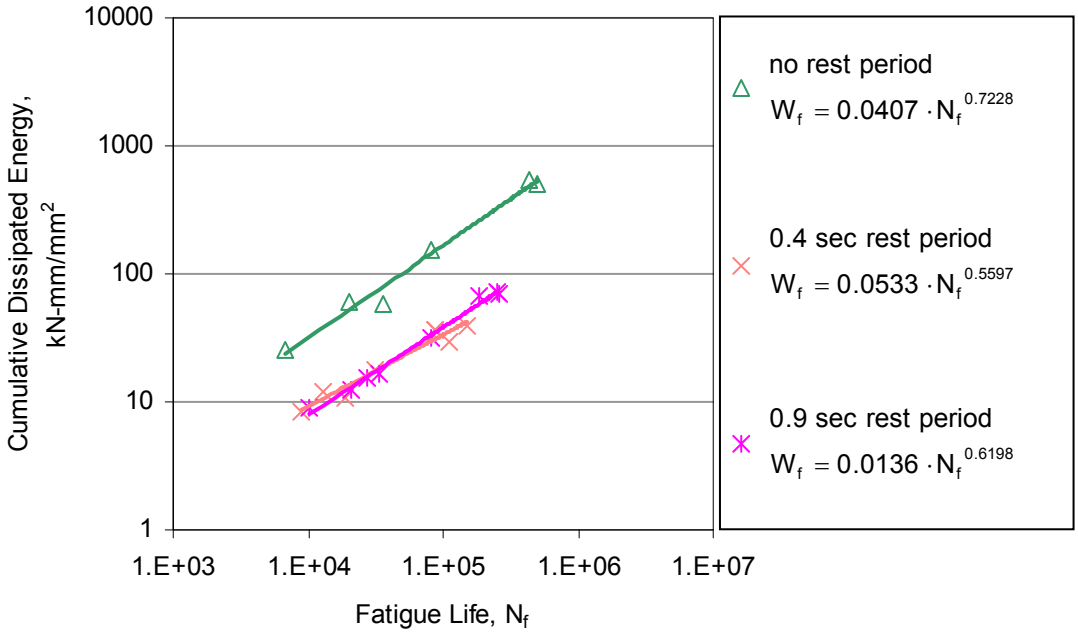

Figure E.8 Fatigue life versus cumulative dissipated energy for SM-9.5E field-field mixtures, section C, with varying locations.

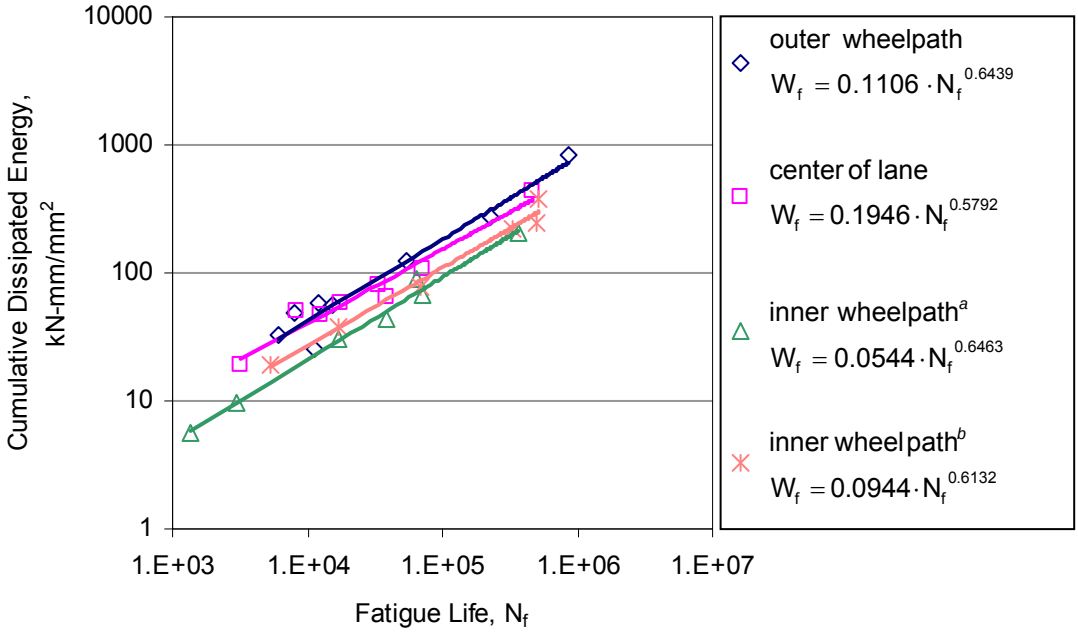

[a]Sample cut with longitudinal axis perpendicular to direction of traffic.
[b]Sample cut with longitudinal axis parallel to direction of traffic.

Figure E.9 Fatigue life versus cumulative dissipated energy for SM-12.5D mixtures, section A.

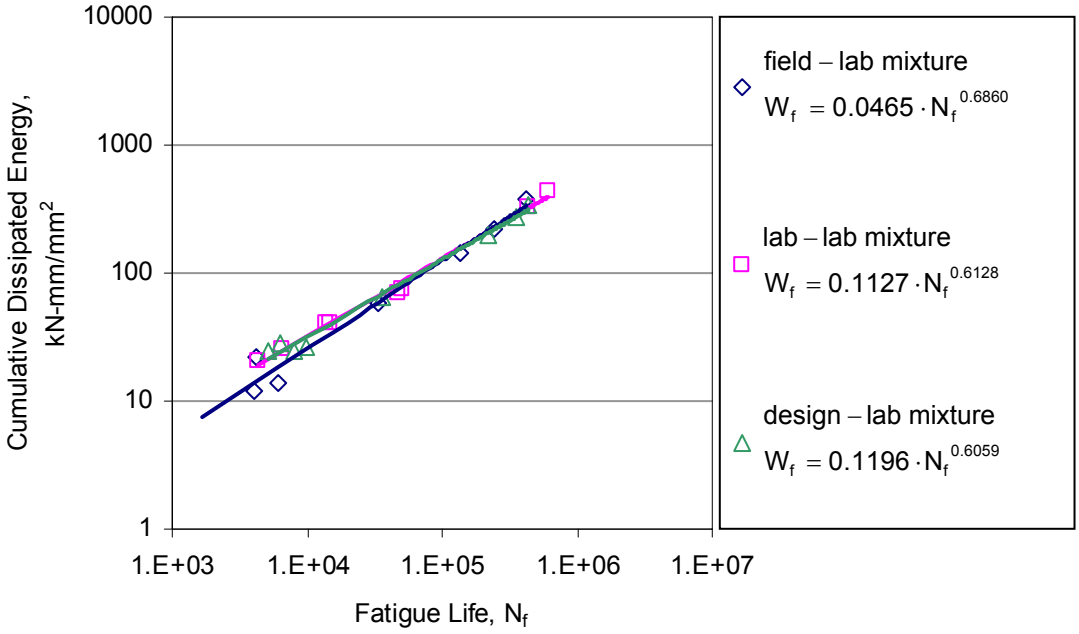

Figure E.10 Fatigue life versus cumulative dissipated energy for SMA-12.5 mixtures, section L.